ABSTRACT

Title of Document: A NOVEL PRE-FLUORESCENT NITROXIDE PROBE FOR THE HIGHLY SENSITIVE DETERMINATION OF PEROXYL AND OTHER RADICAL OXIDANTS

Min Jia, Doctor of Philosophy, 2009

Directed By: Professor Neil V. Blough, Department of Chemistry and Biochemistry

Peroxyl and other radical oxidants react with stable cyclic nitroxides, such as the piperidinyl and pyrrolidinyl nitroxides to form initially the one electron oxidation product, the oxoammonium cation. For most of the nitroxides studied thus far, the oxoammonium cation can in part be regenerated to the nitroxide through reduction by solution constituents. The reaction mechanisms, however, remain a matter of debate. Further, the highly-sensitive, quantitative determination of peroxyl and other radical oxidants has yet to be achieved, posing a major hurdle to a further understanding of the impact of peroxyl radicals in many biological and environmental processes.

A unique, amino-pyrrolidinyl nitroxide, 3-amino-2,2,5,5,-tetramethyl-1-pyrrolidinyloxy (3-ap) is shown to undergo an irreversible reaction with peroxyl radicals and other radical oxidants to generate a diamagnetic product. When a fluorophore, fluorescamine is covalently coupled to the nitroxide, the resulting

compound (3-apf, or **I**) has very low fluorescence quantum yield. Upon reaction with peroxyl and other radical oxidants, the quantum yield of the product increases dramatically (~100 fold), thus 3-ap or 3-apf can be used as a highly sensitive and versatile probe to determine oxidant production optically, either by monitoring the changes in fluorescence intensity using a spectrofluorometer, by HPLC analysis with fluorescence detection, or by a combination of both approaches.

By changing the $[O_2]$/[nitroxide] ratio, it is shown that peroxyl radicals can be detected and quantified preferentially in the presence of other radical oxidants, such as $\bullet NO_2$ and $CO_3^{\bullet -}$. When decreasing the $[O_2]$/[nitroxide] ratio, the oxidation product decreases, with a concomitant increase of the alkoxylamine product resulting from reaction of 3-ap (3-apf) with alkyl radicals.

High resolution mass spectrometry and NMR studies indicate that 3-ap is oxidized to form a cyclic peroxide structure, while 3-apf is oxidized to form a cyclic -NH-O- structure, with this difference resulting possibly from the presence of the fluorescamine moiety in 3-apf.

Detection of photochemically produced peroxyl radicals is achieved by employing 3-ap alone, followed by derivatization with fluorescamine, while detection of thermally-generated peroxyl radicals employs 3-apf. Preliminary applications include the detection of peroxyl radicals generated thermally in soybean phosphatidylcholine liposomes by 3-apf and produced photochemically in tap water by 3-ap.

A NOVEL PRE-FLUORESCENT NITROXIDE PROBE FOR THE HIGHLY SENSITIVE DETERMINATION OF PEROXYL AND OTHER RADICAL OXIDANTS.

By

Min Jia

Dissertation submitted to the Faculty of the Graduate School of the
University of Maryland, College Park, in partial fulfillment
of the requirements for the degree of
Doctor of Philosophy
2009

Advisory Committee:
Professor Neil V. Blough, Chair
Professor Mohamad Al-Sheikhly
Professor Daniel Falvey
Professor Catherine Fenselau
Professor Janice Reutt-Robey
Professor Yuhuang Wang

© Copyright by
Min Jia
2009

ACKNOWLEDGEMENTS

I would like to sincerely thank my research advisor, Dr. Neil V. Blough for his patience, guidance, support and encouragement throughout all the phases of my study and research. From him, I learned not only knowledge in chemistry, but also the way to do research, to identify and solve scientific problems, which will greatly benefit my future research career. My sincere appreciation extends to my advisory committee members, Dr. Mohamad Al-Sheikhly, Dr. Daniel Falvey, Dr. Catherine Fenselau, Dr. Janice Reutt-Robey and Dr. Yuhuang Wang for their assistance and time.

I'd like to express my special thanks to Dr. Mohamad Al-Sheikhly at the Department of Materials Science and Engineering, from whom I received tremendous help utilizing the pulse radiolysis system and ^{60}Co source in his lab. I also thank him for his discussion and advice regarding my research. I thank Ms. Alia weaver in Dr. Al-Sheikhly's lab for her assistance running radiolysis experiments.

I truly appreciate Dr. Sarah Green's insightful discussion regarding my research and her help in my manuscript revision.

It would have been impossible to finish this thesis without the help of Dr. Yiufai Lam at the NMR center who helped me obtain 2D NMR data and offered critical discussion and advice.

My appreciation also goes to Dr. Elizabeth Kujawinski and Melissa Soule at Woods Hole Oceanographic Institution for the FT-ICR mass spectra measurements.

I also would like to thank my friends and colleagues in the Blough research group, Dr. Rossana Del Vecchio, Dr. Yu Tang, Dr. Qing Zhu, Lynne Heighton, Yi Zhang, Kelli Golanoski, Andrea Andrew.

I'd like to thank my parents and my brother, my sister for their continuous support and encouragement; and finally a lot of thanks go to my wife, Linlin Cao. Thank you for always loving, understanding and supporting me.

Table of Contents

List of Tables

List of Figures

List of Schemes

Chapter I Introduction

1.1 Introduction

A free radical can be defined as any species capable of independent existence that contains one or more unpaired electrons.[1] The presence of this unpaired electron causes free radicals to be paramagnetic, and the concentration of free radicals can be followed directly by electron paramagnetic spectroscopy (EPR). The chemical reactivity of free radicals varies dramatically depending on their structures, but most of them are highly reactive and have low steady state concentrations due to their short life time, making the direct measurement by EPR often difficult.

Free radicals can be formed in three fashions:

1) losing one electron from a non-radical molecule to form a radical cation;

$$X \longrightarrow X^{\bullet +} + e \qquad (1.1)$$

2) obtaining one electron to form a radical anion;

$$Y + e \longrightarrow Y^{\bullet -} \qquad (1.2)$$

3) through homolytic scission of a covalent bond to form neutral radicals.

$$X:Y \longrightarrow X^{\bullet} + Y^{\bullet} \qquad (1.3)$$

Some basic reactions of free radicals are listed below:[1]

1. Radical combination reaction, where two radicals combine their unpaired electrons to form a new covalent bond.

$$X^{\bullet} + Y^{\bullet} \longrightarrow X:Y \qquad (1.4)$$

2. Radical addition reaction, where a free radical may react with a non-radical molecule to form a new radical.

$$X^{\cdot} + Y \longrightarrow [X\text{-}Y]^{\bullet} \qquad (1.5)$$

3. Radical redox reaction, where a free radical may serve as a reducing agent, donating one electron and becoming a cation (equation 1.6), or as an oxidizing agent, accepting one electron and becoming an anion (equation 1.7).

$$X^{\cdot} + Y \longrightarrow X^{+} + Y^{\bullet -} \qquad (1.6)$$

$$X^{\cdot} + Y \longrightarrow X^{-} + Y^{\bullet +} \qquad (1.7)$$

4. Hydrogen abstraction, where a free radical abstracts a hydrogen atom from C-H bond to form a new carbon centered radical. In the presence of oxygen, carbon centered radicals react with oxygen at diffusion controlled rate to form peroxyl radicals.

$$X^{\cdot} + RH \longrightarrow XH + R^{\cdot} \qquad (1.8)$$

5. Radical cleavage reaction such as β-elimination, where the β position of the unpaired electron cleaves and forms a new radical, sometimes with the concomitant generation of a new compound.

(1.9)

Most of the metals in the first row of the d-block in the periodic table (except Zn) could qualify as free radicals since they contain unpaired electrons in either atoms or ions. Many of their biological functions involve donating or accepting single electrons.[2-8] Many enzymes utilize these metals to catalyze different biological reactions. Transition

metals, however, can also catalyze deleterious free radical reactions, such as autoxidation and OH formation. One example is the famous Fenton reaction:

$$Fe^{2+} + H_2O_2 \longrightarrow Fe^{3+} + HO\cdot + HO^- \qquad (1.10)$$

1.2 Chemistry of some important free radicals

1.2.1 Biological Systems. Some free radicals play important roles in the auto-oxidation of lipids and cell membranes[9-10] and have also been implicated in oxidative DNA damage, [11-15] in aging,[16-18] and in many human chronic diseases.[19-20] These include hydroxyl/alkoxyl radicals, superoxide radical, carbonate radical and peroxyl radicals.

1. Hydroxyl radical. This is a highly reactive and very strong oxidizing agent. It can be generated by:

1) reaction of metal ions with hydrogen peroxide (reaction 1.10);

2) UV-induced homolytic scission of hydrogen peroxide;

$$H{-}O{-}O{-}H \xrightarrow{UV} 2\,HO\cdot \qquad (1.11)$$

3) the radiolysis of water.

$$H_2O \longrightarrow \cdot OH + e_{aq}^- + H_3O^+ + \cdot H + OH^- + H_2 + H_2O_2 \qquad (1.12)$$

The hydroxyl radical undergoes 3 main types of reactions with other species:

1) hydrogen atom abstraction;

$$HO\cdot + RH \longrightarrow R\cdot + H_2O \qquad (1.13)$$

2) addition to unsaturated bonds;

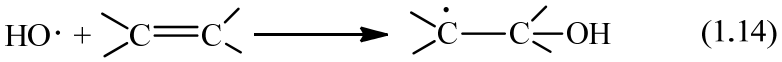

(1.14)

3) electron transfer reactions.

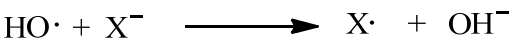

(1.15)

Although the recombination of two •OH can occur in spurs during radiolysis[21], when it is in high concentrations, generally OH will react primarily with other solution constituents, because of its very high rate constant for reaction with most organic and many inorganic compounds.[1]

The hydroxyl radical can abstract a hydrogen atom from saturated organic compounds, undergoes an addition reaction to aromatic or unsaturated compounds. Both types of reactions lead to the formation of carbon centered radicals (R•). In the presence of molecular oxygen, peroxyl radicals (equation 1.17) or superoxide radical (equation 1.16) will be formed secondarily.

(1.16)

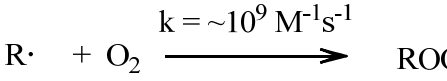

(1.17)

•OH can oxidize many types of compounds due to its high oxidation potential (2.31V vs. SHE).[1] For example, it can react with CO_3^{2-} ion to produce carbonate radical ($CO_3^{\bullet-}$), or nitrite to produce $\bullet NO_2$.

$$\bullet OH + NO_2^- \xrightarrow{k = 6.0 \times 10^9\ M^{-1}s^{-1}} \bullet NO_2 + OH^- \qquad (1.18)$$

$$\bullet OH + CO_3^{2-} \xrightarrow{k = 3.9 \times 10^8\ M^{-1}s^{-1}} CO_3^{\bullet -} + OH^- \qquad (1.19)$$

2. Superoxide radical. Superoxide radical is far less reactive than OH radical. In aqueous solution at neutral to alkaline pH, superoxide is unreactive to most of the biomolecules, such as DNA, proteins, lipids and other molecules. It can selectively react with some proteins such as catalase and glutathione peroxidase to cause damage.[22] At low pH, superoxide is protonated to form HO_2 radical (hydroperoxyl, pKa = 4.88),[1] which is a stronger oxidizing agent than superoxide (equation 1.19). At neutral pH, $HO_2\bullet$ constitutes about 1% of the superoxide pool.

$$O_2^{\bullet -} + H^+ \rightleftharpoons HO_2^{\bullet} \qquad (1.20)$$

$$HO_2^{\bullet} + O_2^{\bullet -} + H^+ \xrightarrow{k = 10^8\ M^{-1}s^{-1}} H_2O_2 + O_2 \qquad (1.21)$$

$$2O_2^{\bullet -} + 2H^+ \longrightarrow H_2O_2 + O_2 \qquad (1.22)$$

Especially at lower pH, the most significant reaction of superoxide in aqueous solution is its dismutation reaction, which usually proceeds via protonation of $O_2^{\bullet -}$ followed by reaction of $HO_2\bullet$ with $O_2^{\bullet -}$ to form H_2O_2 and O_2 (equations 1.20-1.22). The overall dismutation reaction is shown in equation 1.22.

Superoxide radical can act as a reducing agent,[23] for example, reducing Fe(III) to Fe^{2+} (equation 1.23), and can therefore accelerate the generation of •OH in Fenton reaction (equation 1.24). This is called superoxide-assisted/driven Fenton reaction.

$$H_2O_2 + Fe^{2+} \longrightarrow Fe(III) + \cdot OH + OH^- \qquad (1.10)$$

$$Fe(III) + O_2^{\bullet -} \longrightarrow Fe^{2+} + O_2 \qquad (1.23)$$

$$H_2O_2 + O_2^{\bullet -} \xrightarrow{\text{Fe catalyst}} \cdot OH + OH^- + O_2 \qquad (1.24)$$

Superoxide radical can also act as a weak oxidizing species,[24] oxidizing Fe^{2+} to Fe(III), while HO_2• can oxidize NADH directly.

3. Peroxyl radicals.

O_2 reacts with most carbon-centered radicals at the diffusion controlled limit to form peroxyl radicals (equation 1.17). Peroxyl radicals are less reactive and thus more selective in their reactions than hydroxyl radical, therefore potentially more toxic. Peroxyl radicals can also be formed via oxidation of hydroperoxides by Fe^{3+}: [1]

$$ROOH + Fe(III) \longrightarrow ROO\cdot + Fe^{2+} + H^+ \qquad (1.25)$$

In the laboratory, azo compounds are often employed to generate carbon-centered radicals which are rapidly transformed to peroxyl radicals thermally in the presence of molecular oxygen. Common examples are thermolysis of 2,2'-azo-bis-(2-amidinopropane) dihydrochloride (AAPH) in aqueous solution and azobisisobutyronitrile (AIBN) in nonpolar environments.

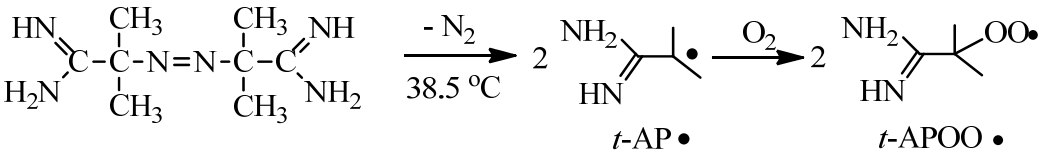

t-APOO generation: Thermolysis of 2,2'-azo-bis-(2-amidinopropane) dihydrochloride

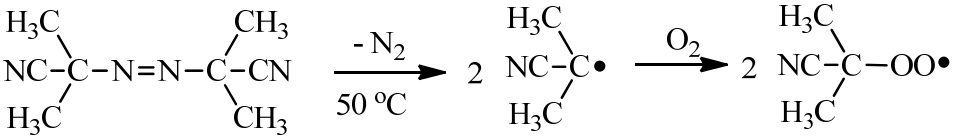

Thermolysis of azobisisobutyronitrile

Scheme 1.1 Generation of Peroxyl Radicals by Thermolysis of azo compounds

Aliphatic peroxyl radicals have relatively high oxidation potential (0.77-1.44V vs. NHE).[25] These peroxyl radicals can oxidize some transition metal ions as well as nitroxide radicals as shown in equation 1.26, where X• stands for nitroxide radicals or transition metals.

$$ROO^{\cdot} + X^{\cdot} \longrightarrow ROO^{-} + X^{+} \qquad (1.26)$$

Peroxyl radicals can also abstract H atoms from other molecules, which is an important step in lipid peroxidation (Scheme 1.2). Because of the electron delocalization, aromatic peroxyl radicals are less oxidizing and less reactive than their aliphatic counterpart.

In biological systems, a free radical initiated chain reaction, lipid peroxidation, is a well known example of how peroxyl radicals can selectively attack biomolecules, leading to cell damage. The initiator, usually •OH, abstracts one active hydrogen atom from the

polyunsaturated fatty acids in the cell membrane, to produce a carbon centered radical. Rapid addition of O_2 to the fatty acid carbon-centered radicals leads to the formation of peroxyl radicals, which will subsequently abstract hydrogen atoms to form new carbon centered radicals, while the initial peroxyl radicals were transformed into lipid peroxide. The same cycle will continue, resulting more peroxide product and new peroxyl radicals. This radical chain reaction will terminate when two radicals (carbon-centered or peroxyl radicals) react with each other to form a non radical product, when the concentration of the free radicals is high enough. Living organisms developed protection mechanisms by utilizing antioxidants and enzymes to eliminate the initiation reaction or to terminate the radical chain, in order to prevent cell damage.

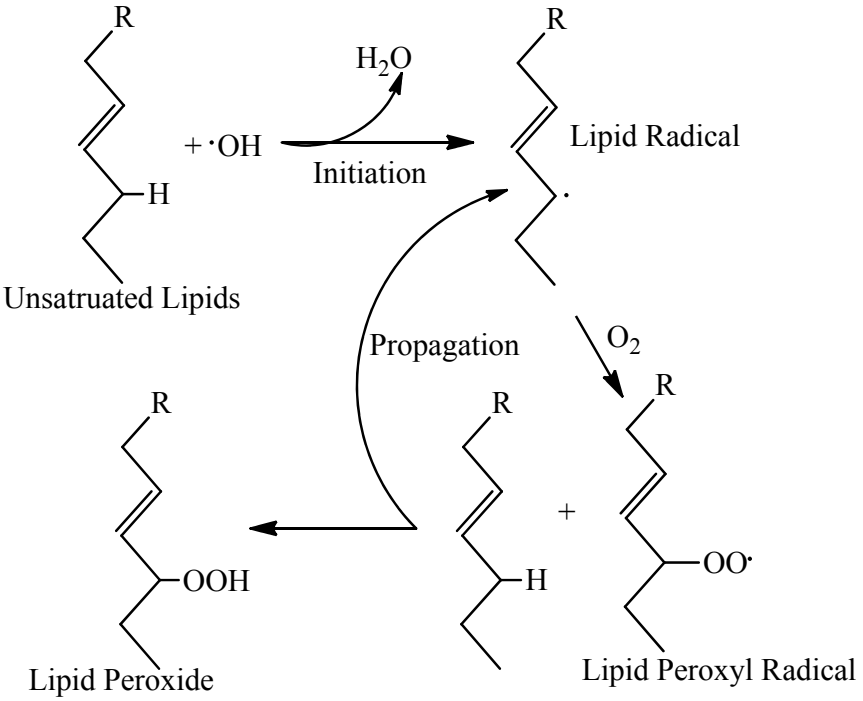

Scheme 1.2 Reaction Mechanism of Lipid Peroxidation

Peroxyl radicals can undergo recombination reaction through Russell Mechanism and generate singlet dioxygen through a tetraoxide intermediate.[26]

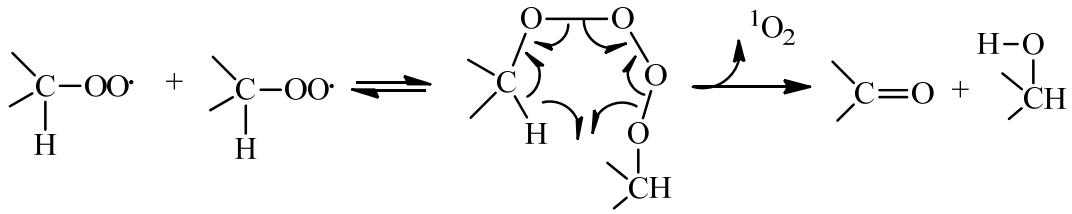

Scheme 1.3 Peroxyl Radical Self Reaction

They can also react with each other to form alkoxyl radical and singlet dioxygen:

$$ROO^{\cdot} + ROO^{\cdot} \longrightarrow 2RO^{\cdot} + {}^1O_2 \quad (1.27)$$

4. Carbonate radical. Carbonate radical can be formed by •OH reaction with carbonate or bicarbonate ions (reactions 1.17 and 1.26).

$$^{\bullet}OH + HCO_3^- \xrightarrow{k = 1 \times 10^7\ M^{-1}s^{-1}} CO_3^{\bullet -} + H_2O \quad (1.28)$$

Since the steady state concentration of bicarbonate ion in vivo is high (25 mM in blood plasm),[1] the generation of carbonate radical could be important despite a relatively low reaction rate constant with •OH radical (10^7-10^8 $M^{-1}s^{-1}$).

Carbonate radical is also a potent oxidizing species (1.78V vs. Ag/AgCl).[1] As a result, it can oxidize ascorbate, methionine and guanine. Carbonate radicals also abstract H atom from amino acids, such as cysteine and tyrosine, and from NAD(P)H.[27] It is however a more selective oxidizing agent than OH radical towards biomolecules.

1.3 Chemistry of some important non radicals

There are some non radical species that are closely related to the radicals discussed above. Understanding the chemistry of these non-radicals is necessary to understand the chemistry of the free radicals. These non-radicals include singlet dioxygen and hydrogen peroxide.

1. Hydrogen peroxide.[1] Hydrogen peroxide is a pale blue liquid under room temperature and readily mixes with water. At low concentrations (< 10 μM), it can increase the proliferation of certain cell types, but it is toxic to cells at high concentration levels (10-100 μM). In biological systems, H_2O_2 can be produced by enzymes, such as xanthine, urate, glucose oxidases. H_2O_2 itself is a relatively weak oxidizing and reducing species. It is not very reactive towards biomolecules such as DNA, lipids and proteins. However, in the presence of transition metal ions such as iron and copper ions, H_2O_2 can be converted to hydroxyl radical through the Fenton or Fenton-like reactions (equations 1.10, 1.23-1.24).

2. Singlet dioxygen.[1] Singlet dioxygen ($^1O_2$) is more reactive than ground state oxygen ($^3O_2$) since the spin restriction that slows the reaction of oxygen with non-radicals is removed. Singlet dioxygen is commonly generated by photosensitization reactions of many organic dye molecules, such as rose Bengal and methylene blue. When excited by light, organic dye molecules can often transfer their excitation energy to molecular oxygen and in this process, convert ground state $^3O_2$ to excited singlet dioxygen $^1O_2$.

Peroxyl radicals can also produce singlet oxygen through Russell mechanism as

discussed above (Scheme 1.3).

In aqueous solution, singlet dioxygen readily relaxes to $^3O_2$ in 2~3 μs. In competition with this relaxation, $^1O_2$ can react with compounds through several mechanisms:[28] 1) reaction with molecules containing carbon-carbon double bonds in ene reactions or Diels-Alder reactions, via hydrogen abstraction pathway.

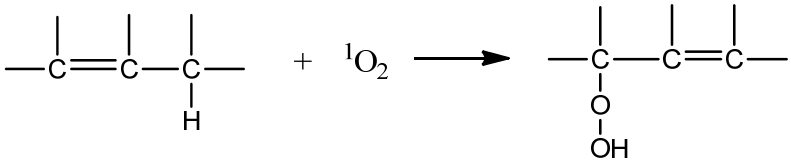

(1.29)

2) Singlet dioxygen reactions can also proceed by electron/H atom transfer from the electron rich compounds, giving neutral radical and HO_2, or a charge-transfer complex.

1.4 Chemistry of stable cyclic nitroxides

Nitroxides are N,N-disubstituted >NO radicals. In the literature they are also termed nitroxyl or aminoxyl radicals. Common types of cyclic nitroxides include piperidinyl (six-membered ring), oxazolidinyl, pyrrolinyl, and pyrrolidinyl (five-membered ring) as shown in Scheme 1.4.

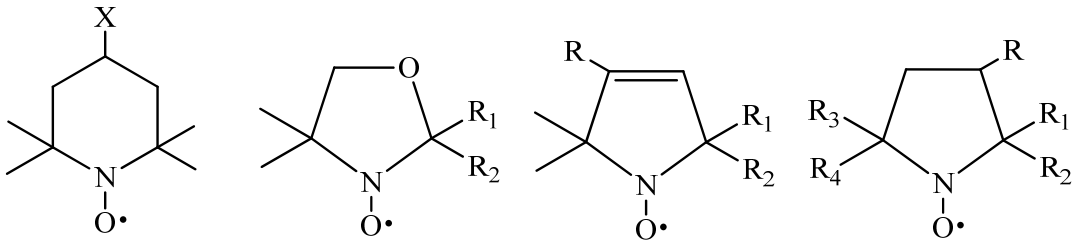

Scheme 1.4 Structures of common types of cyclic nitroxides

Due to the delocalization of the unpaired electron between the oxygen and nitrogen atoms (Scheme 1.5), and the steric effect of the N,N-disubstituted groups, usually methyl groups, nitroxides are relatively stable.[29] However, there are several types of reactions that nitroxides can undergo, often resulting in a loss of their paramagnetism.[30]

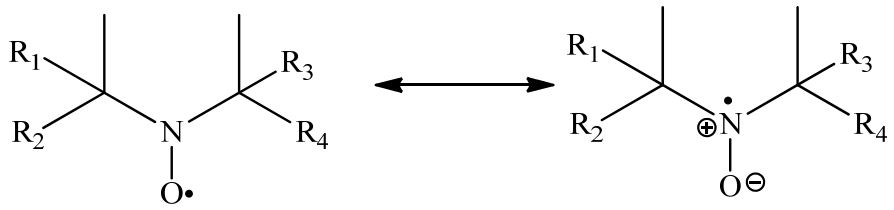

Scheme 1.5 Common structure of nitroxide group and its resonance forms

a. Disproportionation reaction

Although nitroxides with only tertiary carbons adjacent to the nitroxide nitrogen do not undergo this type of reaction, this reaction is important for adducts (nitroxides) of spin traps. The spin adduct of commonly employed spin traps, Phenyl butyl nitrone (PBN), α-(4-pyridyl-1-oxide)-N-tert-butylnitrone (4-POBN) and 5,5-dimethyl-1-pyrroline-N-oxide (DMPO) (structures are shown in Scheme 1.6) all have this potential problem (equation 1.30):

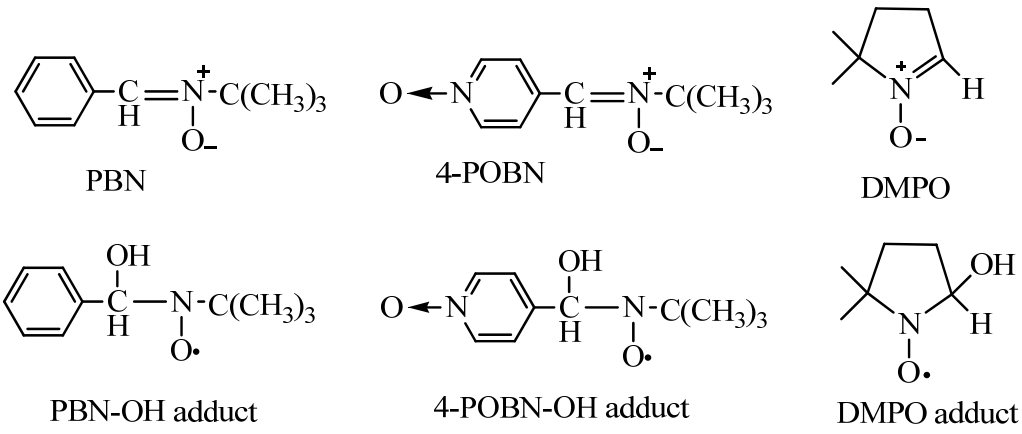

Scheme 1.6 Structures of commonly employed spin traps and their corresponding spin adducts with OH

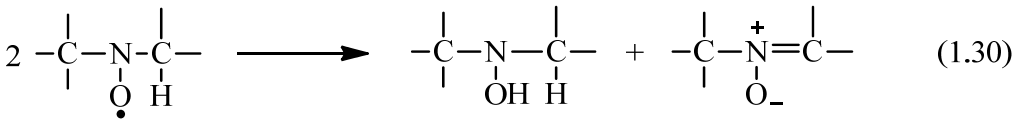

At very low pH, nitroxides with only tertiary carbons adjacent to the nitroxide nitrogen can also undergo a disproportionation reaction (equation 1.31):

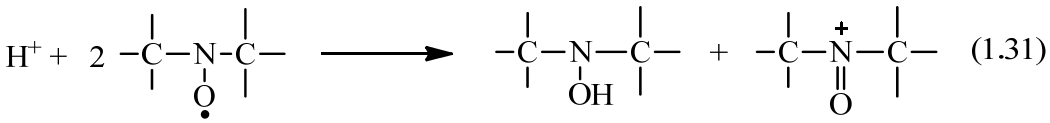

Monoalkyl nitroxides disproportionate easily to yield hydroxylamines and nitroso compounds (equation 1.32):

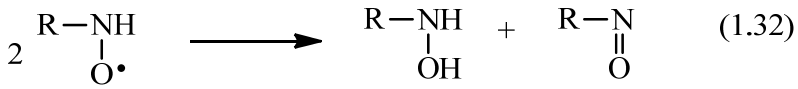

b. Redox reactions[30]

Through one electron redox reactions, nitroxides can be oxidized to their respective oxoammonium cations by strong oxidants and be reduced to their respective hydroxylamines by reductants. The reported redox potential (vs NHE) for

nitroxide/oxoammonium-cation couple varies from 720 to 982 mV, while it ranges from 120 to 760 mV (vs mercury electrode) for nitroxide/hydroxyl-amine redox couple.31 Oxoammonium cations can be reduced directly to their respective hydroxylamines by certain reductants such as NADH, formate and methanol while hydroxylamines can be oxidized to their respective oxoammonium cations, through two-electron transfer reactions (Scheme 1.7).

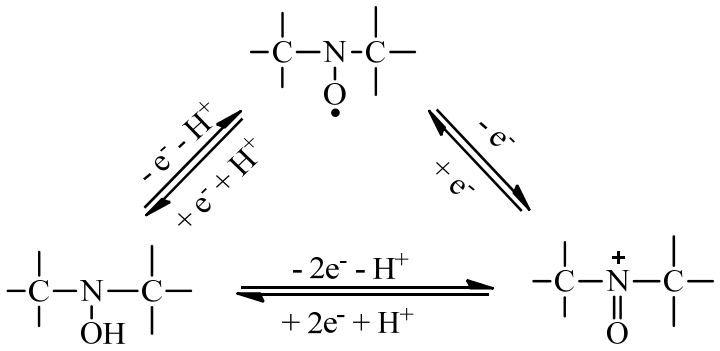

Scheme 1.7 redox reaction of nitroxide radicals

c. Free radical combination reaction

Nitroxides can react with carbon centered radicals at high rate constant (10^8-10^9 $M^{-1}s^{-1}$) to form stable alkoxylamine products (reaction 1.33).

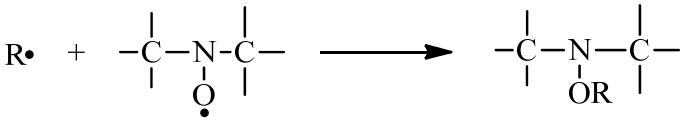

(1.33)

A variety of nitroxides can be synthesized without affecting the unpaired electron. Because of their chemical stability, cell permeability and the sensitivity of their electron paramagnetic resonance spectra to the microenvironment, nitroxides have been employed extensively as spin probes and labels, especially for the study of the dynamics of

membranes and proteins.

Nitroxides have also been used as contrast agents for nuclear magnetic resonance imaging and spectroscopy, due to their ability to alter proton relaxation time. Among the advantages of using nitroxides as contrast agents is their chemical versatility which allows them to be positioned in different locales within the body. One disadvantage of nitroxides as contrast agents is their potential to be reduced to the diamagnetic hydroxylamine by common biological reductants. Because the hydroxylamines can also be reoxidized back to nitroxides, however, the metabolism of nitroxides by cells can be a useful means to study their metabolism in vivo when coupled with in vivo NMR techniques.

Stable nitroxides have also been widely employed as antioxidants against oxidative stress.[32-39] Previous research concerning the mechanisms of antioxidant protection by nitroxides mainly focused on three areas:

a. Removal of superoxide by acting as SOD-mimics;[40-42]

Nitroxides were reported to catalyze the dismutation of superoxide via different reaction routes depending on the ring structure of the nitroxides. For piperidinyl and pyrrolidinyl nitroxides, an oxoammonium cation intermediate (oxidative mode) was proposed to be involved (Scheme 1.9), while nitroxide/hydroxylamine couple (reductive mode) was proposed for oxazolidinyl nitroxides (Scheme 1.9). It was also reported, however, that all nitroxides either do not react or react very slowly with superoxide radical. Therefore nitroxides are inefficient SOD mimics at physiological pH.

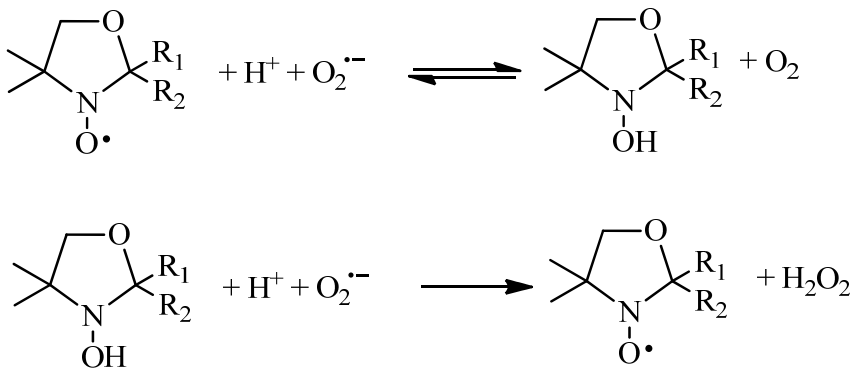

Scheme 1.8 Dismutation of superoxide radical through nitroxide/hydroxylamine

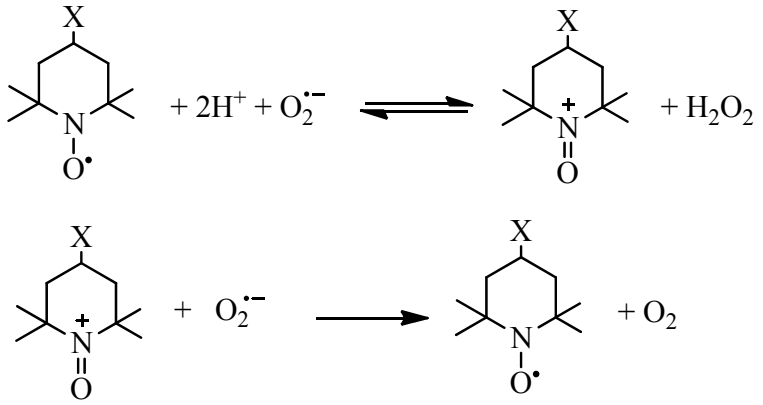

Scheme 1.9 Dismutation of superoxide radical through oxoammonium cation/nitroxide

b. Preventing the formation of hydroxyl radical via the Fenton reaction by removing the reduced transition metal ions (reaction 1.34-1.35):[30]

$$Fe^{2+} + H_2O_2 \longrightarrow Fe^{3+} + HO^{\cdot} + HO^{-} \qquad (1.34)$$

$$Fe^{2+} + RNO^{\cdot} + H^{+} \longrightarrow Fe^{3+} + RNOH \qquad (1.35)$$

c. Reaction with carbon centered radicals:[43-45]

$$RNO^{\cdot} + R^{\cdot} \longrightarrow RNO\text{-}R \qquad (1.36)$$

d. Reaction with secondary radicals such as peroxyl radicals. To date, there is much less

information regarding the reaction mechanisms and there is some controversy surrounding the very few mechanisms that have been proposed.

1.5 Reaction of stable cyclic nitroxides with peroxyl radicals

Current information on the protection mechanism of nitroxides on peroxy radical-induced oxidative degradation is very scarce, although the antioxidant properties were identified almost three decades ago. Early studies mainly focused on the biological aspects of the nitroxide antioxidant protection against peroxyl radical induced oxidative damage, such as peroxidation of linolenic acid, rat liver microsomes, low density lipoproteins, albumin, trout erythrocytes and DNA.[33, 46-49] All of these studies indicated that indolinonic/quinolinic and cyclic piperidine nitroxides are effective antioxidants toward peroxyl radical induced biological damage. However, very few of these studies investigated the possible chemical mechanisms of these reactions and the conclusions are controversial.

Piperidines

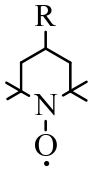

TEMPO: R = H
4-ht: R = OH
4-at: R = NH_2

Pyrrolidines

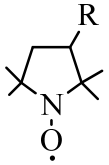

3-ap: R = NH_2
3-amp: R = CH_2NH_2
3-cp: R = $CONH_2$
3-cap: R = COOH

Scheme 1.10 Structures of nitroxide radicals

Damiani et al[50] studied the effect of nitroxide radicals on oxidative DNA damage generated by tert-amidinopropane peroxyl radical (t-APOO•) formed by thermolysis of 2,2'-azobis(2-amidinopropane) dihydrochloride (AAPH) under aerobic conditions. They tested the antioxidant effect of both indolinonic/quinolinic aromatic nitroxides and piperidinyl aliphatic nitroxides (TEMPO and 4-ht) (Scheme 1.10) by gel electrophoresis. All the nitroxide radicals were observed to protect against peroxyl radical attack on plasmid DNA to various degrees depending on the concentrations used. They proposed that the possible protection mechanism of the piperidinyl nitroxides against t-APOO• is due to the scavenging of carbon-centered radicals initially formed upon the AAPH decomposition (Scheme 1.11); the piperidinyl nitroxides were suggested to protect DNA from oxidative damage by reacting with t-AP• not t-APOO•, as shown in Scheme 1.11. Reaction of the aromatic nitroxides was proposed to occur through addition of carbon-centered radicals to the nitroxide moiety as in the piperidinyl nitroxides. Faucitano et al[51] proposed that the indolinonic/quinolinic aromatic nitroxides reacted with peroxyl radicals via the aromatic ring (Scheme 1.12). In both cases, the products of the reactions would be diamagnetic. However, these proposals are speculative as the products of these reactions were never characterized.

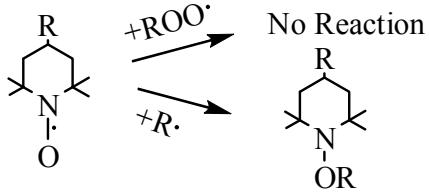

Scheme 1.11 Proposed mechanism for peroxyl radical reaction with piperidinyl nitroxides

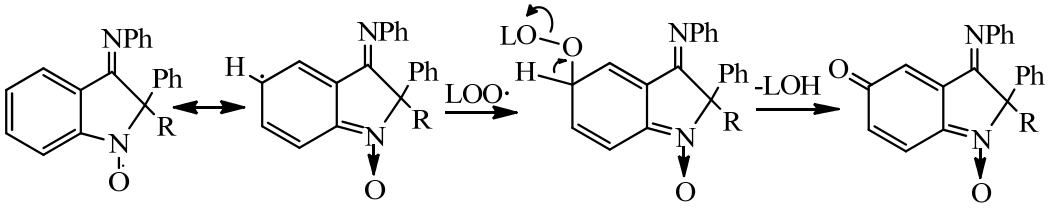

Scheme 1.12 Proposed mechanism for peroxyl radical reaction with aromatic nitroxides

Barton et al[52] studied the reaction of TEMPO with t-butyl peroxide. t-butyl hydroperoxide (TBPH) was employed to generate t-butyl peroxyl radical in the presence of catalytic amount of Fe(III). They proposed a reaction mechanism based on a suggestion by Prof. M.I. McKee of a trioxide intermediate (Scheme 1.13). They found that the formation of dioxygen was proportional to the disappearance of the TBPH with the rate of dioxygen formation decreasing as the t-BuOOH was consumed. Upon re-addition of TBPH to the reaction system, dioxygen formation increased again. They monitored the dioxygen formation from the reaction of TEMPO with t-butyl peroxyl radical over a period of one week with regular addition of TBPH to the original reaction system. Each addition triggered "almost quantitative" dioxygen formation. To further test the role of TEMPO in the reaction they added 2,4,6-tri-t-butyl phenol, a peroxyl radical scanvenger. The formation of dioxygen was inhibited, indicating that TEMPO was involved in the reaction with peroxyl radicals as a catalyst. Based on these observations, Barton et al proposed their reaction mechanism (Scheme 1.14).

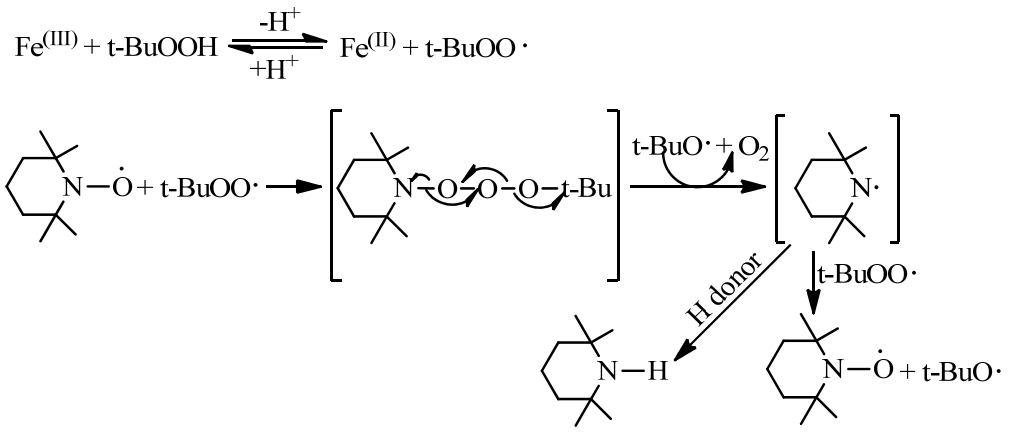

Mechanism A: the McKee Proposal

Scheme 1.13 The McKee Mechanism

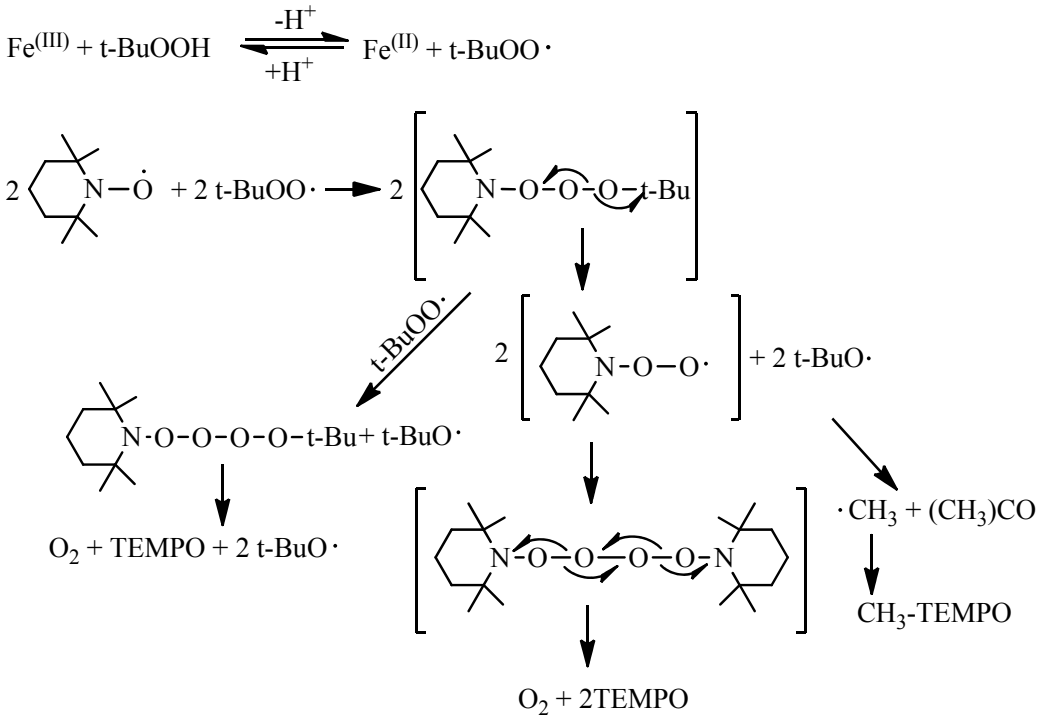

Mechanism B: Barton Proposal

Scheme 1.14 The Barton Mechanism

The McKee mechanism can explain some of the experimental facts, particularly the reaction stoichiometry (2 moles of TBPH consumption for the formation of 1 mole

oxygen). However, this proposed mechanism for the decomposition of the trioxide is very unlikely, since the highly reactive nitrogen radical intermediate is most likely not involved in the reaction as 2,2,6,6-tetramethylpiperidine, as its reduction product, was never detected even at the presence of H donors.

Samuni et al[38] studied the protective effect of three piperidinyl nitroxides (TEMPO, 4-ht and 4-at) on plasmid DNA cleavage upon thermolysis of AAPH under both anoxic and aerobic conditions. Under aerobic experimental conditions, peroxyl radicals are the main damaging species. All three nitroxides, at concentrations as low as 1 μM, effectively protected DNA although the amount of t-APOO• generated was 7-10 times higher than that of the nitroxides. This result suggested that the reaction between piperidinyl nitroxides and peroxyl radicals is not stoichiometric and some of the nitroxides must be regenerated. Nitroxide concentrations continued to decrease during the process of exposure to t-APOO•, indicating that nitroxides were eventually converted to diamagnetic species and depleted. Organic peroxides were reported to be formed and detected by iodometric assay. They presented a reaction mechanism for this reaction involving a trioxide intermediate (Scheme 1.15), same as the McKee mechanism.

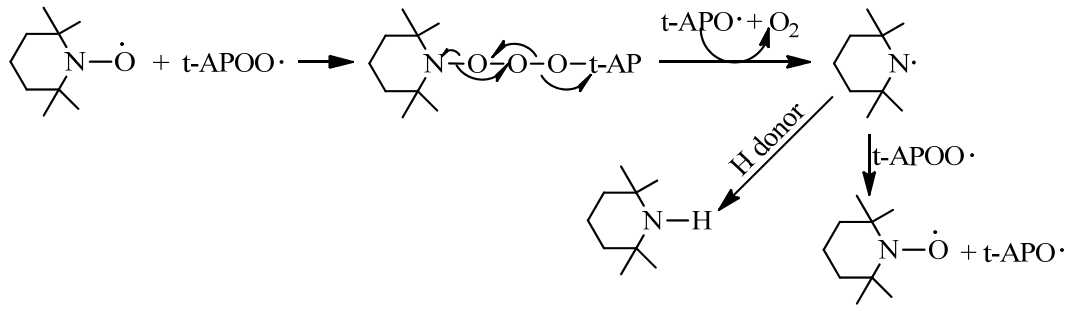

Scheme 1.15 Peroxyl radical- Piperidinyl nitroxide reaction mechanism proposed by Samuni et.al[35]

This conclusion is partially contradictory with that of Barton's work, where they stated that the nitroxides reacted with peroxyl radicals catalytically and was not consumed.

More recent studies suggested that the decomposition of the trioxide intermediate most likely leads to the oxoammonium cation formation, which may undergo further secondary reactions or can be reduced back to original nitroxides, depending on their structures. Goldstein and Samuni[53] studied the kinetics and mechanism of the reaction of alkyl peroxyl radicals with several piperidinyl, pyrrolidinyl and oxazolidinyl nitroxides. They demonstrated that nitroxides reduce peroxyl radicals and form the respective oxoammonium cations. The efficiency as radical scavengers of these nitroxides against the inactivation of glucose oxidase induced by peroxyl radicals was correlated with the kinetics, i.e., the higher the reaction rate constant for reaction with peroxyl radicals, the more efficient the nitroxide as a peroxyl radical scavenger, with piperidinyl > pyrrolidinyl > oxazolidinyl nitroxides. Nitroxides can be regenerated by a two-electron reduction of the oxoammonium cation to the hydroxylamine, followed by the oxidation of the hydroxylamine by peroxyl radicals (Scheme 1.7).

In an earlier study, Goldstein and Samuni[36] proposed a different mechanism for a piperidinyl nitroxide, 4-oxo-TEMPO. Electrochemical oxidation of this nitroxide proceeded to an unstable oxoammonium cation, which decayed to a relatively unreactive species, unlike other oxoammonium cations. HPLC-MS and NMR analysis suggested that this oxoammonium cation undergoes a rapid β-elimination of proton to form a nitroso compound (Scheme 1.16):

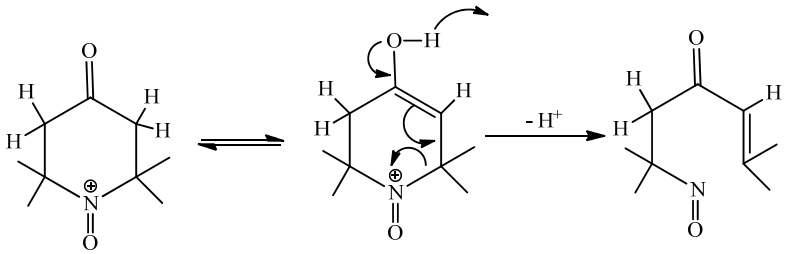

Scheme 1.16 Proposed mechanism for 4-oxo-TEMPO oxoammonium cation decompostion

1.6 Detection of peroxyl radicals

Because peroxyl radicals are not as reactive as and more selective than some primary radicals such as hydroxyl radical, they have the ability to migrate a longer distance before initiating damage, and can thus play a major role in cell damage. These species are primarily responsible for the auto-oxidation of lipids and cell membranes and have also been implicated in oxidative DNA damage, in aging, and in many human chronic diseases. Peroxy radicals can also play important roles in many environmental processes.[54] However, the lack of highly sensitive and selective methods for peroxy radical detection at very low concentrations poses a major hurdle for further understanding of the role of peroxy radicals in these processes.

Direct EPR detection of peroxy radicals in aqueous phase such as biological and environmental systems is generally not possible due to the very low steady state concentration of peroxy radicals in many systems. However, numerous qualitative analyses in some model systems have been reported.[55-58]

More often, indirect detection methods such as EPR spin trapping and radical probes are employed for peroxy radical detection.[59-61] Spin traps (diamagnetic nitrones and nitroso compounds) react with peroxy radicals and convert them into more stable spin adducts (Scheme 1.17).

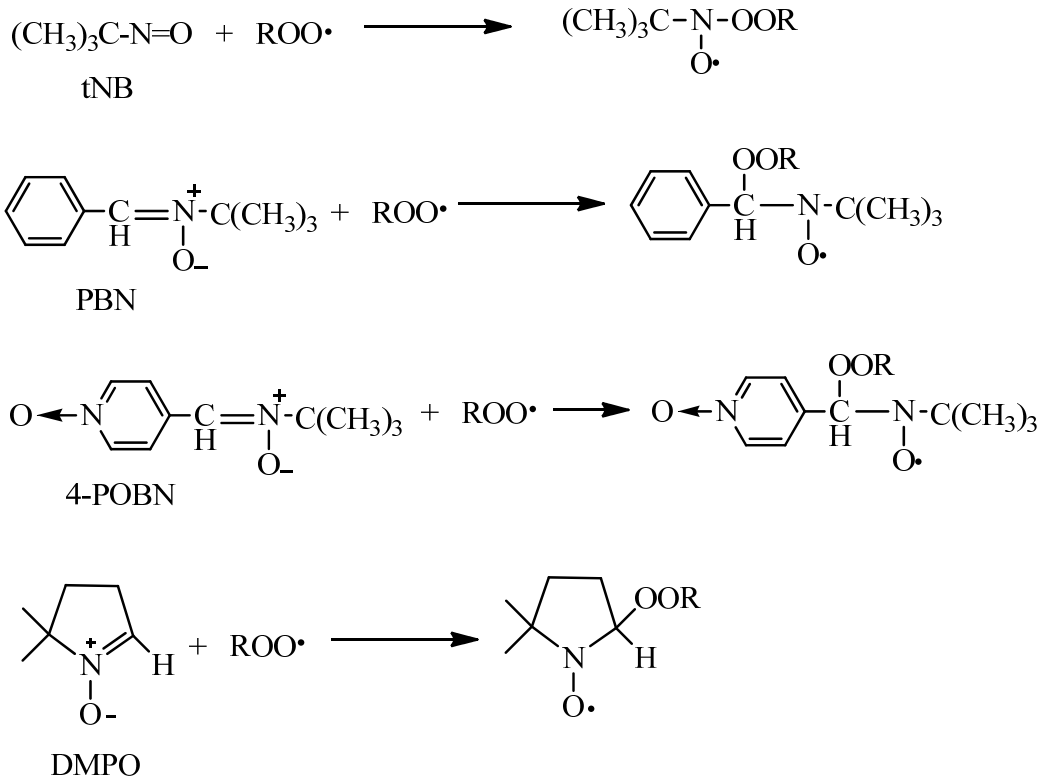

Scheme 1.17 Reactions of peroxyl radicals with common spin traps

In this way, the steady state concentration of the spin adducts can be much higher than the original peroxyl radicals and easier to detect. The pattern and amplitude of the hyperfine splitting of these adducts can often be used to obtain information about the structure of the original radicals. Although spin trapping can be employed to detect the peroxy radicals, it is rather insensitive and subject to certain limitations, including 1) spin adducts instability, [62-63] 2) the need for high concentrations of spin traps due to the small rate constant of the spin trapping reaction[64] and 3) and inability to resolve structurally similar spin adducts. [65] The third drawback can be alleviated to some extent by coupling HPLC with EPR, optical or electrochemical detection. [66-68] However, the instability of spin adduct make this method ineffective in quantifing peroxyl radicals in most cases. Therefore, the results of these detection methods need to be interpreted with extreme caution.

Other detection methods for peroxyl radicals include fluorometric detection employing phycoerythrin, fluorescein, dihydroxynaphthalenes or dipyridamole. [69-73] These methods, which are based on measurement of the fluorescence quenching of these compounds by reacting with peroxy radicals and other ROS, are insensitive and nonspecific toward peroxy radicals and in some cases, the compounds are not stable. Recently, new fluorescence sensors, such as 2',7'-dichlorodihydrofluorescein (DCFH) and dihydrorhodamine 123, 2-[6-(4'-hydroxy)phenoxy-3H-xanthen-3-on-9-yl]benzoic acid (HPF), 2- [6-(4'-amino)phenoxy-3H-xanthen-3-on-9-yl]benzoic acid (APF) and 4[N-methyl-N(4-hydroxyphenyl)amino]-7-nitrobenzofurazan(NBFhd) were reported. [74-75]

These compounds are initially non-fluorescent or very weakly fluorescent, but highly fluorescent upon reaction with ROS. However, HPF and APF can only react with highly reactive ROS such as hydroxyl radical and hypochlorite, but not other ROS (Scheme 1.18):

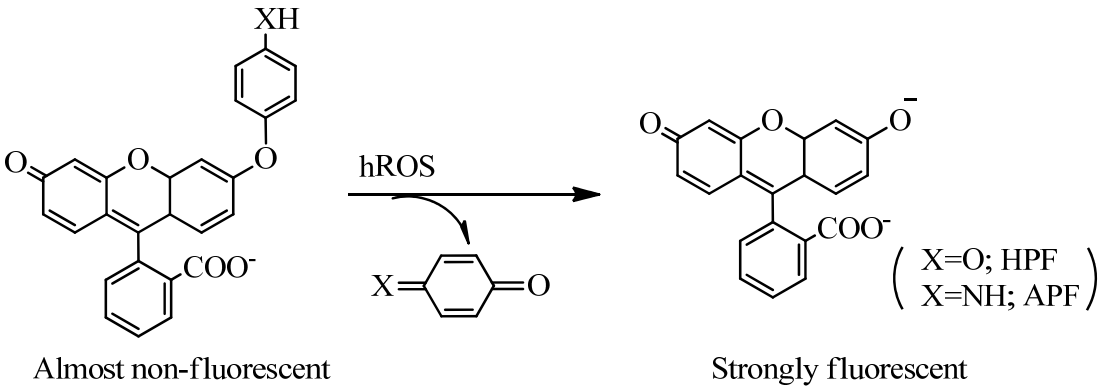

Scheme 1.18 Detection of highly reactive oxygen species by HPF or APF

NBFhd, DCFH and dihydrorhodamine 123 will react non-specifically with almost all the ROS.

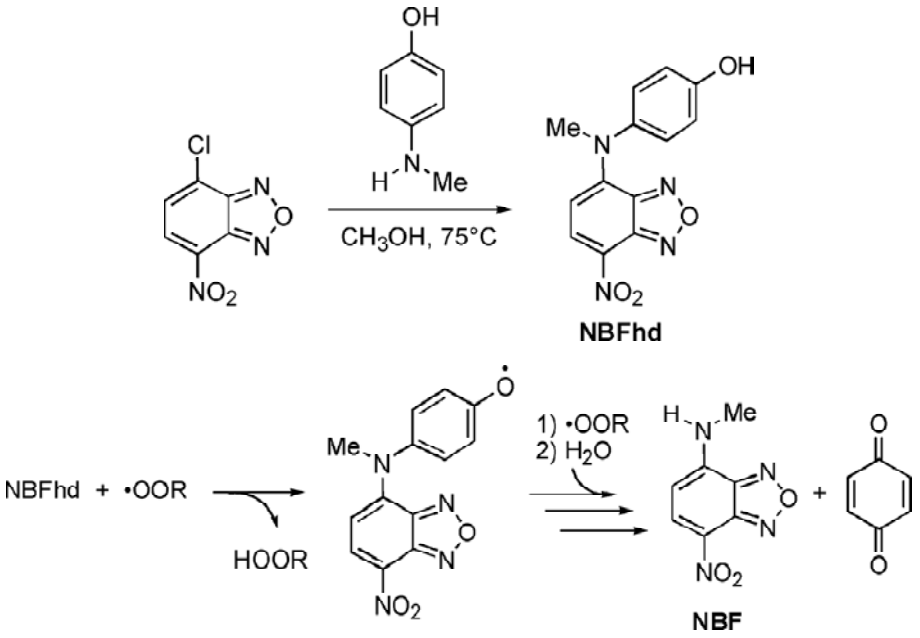

Scheme 1.19 Detection of reactive oxygen species by NBFhd

Although all these fluorescent probes mentioned above are generally more sensitive than the fluorescence quenching methods for ROS detection, they are either unable to detect (APF and HPF) or are nonspecific (NBFhd, DCFH and dihydrorhodamine 123) for peroxy radicals. For example, NBFhd can react with superoxide radicals to form NBF.

In conclusion, most of these methods suffer from one or more problems such as lack of selectivity, low sensitivity, limited stability and most importantly, difficulties in quantification.

Since their initial introduction in the late 1980's and early 1990's,[76-80] the use of pre-fluorescent nitroxide sensors[81] to detect and quantify radical formation has expanded to include a wide range of applications.[82-92] This approach utilizes stable nitroxide radicals as optical switches. By covalently coupling a nitroxide at a short distance from a chromophore, fluorescence emission from the chromophore can be largely quenched.[76,77,93] Upon reaction of the nitroxide moiety with (usually carbon-centered) radicals to form diamagnetic products,[43,94] the intramolecular quenching pathway is eliminated and fluorescence emission is greatly enhanced, thereby allowing radicals to be detected and quantified, either through changes in fluorescence intensity[76,79,80,85,86] or through product analysis by HPLC[87, 95-99] or LC/MS.[100-101] The detection of carbon centered radicals and hydroxyl radical by this approach is shown in Scheme 1.20 and 1.21, respectively:

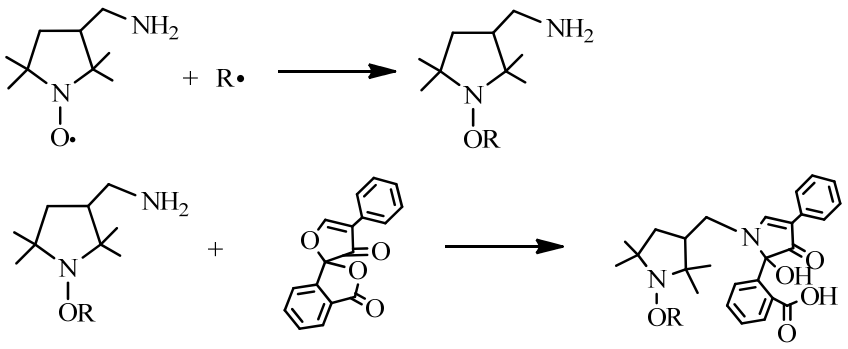

Scheme 1.20 Reaction scheme for detection of carbon centered radicals

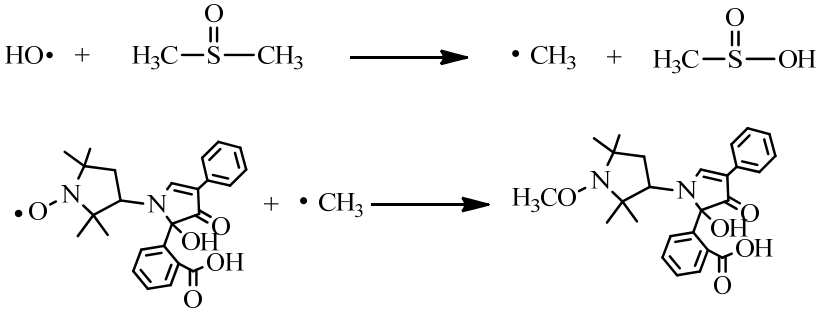

Scheme 1.21 Reaction scheme for detection of hydroxyl radical

Based on this previous work, it appeared feasible to develop a sensitive method for peroxyl radicals detection based on pre-fluorescent nitroxide probe.

Probe Reaction Kinetics

The kinetics for the reaction of the nitroxide probes with carbon centered radicals (as well as peroxyl radicals, see below) can be described by the following series of equations. Carbon centered radicals can react with the probe to form product VI (reaction 1), or react with other compounds (including bimolecular self-reaction) to form other product (reaction 2), as shown in Scheme 1.22. The following equations apply to this reaction system:

$$\frac{d[R\bullet]}{d[t]} = F - k_N[RNO\bullet][R\bullet] - k_{loss}[Reac][R\bullet] \quad (1.37)$$

$$\frac{d[RNO\bullet]}{d[t]} = -k_N[RNO\bullet][R\bullet] \quad (1.38)$$

where F is the generation rate of R•; k_N is the rate constant of nitroxide reaction with R•; k_{loss} is the apparent rate constant for all other reactions with R•.

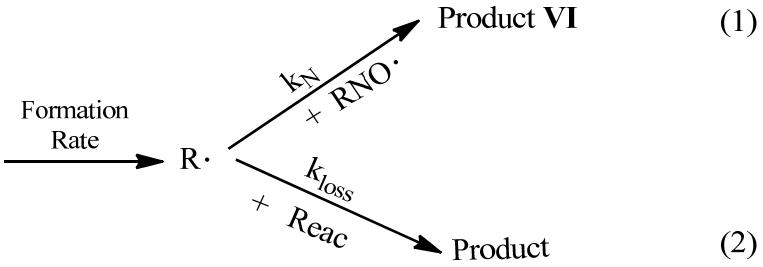

Scheme 1.22 reaction of carbon centered radicals with nitroxides and other reactants

At steady state concentration for the R•, $\frac{d[R\bullet]}{d[t]} = 0$. Rearrange equation 1.37,

$$[R\bullet]_{SS} = \frac{F}{k_N[RNO\bullet] + k_{loss}[Reac]} \quad (1.39)$$

Plug this into equation 1.38:

$$R = -\frac{d[RNO\bullet]}{d[t]} = \frac{Fk_N[RNO\bullet]}{k_N[RNO\bullet] + k_{loss}[Reac]} \quad (1.40)$$

where R is the rate of nitroxide spin loss. When $k_N[RNO\bullet] \gg k_{loss}[Reac]$, equation 1.40 becomes,

$$R = -\frac{d[RNO\bullet]}{d[t]} = F \quad (1.41)$$

And the rate of nitroxide spin loss equals the formation rate of R•, and becomes independent of nitroxide concentration. $[R\bullet]_{SS}$ is unaffected by the nitroxide probe when $k_N[RNO\bullet] \ll k_{loss}[Reac]$. In this situation, the rate for nitroxide spin loss becomes first order with respect to nitroxide concentration:

$$R = -\frac{d[RNO\bullet]}{d[t]} = \frac{Fk_N[RNO\bullet]}{k_{loss}[Reac]} = k_{obs}[RNO\bullet] \qquad (1.42)$$

where $k_{obs} = \frac{Fk_N}{k_{loss}[Reac]}$.

In the presence of >20% O_2, all the R• (>96%) will be quantitatively converted to ROO•,[53] which will undergo reaction with nitroxides. The kinetics of this reaction will be similar to the kinetics discussed above, provided the reaction of this specific nitroxide with peroxyl radicals is stoichiometric.

1.7 Purpose and summary of this research

As mentioned above, despite the fact that peroxyl radicals are very important in cellular regulation processes and their overproduction is involved in a number of human diseases, currently there is no highly sensitive and selective method for peroxyl radical detection, which poses a major hurdle to our understanding the roles of peroxyl radicals in these processes. Stable cyclic nitroxides, which have been studied for their efficient antioxidant and radioprotective effects, are finding more and more applications in biological and medicinal areas due to their cell permeability and low toxicity. However, current information on peroxyl radical reaction with nitroxide radicals is scarce and there has been disagreement on the reaction mechanisms. Therefore, the development of a highly sensitive and selective nitroxide probe for the quantitative determination of peroxyl radicals will aid in our understanding of the role of peroxyl radicals in many processes. Study of the mechanism of the reaction of nitroxide radicals with peroxyl radicals will further aid in our understanding of how nitroxides exert their antioxidant effect and therefore may help in the design of novel and more medicinally useful

nitroxides.

To achieve these goals, the stoichiometry of the reaction of peroxyl radicals with a series of stable cyclic nitroxides, both piperidinyl and pyrrolidinyl nitroxides, was examined, to test whether a nitroxide could be found that reacted stoichiometrically with peroxyl radicals. Most of the nitroxides studied thus far have been found to react with peroxyl radicals reversibly. As discussed above, the respective oxoammonium cations formed are stable enough that they can be reduced back to the nitroxide by other reducing solution constituents. These types of nitroxides could serve as good antioxidants because of their catalytic processing of peroxyl radicals, but cannot be employed as a probe for quantitative analysis.

Provided the nitroxide can react with peroxyl radicals stoichiometrically, a second desirable property is that the nitroxides can be easily coupled to a fluorophore. 4-oxo-TEMPO can react with peroxyl radicals irreversibly based on Samuni's study, making it a potentially suitable probe. However, this nitroxide cannot be easily coupled to a fluorescent chromophore, making it a less desirable candidate.

In this thesis, the reaction stiochiometry of several amino substituted piperidine and pyrrolidine nitroxides with peroxyl radicals was studied. A pre-fluorescent nitroxide probe (3-apf, **I**), synthesized by reaction of 3-amino-2,2,5,5,-tetramethyl-1-pyrrolidinyloxy (3-ap) with fluorescamine, was found to undergo a unique, irreversible reaction with peroxyl radicals to form a more highly fluorescing diamagnetic product , and thus can be employed to detect and quantify peroxyl radicals optically. All other amino-nitroxides

examined were found to undergo a partially reversible reaction and therefore cannot be used as fluorescence probes for quantification.

In Chapter II the stoichiometry of peroxyl radical reaction with 3-apf is first established and is shown to differ from that of other amino-nitroxides. The stability of this probe under various experimental conditions was examined. It was concluded that 3-apf was suitable for thermolysis and gamma radiolysis experiments but was unstable under high intensity polychromatic irradiation. The use of 3-apf to determine the formation rate of peroxyl radicals by thermolysis and radiolysis of simple model systems is shown, with this approach then employed to determine the production of peroxyl radicals in an aqueous dispersion of soybean phosphatidylcholine (PC) liposomes. The selectivity of this probe was demonstrated by the detection of low compositions of peroxyl radicals in the presence of $\bullet NO_2$ and $CO_3^{\bullet-}$ radicals, which can also react with the probe to generate the same product, by means of simply changing the $[O_2]$/[3-apf] ratio. The product of 3-apf reaction with peroxyl radicals was purified by HPLC and the structure was analyzed by ESI-MS, FT-ICR MS and NMR in an attempt to elucidate the possible reaction mechanism.

In Chapter III the reaction of 3-ap and peroxyl radicals was studied. The stoichiometry was established and its stability under different experimental conditions was examined. 3-ap was first employed in simple model systems to detect the generation of peroxyl radicals. It was then used to determine peroxyl radicals generated photochemically from tap water following derivatization of its product with fluorescamine and subsequent

chromatographic analysis. Structure of the product of 3-ap reaction with peroxyl radicals was also analyzed by mass spectrometry. In chapter IV, the conclusions of this research are presented and future work is suggested.

Chapter II Trace Determination of Peroxyl Radicals in Complex Matrices Employing Fluorescamine Derivatized 3-ap

Abstract

Fluorescamine derivatized 3-amino-2,2,5,5,-tetramethyl-1-pyrrolidinyloxy (3-apf, **I**) is shown to undergo an irreversible reaction with peroxyl radicals and other radical oxidants to generate a more highly fluorescent diamagnetic product (**II**), and thus can be used as a highly sensitive and versatile probe to determine oxidant production optically, either by monitoring the changes in fluorescence intensity, by HPLC analysis with fluorescence detection, or by a combination of both approaches. By changing the [O2]/[**I**] ratio, we show that peroxyl radicals can be detected and quantified preferentially in the presence of other radical oxidants. Employing HPLC analysis, the detection limit of **II** at a S/N of two is ~3 nM for a 125 μL injection. With direct fluorometric measurement, the detection limit is 0.35 μM at a S/N of two. The method was employed for the detection of peroxyl radicals generated thermally in soybean phosphatidylcholine liposomes as a demonstration of a preliminary application.

2.1 Introduction

Peroxyl radicals, formed by the rapid addition of molecular oxygen to carbon-centered radicals, play an important role in many pathological processes, chronic diseases and aging due to their involvement in the oxidative degradation of DNA and proteins, and in the

autoxidation of lipids within cell membranes.[9-20] These species are also key intermediates in thermal and photochemical degradation of both natural and man-made materials.[54]

Although a variety of approaches have been employed to detect peroxyl radicals, including spin trapping with electron paramagnetic resonance (EPR) detection[61] and fluorescence sensors,[69,72,75] most of these methods suffer from one or more problems such as lack of selectivity, low sensitivity, limited stability and most importantly, difficulties in quantification, as discussed in chapter I.

Here we demonstrate that the pre-fluorescent nitroxide probe, **I** (Scheme 2.1), synthesized by reaction of 3-amino-2,2,5,5,-tetramethyl-1-pyrrolidinyloxy (3-ap) with fluorescamine,[95-96] undergoes a unique, irreversible reaction with peroxyl radicals to form a more highly fluorescing diamagnetic product (**II**), and thus can be employed to detect and quantify peroxyl radicals optically. Although other one-electron (radical) oxidants such as $\bullet NO_2$ and $CO_3^{\bullet-}$ are also shown to react with **I** to form **II**, we demonstrate that peroxyl radicals can be preferentially detected in their presence by changing the $[O_2]/[\mathbf{I}]$ ratio (Scheme 2.1).

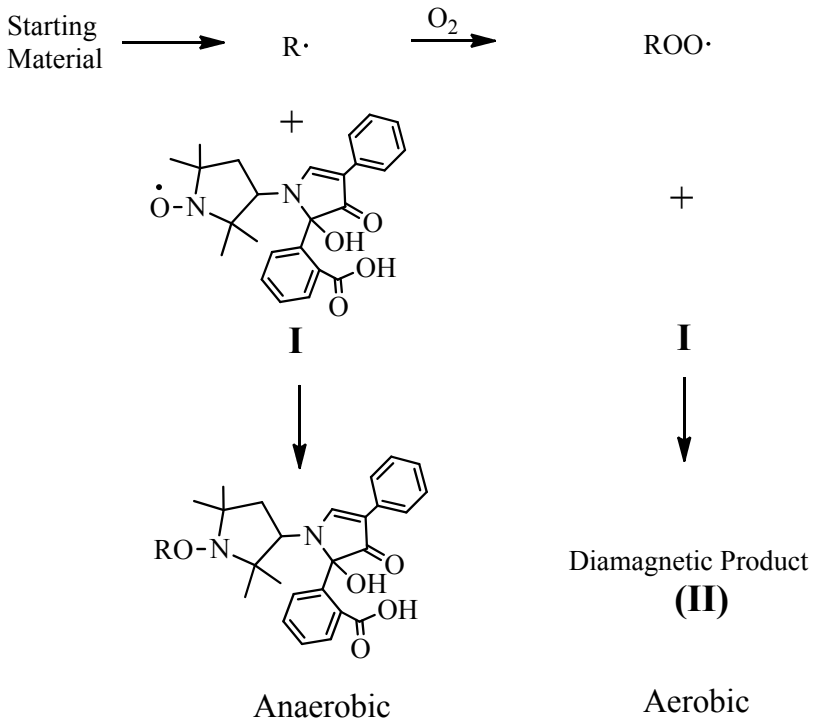

Scheme 2.1 Reaction of **I** with carbon-centered radicals to form the alkoxylamine product under anaerobic conditions and with peroxyl radicals to form **II** under aerobic conditions.

In this chapter, the stoichiometry of peroxyl radical reaction with **I** is first established and is shown to differ from that of other fluorescamine derivatized amino-nitroxides. The use of **I** to determine the formation rate of peroxyl radicals by thermolysis and radiolysis of simple model systems is shown, with this approach then employed to determine the production of peroxyl radicals in an aqueous dispersion of soybean phosphatidylcholine (PC) liposomes, which is commonly used as a model for cell membranes.

2.2 Materials and Methods

2.2.1 Chemicals

Nitroxides (3-ap, 3-aminomethyl-2,2,5,5-tetramethyl-1-pyrrolydinyloxy (3-amp), 3-carbamoyl-2,2,5,5-tetramethyl-1-pyrrolidineoxy (3-cp) and 4-amino-2,2,6,6-tetramethylpiperidinyloxy (4-at)) and fluorescamine were purchased from Acros and Sigma Aldrich, respectively. 2,2'-Azo-bis-(2-amidinopropane) dihydrochloride (AAPH) and azobisisobutyronitrile (AIBN) were purchased from Cyman Chemical Co. Sodium phosphate (99.999%), sodium hydroxide were obtained from Aldrich. Sodium carbonate and sodium nitrite (99.99+%) was purchased from Sigma Aldrich. DMSO, HPLC grade methanol, acetonitrile and glacial acetic acid were all purchased from Fisher. Acetone was obtained from Sigma Aldrich. Refined lecithin was purchased from Alfa Aesar. Nitrogen, air, oxygen and nitrous oxide were all from Airgas. All chemicals were used without further purification. Pure water for all experiments was obtained from a Millipore MilliQ system.

2.2.2 Thermolysis Thermolysis of AAPH was carried out in a 4 mL quartz cuvette in pH 7.4, 50 mM sodium phosphate buffer in a thermostated water bath at 38.5 ± 0.5 °C. The stock AAPH solution (80 mM) was prepared daily and stored in an ice bath prior to thermolysis. Reactions were initiated by immersion of the reaction vessel in the water bath. Reactions were terminated by placing aliquots of the reaction mixture in a -20°C freezer for minimally 10 min. For anaerobic experiments, samples were purged for 20 min with N_2, with the headspace of the cuvette continuously purged with N_2 during thermolysis. The

liposome preparation procedure has been reported previously. Briefly, 1 mg of AIBN and 375 mg of lecithin was dissolved in 5 ml chloroform, with the solvent then evaporated to produce a thin film. **I (**28.4 μM) dissolved in 5 mL of 0.1 M NaCl solution was added to obtain a milky liposome suspension. This suspension was promptly placed into 50±1˚C water bath under an atmospheric of oxygen to initiate the reaction. The reaction was terminated in the same way as in AAPH experiments. The suspensions were filtered through 0.2 μm membrane before injection into HPLC column.

Scheme 2.2 below showed the thermolysis of 2,2'-Azo-bis-(2-amidinopropane) dihydrochloride (AAPH) and azobisisobutyronitrile (AIBN).

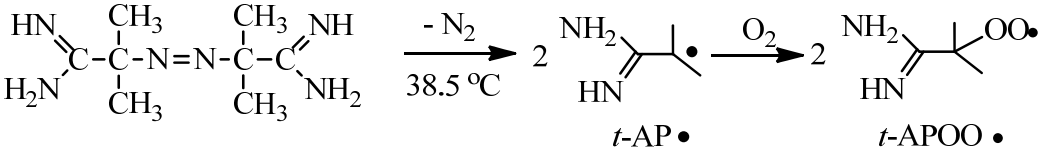

t-APOO generation: Thermolysis of 2,2'-azo-bis-(2-amidinopropane) dihydrochloride

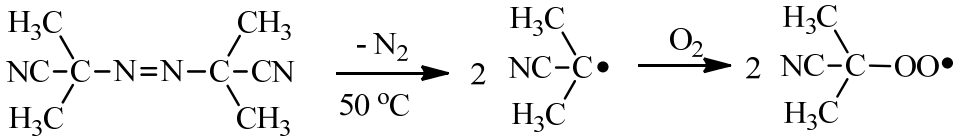

Thermolysis of azobisisobutyronitrile

Scheme 2.2 Radical generation by thermolysis

AAPH is a water-soluble azo compound which is used extensively as a clean source of free radicals and as an initiator of free radical chain reactions. Decomposition of AAPH produces molecular nitrogen and two identical carbon radicals. The carbon radicals may

combine with other radicals to produce stable products or react with molecular oxygen to give peroxyl radicals. The half-life of AAPH is about 175 hours (37°C at neutral pH), making the rate of free radical generation essentially constant during the first several hours in solution at a constant temperature. AIBN is an oil-soluble compound that is often used as free radical initiator in polymerization reactions and in lipid peroxidation studies. Thermal decomposition of AIBN generates nitrogen gas and two identical 2-cyanoprop-2-yl radicals, which will form peroxyl radicals under aerobic conditions.

2.2.3 Steady State Radiolysis Steady state radiolysis was performed using a ^{60}Co source at room temperature. The dose rate was determined in each experiment using a Fricke dosimeter. 20 mM DMSO in 10 mM pH 7.4 phosphate buffer was saturated either with N_2O alone (to generate carbon centered radical) or with 80% N_2O/ 20% O_2 (to generate peroxyl radical) in a Wheaton 5 ml serum vial. The vials were immediately sealed (while still purging) with a Wheaton rubber plug stoppers, which were then fastened by aluminum crimping tool. $CO_3^{\bullet-}$ and $\bullet NO_2$ were produced by gamma irradiation of N_2O saturated, 100 mM Na_2CO_3 solution or 10 mM $NaNO_2$ solution in 5 mM phosphate buffer (pH 7.4), respectively. Superoxide radical was generated by radiolysis of 10 mM formate in the presence of 50 μM DTPA.

Gamma irradiation of water produces mostly OH radical, hydrated electron and H_3O^+ (reaction 2.1). In the presence of N_2O, hydrated electron is converted to OH radical (reaction 2.2). OH radical will then react with DMSO to generate methyl radical, which can further react with O_2 to produce methyl peroxyl radical (reactions 3 and 4). Under 80%

N_2O/20% O_2 and 20 mM DMSO at neutral pH, about 91% of all the radicals formed are converted to ROO radicals. Radiolysis of N_2O saturated Na_2CO_3 solution produces reactions 2.1-2.1 and 2.5 to generate $CO_3^{\bullet-}$ radical. Similarly, radiolysis of N_2O saturated $NaNO_2$ solution will produce $\bullet NO_2$ via reactions 2.1-2.2 and 2.4. Radiolysis of O_2-saturated sodium formate solution is a clean source of superoxide radical. The e_{aq}^- generated in reaction 2.1 can react with O_2 directly to produce superoxide radical (reaction 2.7), while hydrogen atom abstracting from formate by OH produces $CO_2^{\bullet-}$ (reaction 2.8), which subsequently reduces O_2 to superoxide radical (reaction 2.9). This set of reactions converts almost all of the primary radicals to superoxide at neutral pH.

$$H_2O \longrightarrow \bullet OH + e_{aq}^- + H_3O^+ + \bullet H + OH^- + H_2 + H_2O_2 \quad (2.1)$$

$$e_{aq}^- + N_2O + H_2O \xrightarrow{k_2 = 9.1 \times 10^9\ M^{-1}s^{-1}} \bullet OH + OH^- + N_2 \quad (2.2)$$

$$\bullet OH + \begin{matrix} CH_3 \\ CH_3 \end{matrix}\!\!>\!S{=}O \xrightarrow{k_3 = 6.6 \times 10^9\ M^{-1}s^{-1}} \bullet CH_3 + H_3C{-}\overset{\displaystyle O}{\overset{\|}{S}}{-}OH \quad (2.3)$$

$$\bullet OH + NO_2^- \xrightarrow{k_4 = 6.0 \times 10^9\ M^{-1}s^{-1}} \bullet NO_2 + OH^- \quad (2.4)$$

$$\bullet OH + CO_3^{2-} \xrightarrow{k_5 = 3.9 \times 10^8\ M^{-1}s^{-1}} CO_3^{\bullet-} + OH^- \quad (2.5)$$

$$\bullet CH_3 + O_2 \xrightarrow{k_6 = 1.6 \times 10^9\ M^{-1}s^{-1}} CH_3OO\bullet \quad (2.6)$$

$$e_{aq}^- + O_2 \longrightarrow O_2^{\bullet-} \quad (2.7)$$

$$\bullet OH + HCOO^- \longrightarrow CO_2^{\bullet-} + H_2O \quad (2.8)$$

$$CO_2^{\bullet-} + O_2 \longrightarrow CO_2 + O_2^{\bullet-} \quad (2.9)$$

2.2.4 Photolysis For the polychromatic irradiations, samples were placed in a 1-cm cuvette and irradiated with a 300 W xenon lamp. The actinic light was first filtered through 22 cm Milli-Q water and then through a 275 nm long pass filter to provide a light intensity of 150 mW/cm^2. For the monochromatic irradiation experiments, a 1000 W xenon arc lamp was employed as light source. A Spectral Energy GM252 monochrometer was used to select the irradiation wavelength with a bandpass set at 10 nm. The irradiation intensity was determined with an IL 1700 radiometer. Samples were purged with N_2 or oxygen for 10 min before irradiation while the headspace of the cuvette was continuously flushed during irradiation.

2.2.5 HPLC The reversed-phase HPLC system is consisted of a Gilson Model 811B dynamic mixer, an Eldex Model B-100S single piston pump, a 0-5000 psi pressure gauge, a Valco Model C10W injection valve. A 4 μm reversed phase C18 packing Nova-Pack column in a RCM 8×10 cm Waters radial compression module was employed for separation. The column temperature was maintained at 29 ^{0}C by a Buchi B-481 thermostat water bath. In most cases, the mobile phase was 65% sodium acetate buffer (50 mM, pH 4.0) and 35% methanol (v/v), with a flow rate of 1.0 ml/min. A Perkin Elmer 785A UV-Vis detector set at 390nm was employed. The fluorescence detector was a Hitachi Model L4870 set at 390 nm (excitation) and 490 nm (emission). A 125 μL sample loop was employed. OMS Tech Elab software was used for data acquisition and post run processing.

2.2.6 UV/Vis Spectrophotometer A Hewlet-Packard 8452A diode array spectrophotometer was employed for all optical absorption measurements. All measurements were

performed at room temperature except the AAPH thermolysis experiment.

2.2.7 Fluorometer Emission spectra were collected with an Aminco AB2 spectrofluorometer. Wavelengths were set at 390 nm (excitation) and 400-700 nm (emission) with 4 nm bandpasses on both excitation and emission monochromators. All the spectra were recorded at room temperature except the AAPH experiments. Thermo Fisher AB2 software was used to acquire and process all the spectra. Background subtraction and instrument correction were done before peak area integration in quantitative experiments.

2.2.8 Electron Paramagnetic Resonance A Bruker ESP300E EPR spectrometer was used to follow the nitroxide spin loss. Samples were drawn into 50 μL capillary tubes, sealed top and bottom with Critoseal, and placed within standard 3 mm ID quartz EPR tubes. Standard instrument settings were frequency 9.8 GHz; microwave power 9.4 mW; modulation amplitude 1.0 G. Spin levels were determined from areas obtained by double integration of the EPR spectra, as compared with known concentrations of 3-cp.

2.2.9 Cyclic Voltammetry Cyclic voltammetry of the nitroxides was performed using a homemade 3 electrode cell on a CHI660A workstation. Scan range was 0-1.0 volts vs Ag/AgCl reference electrode and scan rate was 100 mV/s. Both working and counter electrodes were platinum wire. Nitroxides were dissolved in pH 7.4, 50 mM sodium phosphate buffer saturated with K_2SO_4.

2.2.10 Synthesis and Purification of 3-apf and product II 100 mg of fluorescamine was dissolved into 3 mL of acetonitrile. 55 mg of 3-ap was dissolved into 3 mL of acetonitrile and was added dropwise to the fluorescamine solution with constant stirring.

The total volume of the completed reaction mixture was reduced to 0.5 mL by flushing with dry nitrogen. A bright yellow precipitate was produced after the reaction mixture was stored in -20°C overnight. The supernatant was carefully removed. The precipitate was rinsed 3 times with ethyl ether and dried under dry nitrogen gas. The final product was sealed and stored at -20°C until use. The purity of the product was analyzed by HPLC with UV detector set at 390 nm. > 95% purity was normally obtained using this synthesis method. The structure of this product was confirmed by ESI-TOF mass spectrometry (Figure 2.1).

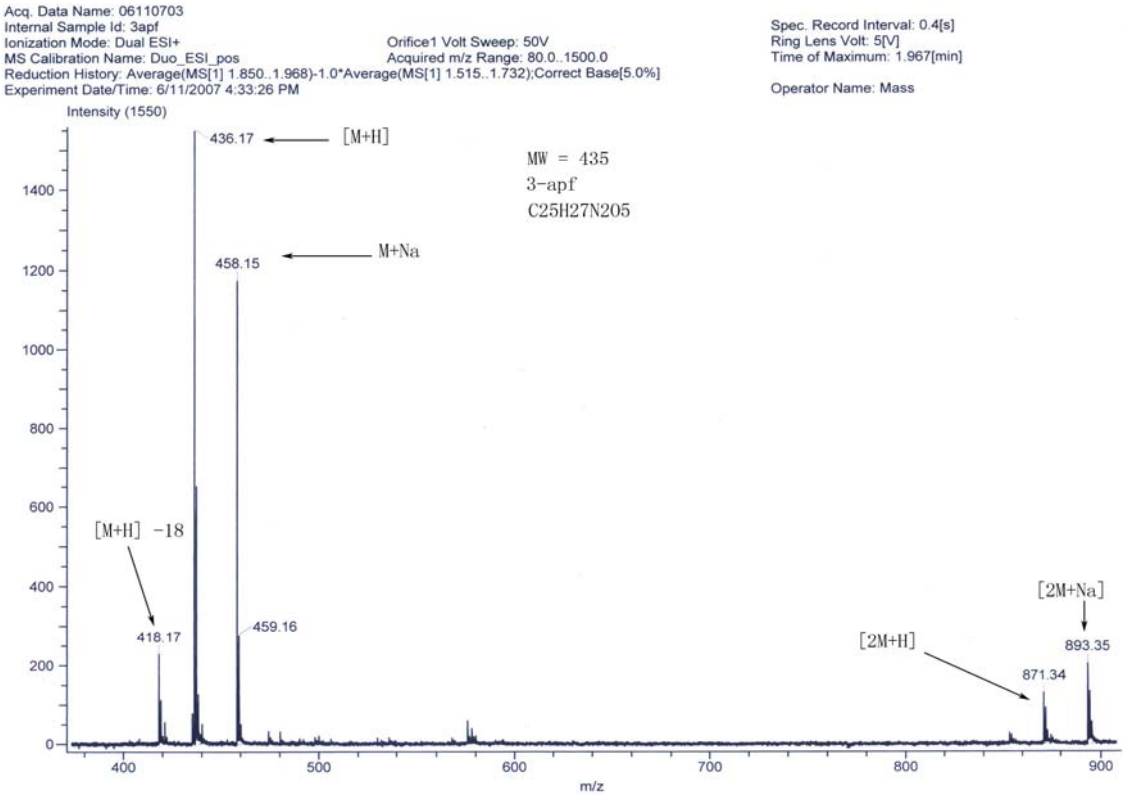

Figure 2.1. AccuTOF-CS ESI-TOF spectrum of 3-apf (**I**). Needle voltage 2kV, orifice 1 voltage 15V, orifice 2 voltage 7V.

Bulk electrolysis of ~2 mM 3-ap, 3-amp and 4-at were performed with a 3-electrode system on a BAS CV-50W voltammetric analyzer in neutral pH buffer saturated with K_2SO_4. The voltage was 750 mV vs. Ag/AgCl and the electrolysis time was 90 min. A 10 mM fluorescamine solution in acetonitrile was added to the reaction mixture in a 1 ml centrifuge tube and vortexed for 1 min at room temperature. The pH of the solution was adjusted to 8.1 and fluorescamine was added in 5 to 10-fold molar excess relative to the product. **II** was then separated and purified by HPLC, followed by extraction with chloroform. **II** was dried under N_2 flow and stored in the freezer at -20°C until use.

Reaction of the 3-ap oxidation product with benzoyl chloride was carried out in aqueous solution. Briefly, 18 mg of 3-ap was oxidized either electrochemically or by t-APOO radical in 10 ml aqueous solution in a 25 mL conical flask. 800 mg of sodium bicarbonate was added while stirring. 24 mg of benzoyl chloride was then added into the solution and the mixture was stirred for 20 min. 20 ml of chloroform was used to extract the product. The solvent was evaporated and the the dry product was redissoved in 3 mL 50%/50% by volume methanol/water. The product was purified by RP HPLC (mobile phase: 75% H_2O/25% methanol), extracted into chloroform and dried under N_2. The dry product was stored at -20 °C until further use.

2.2.11 Quantum Yield Measurement The AB2 spectrofluorometer was used for fluorescence quantum yield measurements. Quinine sulfate solutions at concentrations of 0.1, 0.25, 0.5, 0.75, 1 ppm in 0.1 N sulfuric acid were used as a reference. The absorption of the quinine sulfate solutions at 350 nm were acquired on the HP 8452A spectrophotometer.

Fluorescence spectra were recorded on the AB2 spectrofluorometer with excitation wavelength set at 350 nm and emission wavelengths over 360-800 nm. Absorption of product **II** solutions was taken at 370 nm. Fluorescence intensities were measured with excitation wavelength set at 370 nm and emission wavelength from 380-800 nm. The quantum yield of the product in different solvents was calculated using the equation below (equation 2.10):

$$\varphi_x = \varphi_{qs}(Slope_x/slope_{qs}) \qquad (2.10)$$

where φ_x is quantum yield of **II**, φ_{qs} is quantum yield of quinine sulfate solution; $slope_x$ was calculated from the standard curve of integrated fluorescence peak areas versus absorbance for **II**, and $slope_{qs}$ was calculated from the standard curve of integrated fluorescence peak areas versus absorbance for quinine sulfate solutions.

2.2.12 Product Analysis by NMR and Mass Spectrometry 1H, 13C NMR and COSY, HMBC, HSQC, NOESY and H2BC were performed on Bruker 500 and 600 MHz spectrometers located at the NMR facility at the University of Maryland. Samples were prepared in deuterated chloroform at room temperature. High resolution mass spectra were taken on a linear quadrupole-ion trap (LTQ) Fourier-transform ion cyclotron resonance (FT-ICR) mass spectrometer (LTQ FT Ultra, Thermo Scientific) at the Woods Hole Oceanographic Institution. Data were collected as processed mass spectra with associated

peak lists (XCalibur, version 2.0, Thermo Fisher Scientific). The instrument was externally calibrated using a standard solution from Thermo Fisher Scientific, and the resulting mass accuracy was < 2 ppm. Conventional ESI was employed for ionization process. The ESI spray voltage was 4.3 kV for positive ion mode and 4.0 kV for negative ion mode. Capillary temperature was 250˚C. A JEOL AccuTOF-CS ESI-TOF mass spectrometer coupled with an Agilent 1100 HPLC module at the University of Maryland was also employed for part of the product analysis. Mobile phase for the HPLC was 50/50 v/v ACN/water with a flow rate of 100 μL/min. The accurate mass data were determined by single ion mass drift correction of an internal standard compound.

2.2.13 Tests for the reaction of I with other radical and oxidants. Under neutral pH conditions, 15 μM **I** was exposed to 8 μM/min superoxide generated by steady state radiolysis of 10 mM formate in the presence of 50 μM DTPA. We further tested the effect of superoxide radical on **I** in a xathine/xanthine oxidase system. Xathine (400 μM) and xathine oxidase (9 mg/ml) in the presence of 50 μM DTPA was employed to generate a superoxide flux of 4.5 μM/min. HPLC with UV/Vis detection and UV/Vis spectroscopy were employed to follow the concentration of **I** during the process. The reactivity of **I** towards singlet dioxygen at neutral pH was tested by irradiating a 10 μM Rose Bengal solution in the presence of 11.4 μM of the nitroxide. The solution was placed 20 cm from a lab fluorescent light and aliquots of the solution were subjected to HPLC and ERP analysis. $CO_3^{\bullet-}$ and $\bullet NO_2$ were produced by gamma irradiation of N_2O saturated, 100 mM Na_2CO_3 solution or 10 mM $NaNO_2$ solution in 5 mM phosphate buffer (pH 7.4),

respectively. The product was analyzed by HPLC with fluorescence detection and by mass spectrometry.

2.3 Results

2.3.1 Reaction Stoichiometry and Kinetics

Alkyl radicals (t-AP•) were produced by thermolysis of AAPH under anaerobic conditions (Scheme 2.2). Under aerobic conditions, these alkyl radicals were converted quantitatively to peroxyl radicals (t-APOO•; ~95%), owing to the high $[O_2]/[\mathbf{I}]$ ratios employed (varying from ~5 to 20), as well as to the higher reaction rates of t-AP• with O_2 (~$2\text{-}4\times10^9$ $M^{-1}s^{-1}$) [102] as compared with typical nitroxides (~$1\text{-}8\times10^8$ $M^{-1}s^{-1}$).[43,94] EPR was then used to follow the spin loss of **I** under anaerobic and aerobic conditions to compare the reactivity of **I** with t-AP• and t-APOO•, respectively (Scheme 2.1; a representative example of EPR spectra is provided in Figure 2.2).

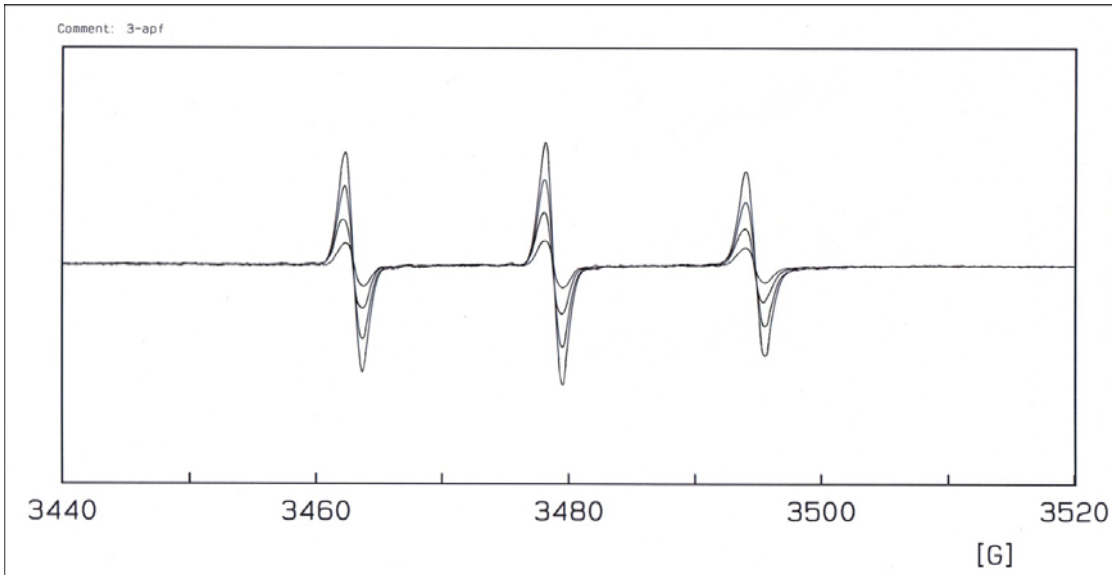

Figure 2.2 EPR spectrum showing the decrease of I when reacted with CH3OO• produced by steady state radiolysis of 10 mM, pH 7.4 phosphate buffer saturated with 80% N2O/ 20% O2 in the presence of DMSO. [I] = 48.3 μM, [DMSO] = 20 mM. Dose rate was 5 Gy/min. Irradiation time from higher peak to lower peak: 0, 5.7, 11.5, 17.2 min. Standard instrument settings were frequency 9.8 GHz; microwave power 9.4 mW; modulation amplitude 1.0 G. Spin levels were determined from areas obtained by double integration of the EPR spectra, as compared with these obtained from known concentration of 3-cp.

Identical rates of spin loss were observed for **I** under N_2 and air during the thermolysis of AAPH (Figure 2.3A), demonstrating that t-APOO• reacted with **I** to the same extent as t-AP•. Further, the rates were independent of [**I**], indicating that both t-AP• (under N_2) and t-APOO• (under air) were reacting quantitatively with **I**. Identical rates of loss were also observed in the reaction of **I** with CH_3• and CH_3OO• radicals generated by steady-state radiolysis in the absence and presence of 20% O_2, respectively (Figure 2.3B), showing that this reaction is not unique to t-APOO•. At the temperatures employed in this study, nitroxides are known to react irreversibly with carbon-centered radicals to produce stable alkoxylamine products. [43,94, 77-80] Thus, the identical rates of loss in the presence and

absence of O_2 and with increasing [**I**], demonstrates that **I** also reacts irreversibly with peroxyl radicals.

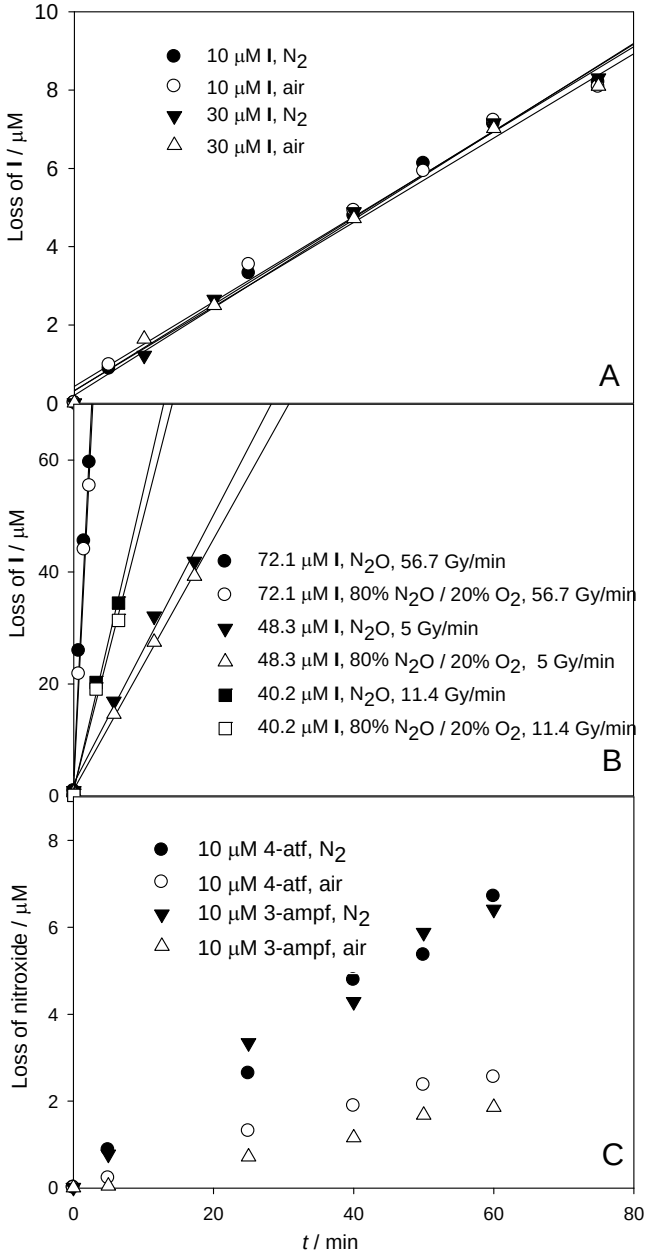

Figure 2.3. Reaction of nitroxides with peroxyl radicals. Panel A: Time course for the reaction of **I** with t-AP• (under N_2) and t-APOO• (under air) generated by thermolysis of AAPH (1 mM) in 50 mM phosphate buffer, pH 7.4 at 38.5 ± 0.5 ˚C. [O_2] = 210 μM at this temperature. Panel B: Time course for the reaction of **I** with CH_3• (under N_2O) and CH_3OO• (80% N_2O/ 20% O_2) generated by gamma radiolysis in 10 mM phosphate buffer, pH 7.4 contains [DMSO] = 20 mM, [O_2] = 250 μM. Panel C: Time course for the reaction of

fluorescamine derivatized 4-at (4-atf) and fluorescamine derivatized 3-amp (3-ampf) with t-AP• (under N_2) and t-APOO• (under air) in 50 mM phosphate buffer, pH 7.4. [4-atf] or [3-ampf] = 10 μM. Other reaction conditions as in Panel A.

Reaction of **I** with t-APOO• and CH_3OO• also led to a dramatic increase in the steady-state fluorescence intensity (Figure 2.4), which exhibited a linear relationship with the loss of **I** as determined by EPR (Figure 2.4 inset).

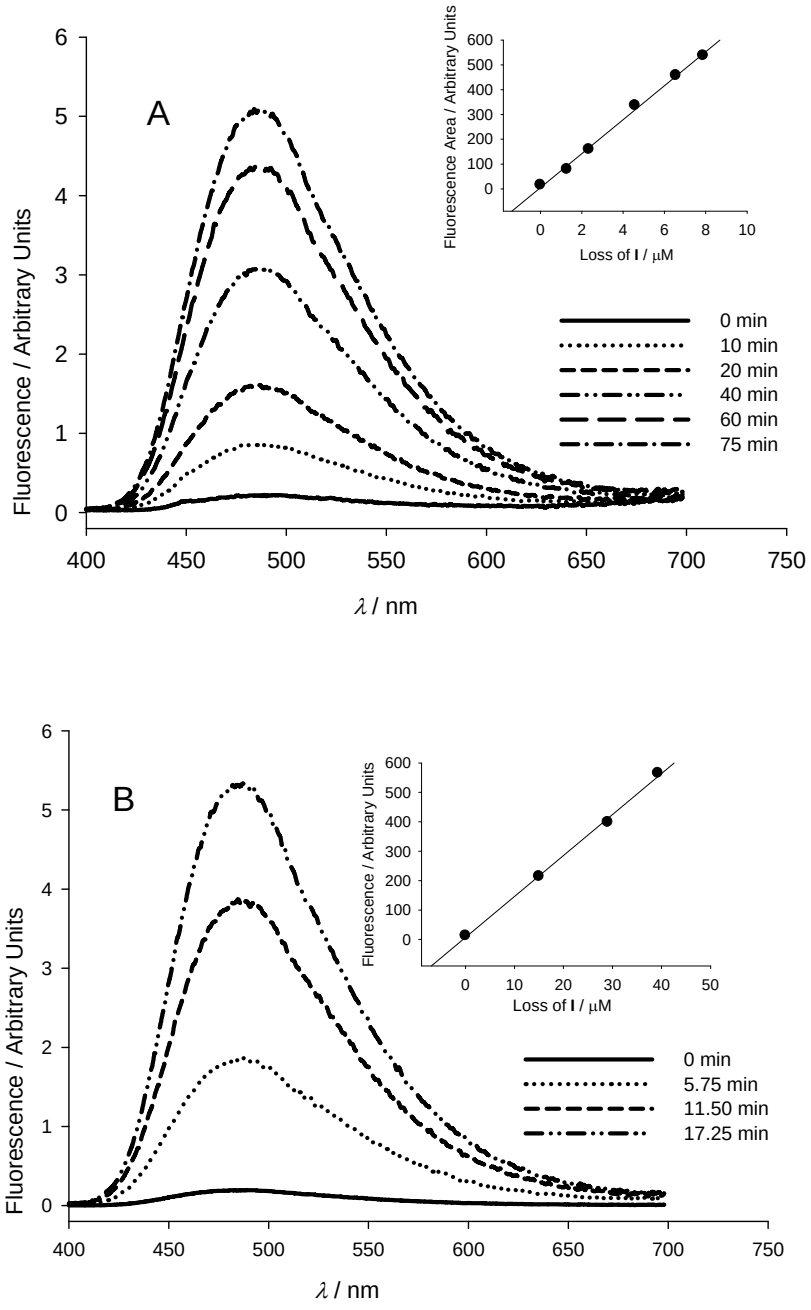

Figure 2.4. Panel A: fluorescence emission spectra of **II** formed by reaction of **I** with t-APOO• produced by thermolysis of AAPH (1 mM) at 38.5 ± 0.5 ˚C in 50 mM phosphate buffer, pH 7.4. [O_2] = 210 μM and [**I**] = 10 μM. Excitation wavelength was at 386 nm. Inset: Dependence of fluorescence area on the loss of **I** as determined by EPR. Panel B: fluorescence emission spectra of **II** formed by reaction of **I** with CH_3OO• produced by steady state radiolysis of 10 mM, pH 7.4 phosphate buffer saturated with 80% N_2O/ 20% O_2 in the presence of DMSO. [**I**] = 48.3 μM, [DMSO] = 20 mM. Dose rate was 5 Gy/min. Fluorometric

conditions were as in Panel A. Note that these samples were diluted 5-fold before analysis to avoid detector saturation and inner-filter effects.

HPLC analysis employing fluorescence detection showed that reaction of either t-APOO• or CH_3OO• with **I** produced a single product (**II**) that was not formed under anaerobic conditions (Figure 2.5). The fluorescence peak area of **II** increased linearly with the loss of **I** as determined by EPR (Panel A, inset).

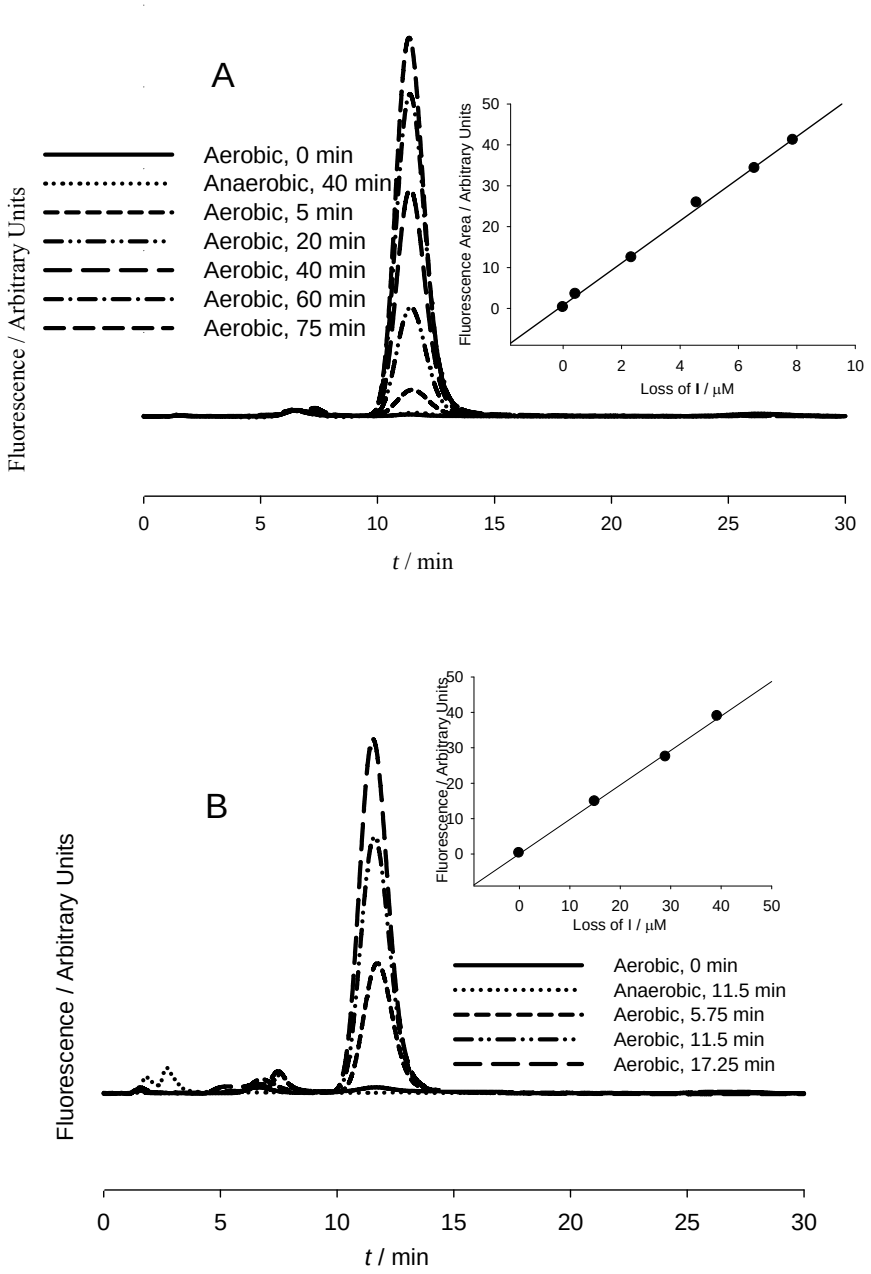

Figure 2.5 Panel A: Reversed phase HPLC chromatograms showing the formation of **II** upon reaction of I with t-APOO• produced by thermolysis of AAPH (1 mM) at 38.5 ± 0.5 ˚C in 50 mM phosphate buffer, pH 7.4. $[O_2]$ = 210 μM and [**I**] = 10 μM. The HPLC mobile phase was 65% sodium acetate buffer / 35% MeOH v/v. Excitation wavelength 390 nm, emission wavelength 490 nm. Injection volume was 125 μL. Inset: Dependence of fluorescence peak area on the loss of **I** as determined by EPR. Panel B: Reversed phase HPLC chromatograms showing the formation of **II** upon reaction of **I** with CH_3OO• produced by steady state radiolysis of 10 mM, pH 7.4 phosphate buffer saturated with 80% N_2O/ 20% O_2 in the presence of DMSO. [**I**] = 48 μM, [DMSO] = 20 mM. Dose rate was 5 Gy/min. HPLC conditions as in Panel A. Inset:

Dependence of fluorescence peak area on loss of **I** as determined by EPR. Note that these samples were diluted 5-fold before sample injection to avoid detector saturation.

II was also generated either by the electrochemical oxidation of 3-ap (see below) or by 3-ap reaction with peroxyl radicals when followed immediately by derivatization with fluorescamine at pH 8.1 (Figure 2.6).

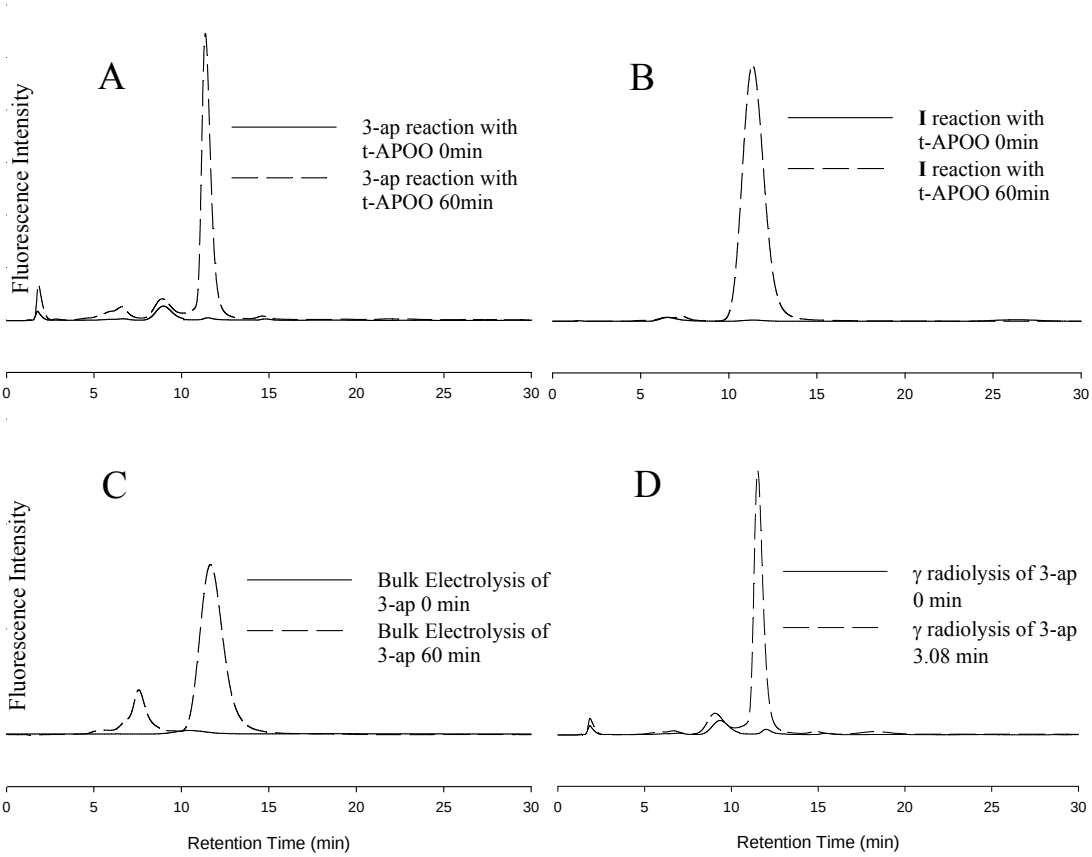

Figure 2.6 Comparison of the products obtained from the reaction of **I** and from the reaction of 3-ap followed by immediate derivatization with fluorescamine. In A, C and D, 3-ap was employed; in B, **I** was used. Reactions were all in pH 7.4 phosphate buffer. D has a dose rate of 56.7 Gy/min. An excitation wavelength of 390 nm and an emission wavelength of 490 nm were employed for fluorescence detection.

Compared to **I**, the fluorescence quantum yield of the product **II** is significantly increased, due to the removal of the paramagnetic nitroxide moiety. Using equation 2.10, the calculated quantum yield of **II** in different solvents are listed in table 2.1. The quantum yield of **I** in different solvents are listed in table 2.

Fluorescence quantum yields of HPLC-purified **II** in H_2O (0.045) and in pH 7.4, 50 mM phosphate buffer (0.041) were about 90-fold higher than that obtained previously for **I** (0.00046)[93] and only about 2-fold lower than that obtained previously for an alkoxyamine adduct of **I** (0.097).[93]

Table 2.1 Fluorescence quantum yield of **II** in different solvents

Solvent	H2O	MeOH	Dioxane	Acetonitrile	Acetate Buffer pH 4.01	Phosphate buffer, pH 7.0	borate buffer, pH 8.4	65% acetate/35 MeOH
Φ	0.0451	0.0233	0.0241	0.0110	0.0440	0.0400	0.0453	0.0318

Table 2.2 Fluorescence quantum yield of **I** in different solvents (from reference 93)

Solvent	borate buffer	MeOH	Dioxane
Φ	0.00046	0.00023	0.0005

Prior work has shown that nitroxides react with peroxyl,[53] $\bullet NO_2$[36] and $CO_3^{\bullet -}$[103] radicals to form initially the oxoammonium cation. However, **II** was stable in aqueous solution at room temperature for at least several hours, both in the absence and presence of NADH, [36,37,39,53] illustrating that **II** was not the oxoammonium cation.

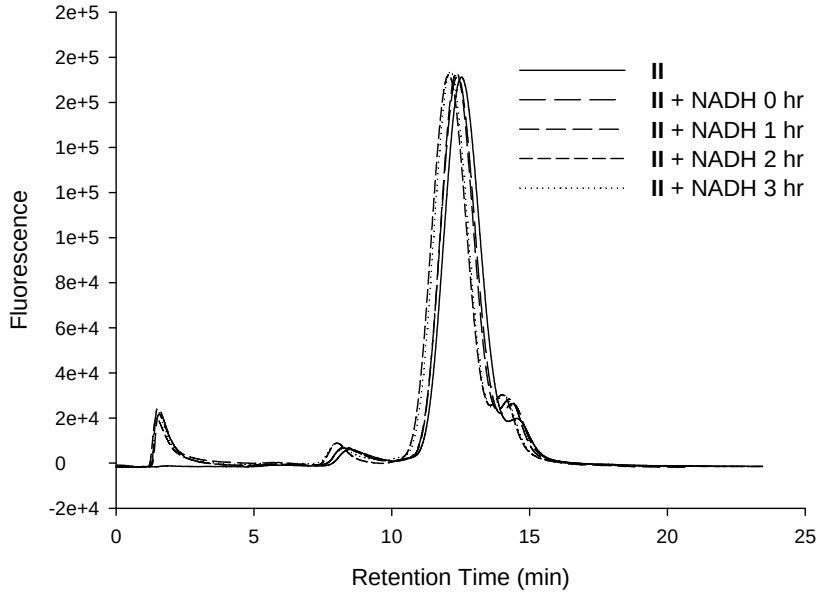

Figure 2.7 Time course of reversed phase HPLC chromatograms of **II** in the presence of NADH. [**II**] = 20 μM, [NADH] = 20 μM. The HPLC mobile phase was 65% sodium acetate buffer / 35% MeOH v/v. Excitation wavelength 390 nm, emission wavelength 490 nm. Injection volume was 125 μL.

Further, the 1:1 stoichiometric reaction of this amino-nitroxide (**I**) with peroxyl radicals (Figure 2.3) was unique; other fluorescamine-derivatized amino-nitroxides (3-ampf and 4-atf), exhibited much lower rates of spin loss in the presence of air than in its absence (Figure 2.3C). For these nitroxides, the lower rates of spin loss in air presumably result from the reversible regeneration of the nitroxyl moiety via the reduction by solution constituents of the oxoammonium cation.[36,37,39,53] Unlike both 4-at and 3-amp, 3-ap exhibited an irreversible oxidative wave in its cyclic voltammogram (Figure 2.8), clearly revealing that the oxoammonium cation of 3-ap is far less stable than that of 4-at and 3-amp, and reacts rapidly to form a secondary product**.** Increasing the scan rate from 100 to 500 mV/s did not lead to the appearance of a reductive wave in the cyclic voltammogram,

further indicating that the lifetime of this oxoammonium cation must be very short, under roughly one second, and thus that it is much less likely to be intercepted by solution reductants, as is demonstrated by the results in Figure 2.3.

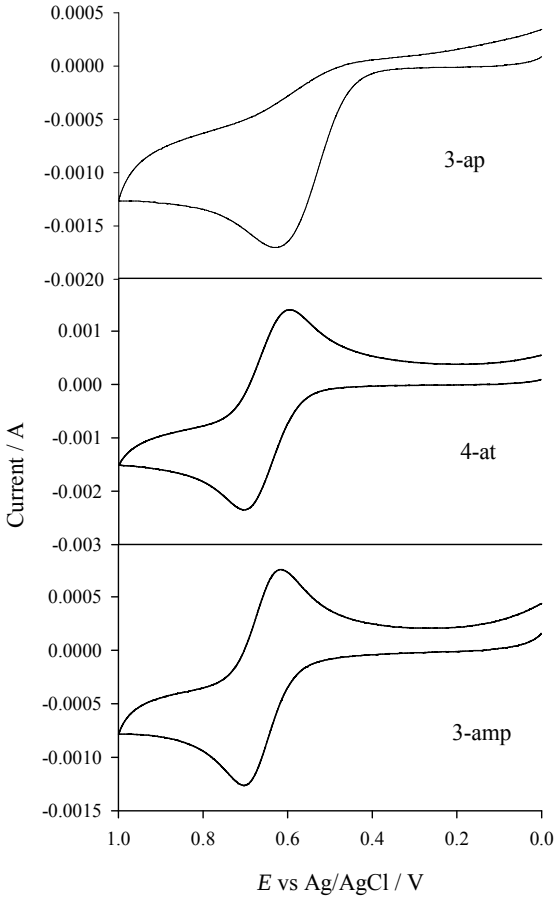

Figure 2.8 Cyclic voltammetry of nitroxides in K_2SO_4-saturated phosphate buffer (50 mM, pH 7.4). Nitroxide concentrations were 2.5-5 mM. Electrodes: Platinum (working and auxiliary), Ag/AgCl (reference). Scan rate was 100 mV/s and scan range was 0-1000 mV.

2.3.2 Product Analysis.

The structure of **II** was characterized by FT-ICR MS following HPLC purification of the fluorescamine-derivatized electrochemical oxidation product of 3-ap. Dominant peaks at m/z 395.1601 and 393.1456 were observed in positive and negative ion mode, respectively (Figure 2.9), corresponding to a molecular formula of $C_{22}H_{22}N_2O_5$ (predicted masses: 395.1602 in positive mode and 393.1456 in negative mode).

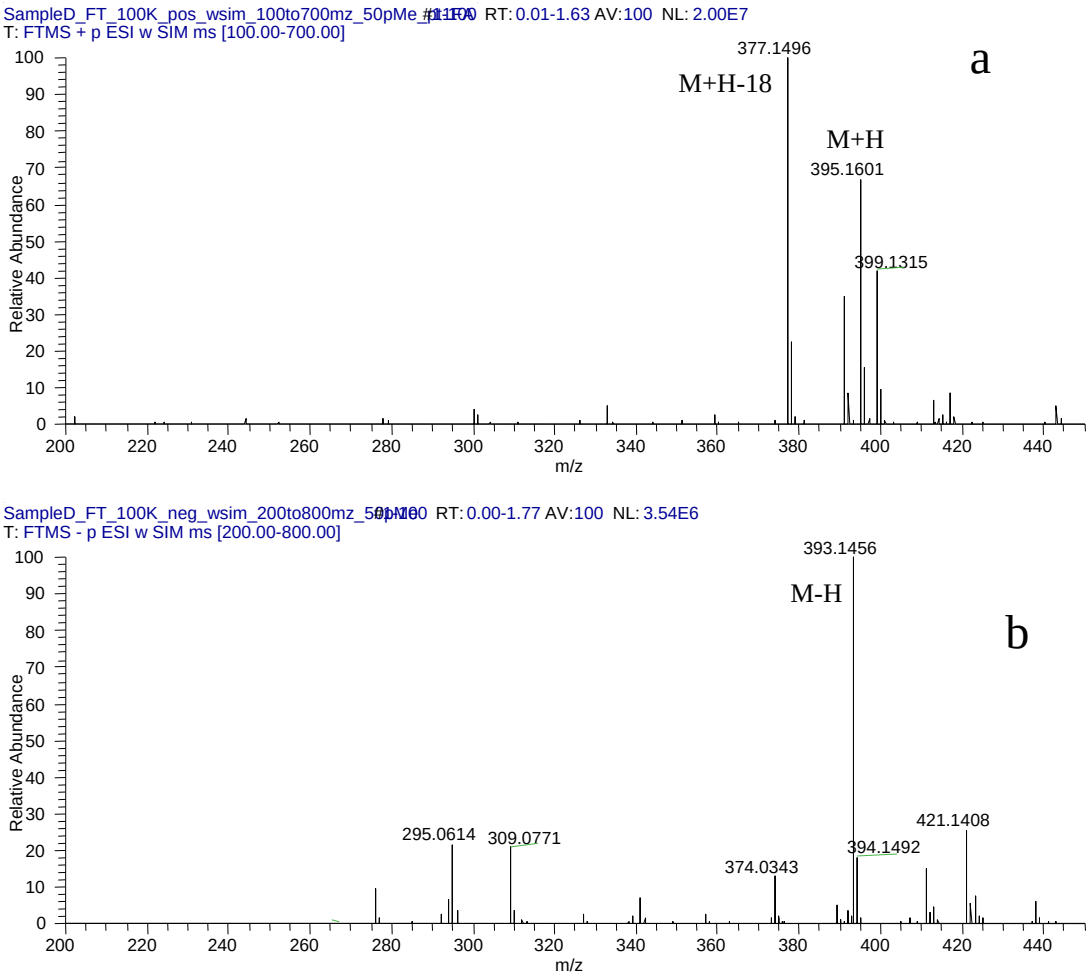

Figure 2.9 High resolution FT-ICR MS of product **II** in 50/50 MeOH/H_2O in positive ion mode (a) and negative ion mode (b). Conventional ESI, no sheath or auxiliary nitrogen gas used. In positive mode, spray voltage: 4.3 kV, syringe flow rate: 4 uL/min and Capillary temperature: 250 ˚C. In negative mode, spray voltage: 4.0 kV, syringe flow rate: 4 uL/min and Capillary temperature: 265 ˚C.

Because the absorption and fluorescence spectra of **II** were identical to that of the alkoxylamine adducts of **I** (Scheme 2.1, Figure 2.4), it was concluded that the fluorescamine moiety within **II** must be structurally intact. On this basis, **II** was tentatively identified as the structure shown in Scheme 2.3. Unfortunately, **II** was not sufficiently stable in chloroform over the time frame needed to obtain an unequivocal identification by

NMR either at room or low temperature (Figure 2.10 and 2.11) **II** was also found to be unstable in acetonitrile and methanol (data not shown).

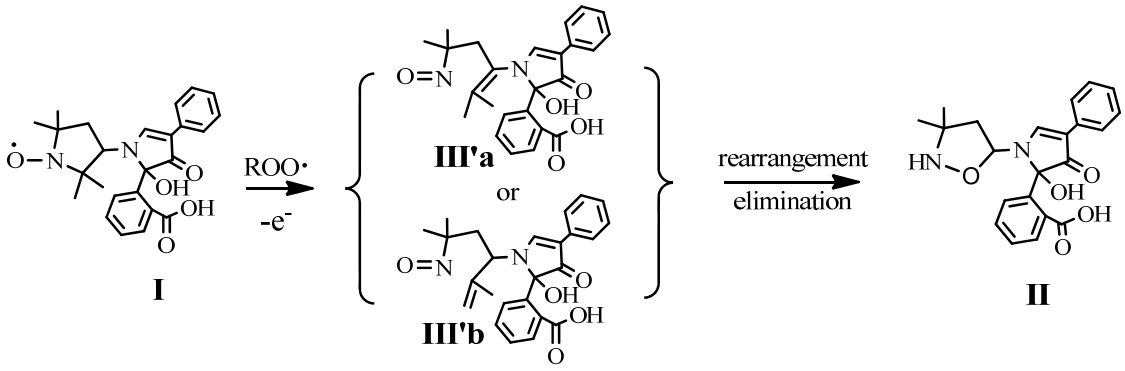

Scheme 2.3 proposed reaction pathway for the reaction of oxoammonium cation of **I**

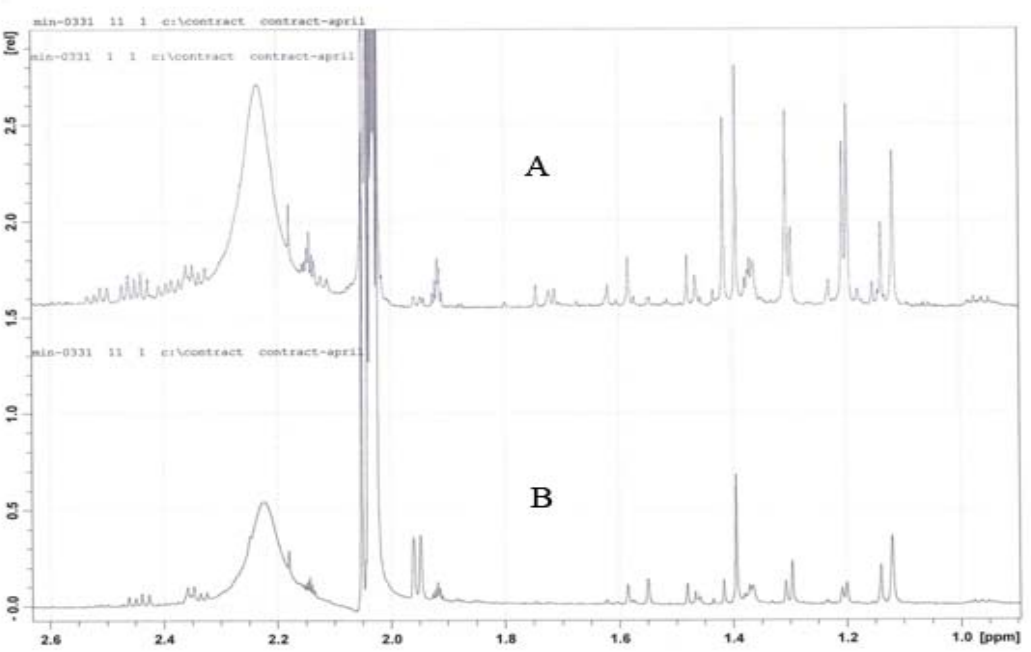

Figure 2.10 1H NMR spectra of **II** in chloroform (D) indicate that the stability of **II** in organic solvents prevents the direct characterization of **II**. Spectrum B was measured one hour after spectrum A at room temperature for the same sample.

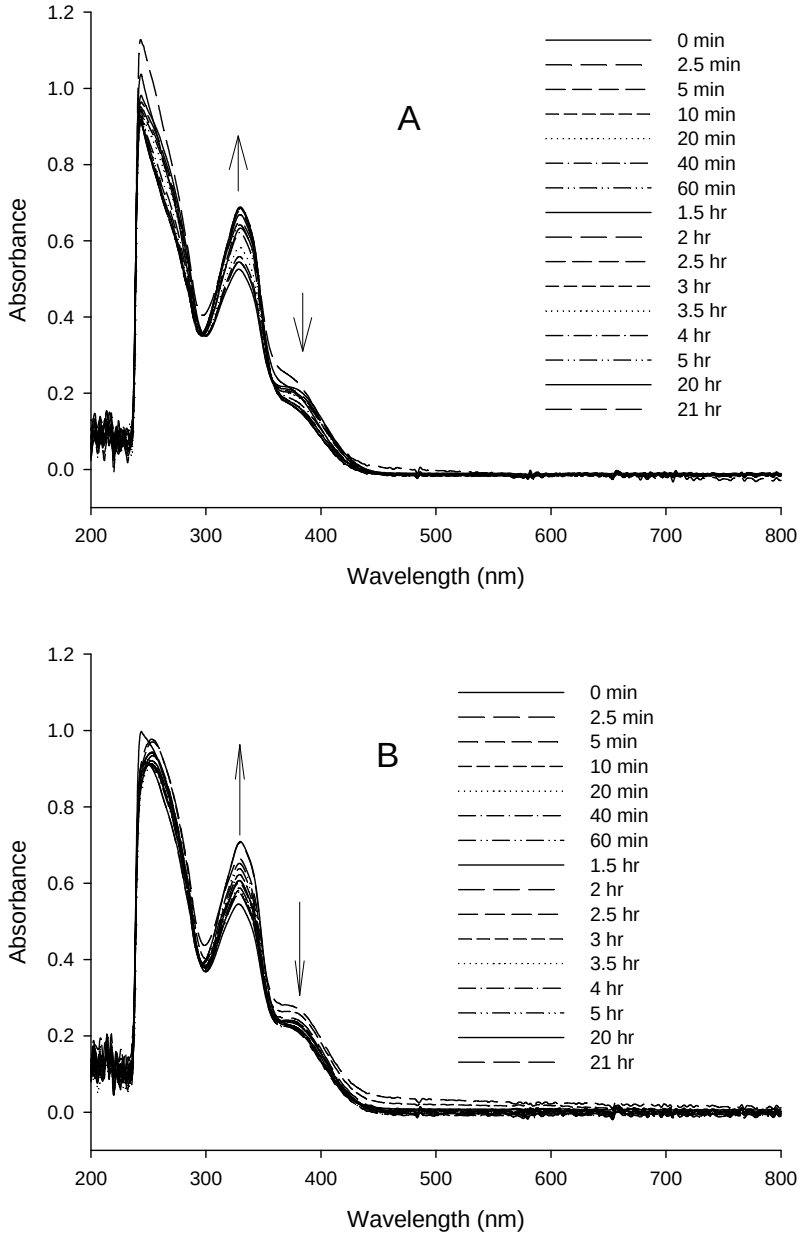

Figure 2.11 Panel A: UV/Vis spectra of **II** in chloroform (D) indicate that the stability of **II** in organic solvents prevents the direct NMR characterization of **II**. Spectra were taken under room temperature. Panel B: Spectra were taken at 0 ˚C. Other conditions are the same as in Panel A.

In an attempt to resolve this issue, the electrochemical oxidation product of 3-ap was reacted with benzoyl chloride at pH 8.5 to form the stable amide (Scheme 2.4). Following HPLC purification, this product was identified as the cyclic peroxide **V** (Scheme 2.4) as established by FT-ICR MS (Figure 2.12) and extensive NMR analyses (Table 2.3, Figure A1-A14 in Appendix I). The reaction mechanisms by which **II** and **V** are formed are not presently obvious to us, as well as why the reaction on the nitroxide moiety yield different final products when derivatized with different chromophores. However, it appears that the presence of the fluorescamine moiety alters the reaction pathway from **III (**and **III')** to produce **II** (Scheme 2.3, Figure 2.6 A,C,D). Regardless, the observation that **I** undergoes irreversible reaction with peroxyl radicals while most other nitroxides do not[53] can be attributed to the presence of the amine moiety at the β-position, which we suggest facilitates a rapid initial ring cleavage and proton loss (Scheme 2.3). In conclusion, although we were unable to propose a complete mechanism for the reaction of peroxyl radicals with **I** due to the lack of stability of **II** in organic solvents, we have established that the oxoammonium cation of **I** is unstable and undergoes a rapid secondary reaction to form a more polar, lesser molecular weight product, consistent with fragmentation of the ring as established by NMR and mass spectrometry for both **II** and **V**.

Table 2.3. 1H and 13C NMR data for product V

Position	δC	δH
1	135.45	-
2	128.52	7.71
3	127.72	7.38
4	130.40	7.43
5	127.72	7.38
6	128.52	7.73
7	165.56	-
8	-	3.10
9	96.06	5.58
10	51.16	2.47-2.50; 2.32, 2.34
11	62.21	-
12	26.34	1.81
13	26.52	1.63

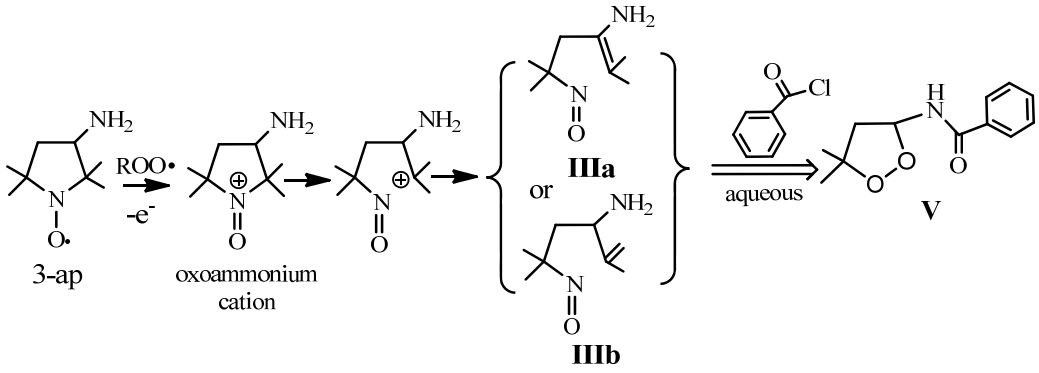

Scheme 2.4 Proposed pathways for the reaction of benzoyl chloride with 3-ap oxidation product.

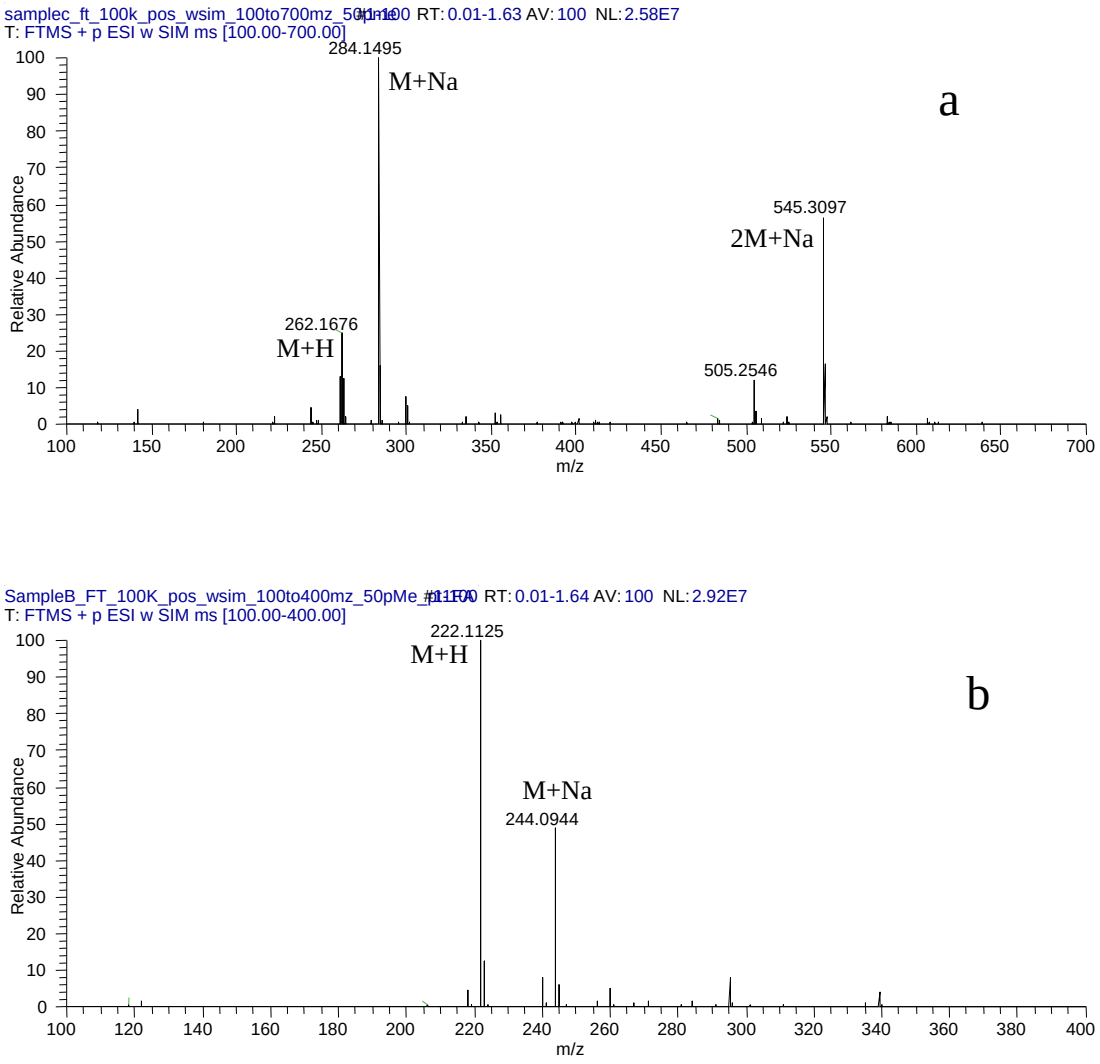

Figure 2.12 High resolution FT-ICR MS of the benzylamide of 3-ap (C15H21N2O2) (a) and **V** (b). MS conditions are the same as in Figure 2.9.

2.3.3 Reaction of nitroxides with other radical and oxidants. Other reactive oxygen species that might interfere with peroxyl radical detection include the hydroxyl (•OH), [39] alkoxyl (RO•), singlet dioxygen and possibly superoxide ($O_2^{\bullet-}$).[103-104] A 15 µM **I** solution was radiolysed in the presence of formate and DTPA at a dose rate of 14.5 Gy/min to produce a superoxide flux rate of 8 µM/min (reaction 2.1, 2.7-2.9). Xathine/Xathine

oxidase was employed to generate superoxide radicals at a flux rate of 4.5 μM/min. In both cases there were no noticeable reaction between superoxide radical and **I** as indicated by HPLC analysis (Figure 2.13) and UV/Vis spectroscopy (Figure 2.14). These findings are consistent with prior results[95-96] and the fact that the rate constants for reaction of superoxide with pyrrolidinyl nitroxides are two to three orders of magnitude lower [103-104] than those for peroxyl radicals[36-37, 53] at neutral to alkaline pH.

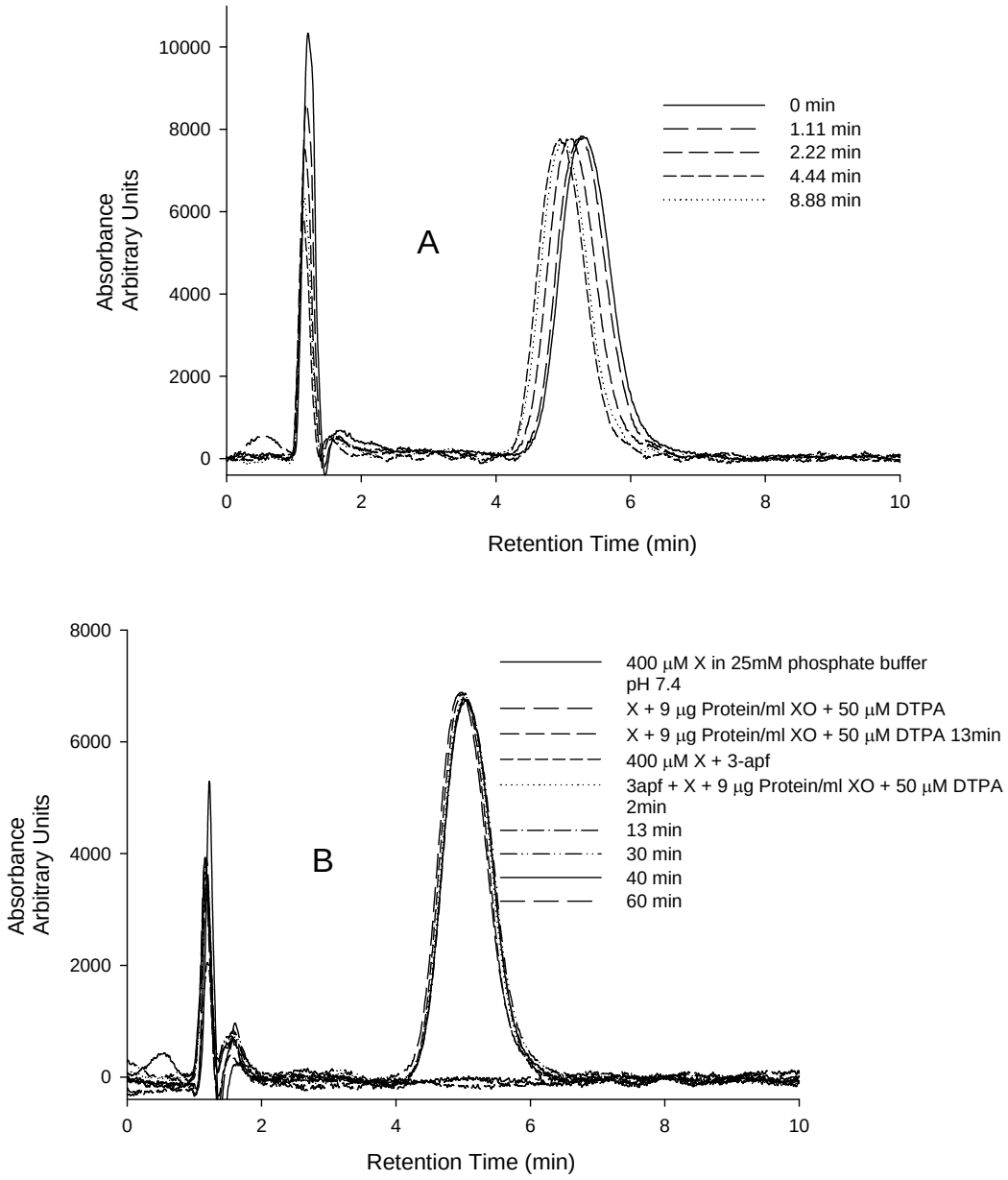

Figure 2.13 Effect of radiolytically (Panel A) and enzymatically (Panel B) generated superoxide radical on **I** as determined by HPLC with UV/Vis detection.

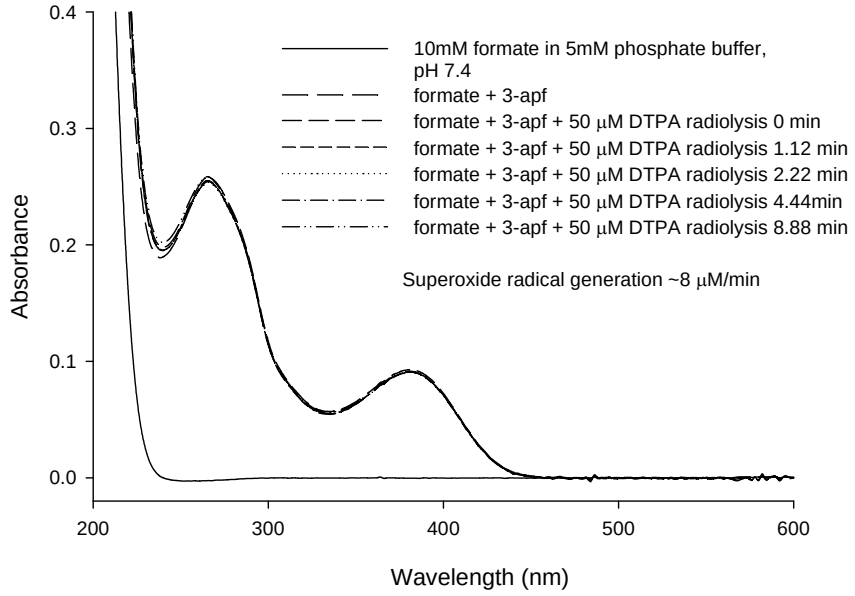

Figure 2.14 effect of radiolytically generated superoxide radical on **I** as determined by UV/Vis spectroscopy.

Although singlet dioxygen is known to oxidize hydroxylamine to its corresponding nitroxide, nitroxides alone are known to quench singlet dioxygen via a physical mechanism,[105] making it highly unlikely that singlet dioxygen reacts with most nitroxides. Nevertheless, this possibility was tested by employing rose Bengal to generate singlet oxygen molecules in the presence of 11.4 μM **I**. HPLC with UV/Vis detection showed that singlet oxygen had no noticeable effect on **I** under our experimental conditions (Scheme 2.15).

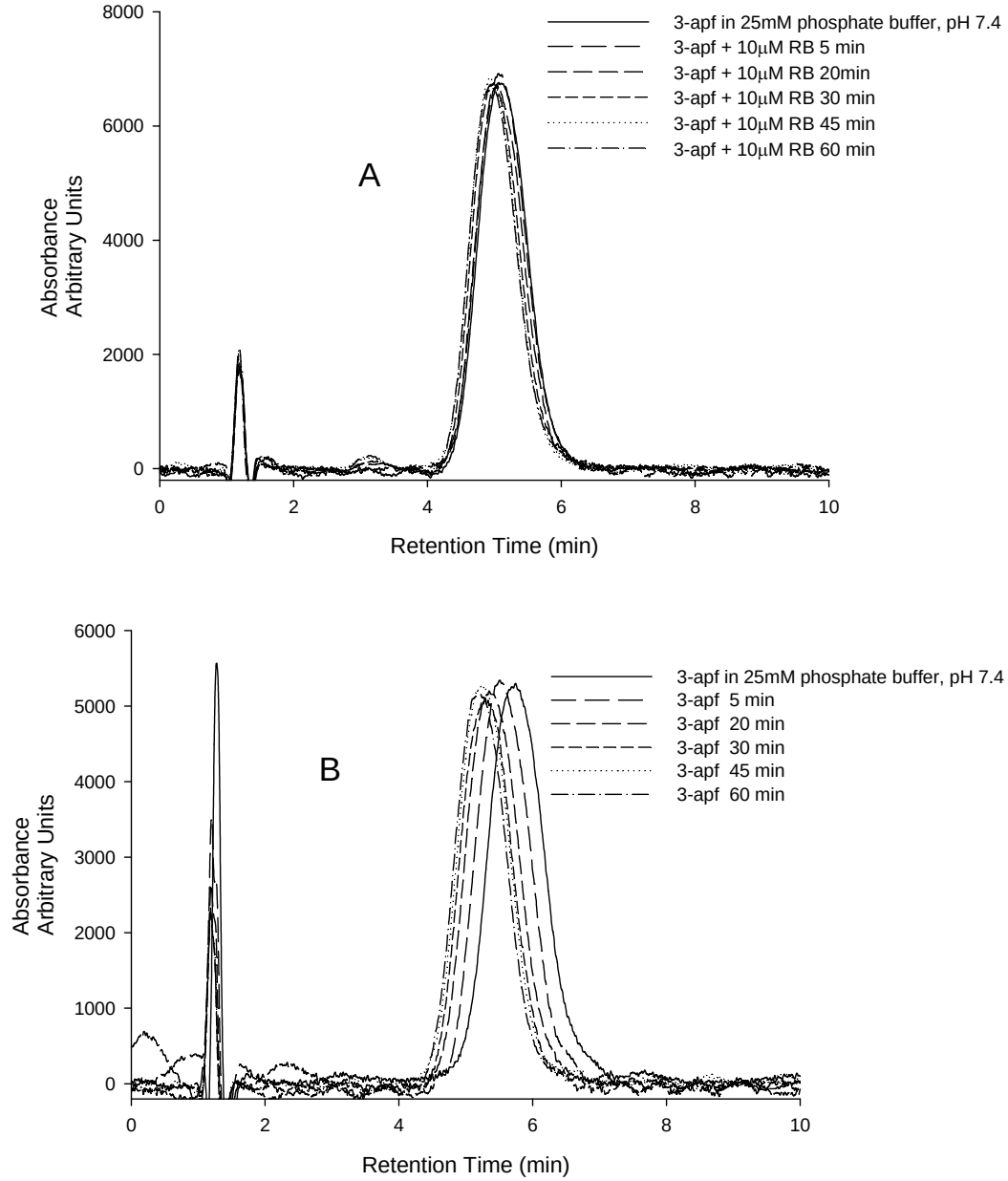

Figure 2.15 Panel A: Reactivity of **I** with singlet oxygen generated by photo-irradiation of rose Bengal by a lab light bulb over a time period of an hour. Panel B was the control experiment under the same conditions at the absence of rose Bengal.

Because published rate constants for reaction of pyrrolidinyl nitroxides with peroxyl radicals are reasonably large (~10^6-10^7 $M^{-1}s^{-1}$),[53] the use of low concentrations of **I** (<40-50 μM) should allow quantitative reaction with peroxyl radicals (eg., Figures 2.3A,C,2.4,2.5), while largely precluding interferences from more highly reactive oxidants such as •OH, and RO•, which under most circumstances will react preferentially with other solution constituents at higher concentrations.

Nevertheless, this may not be the case when other more selective oxidants are also present. For example, our results indicate that radical oxidants such as $•NO_2$ and $CO_3^{•-}$ are also capable of oxidizing **I** to the oxoammonium cation to further generate **II** (reaction 2.13, 2.14 and Figure 2.16) thus will also be detected.

$$•CH_3 + \mathbf{I} \xrightarrow{k_7 = 7.8 \times 10^8\ M^{-1}s^{-1}} \mathbf{VI} \qquad 2.11$$

$$CH_3OO• + \mathbf{I} \xrightarrow{k_8 = 10^6\text{-}10^7\ M^{-1}s^{-1}(39)} \mathbf{II} \qquad 2.12$$

$$•NO_2 + \mathbf{I} \xrightarrow{k_9 = 10^8\ M^{-1}s^{-1}(40)} \mathbf{II} \qquad 2.13$$

$$CO_3^{•-} + \mathbf{I} \xrightarrow{k_{10} = 10^8\ M^{-1}s^{-1}(44)} \mathbf{II} \qquad 2.14$$

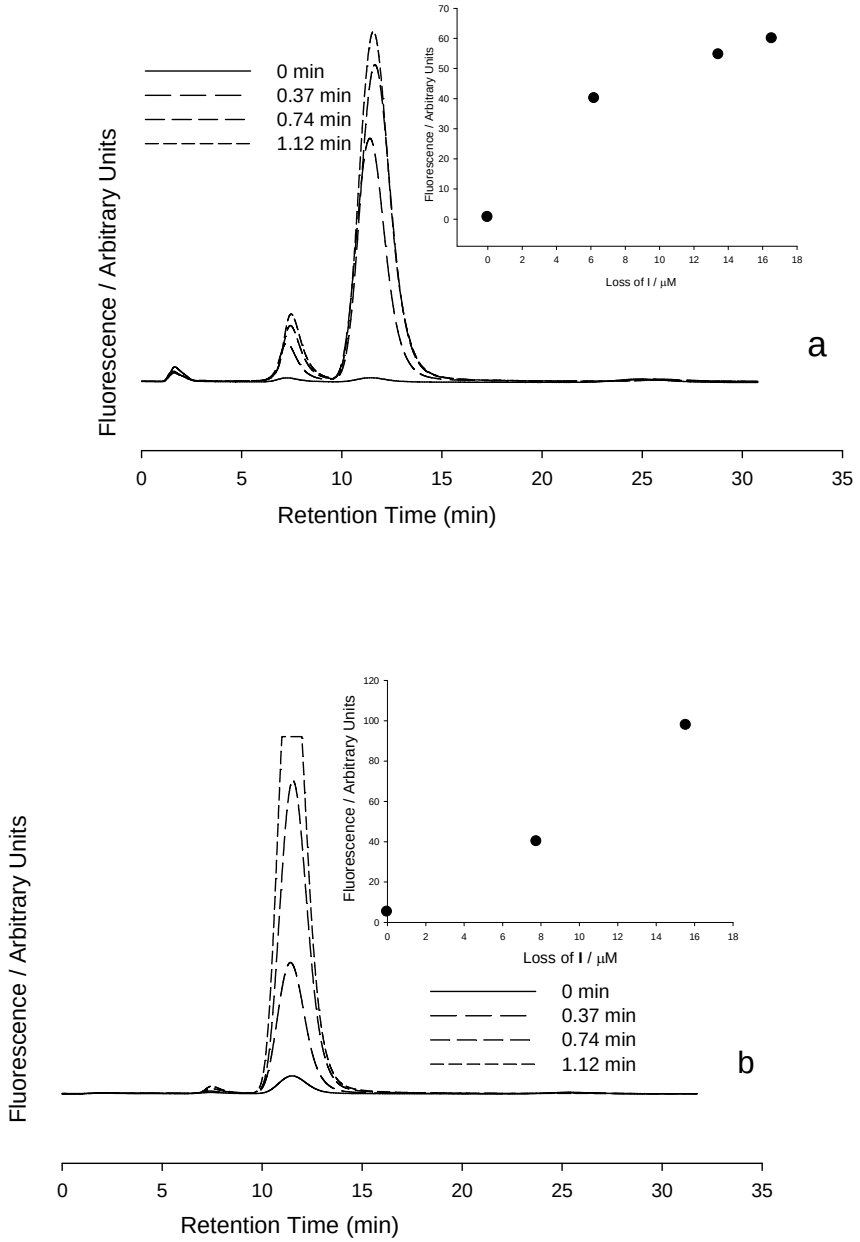

Figure 2.16 Reversed phase HPLC chromatograms showing the formation of **II** upon reaction of **I** with $CO_3^{\bullet-}$ (a) and $\bullet NO_2$ (b), produced by steady state radiolysis of N_2O saturated Na_2CO_3 and $NaNO_2$ solutions, respectively. [**I**] = 30 μM, [Na_2CO_3] = 100 mM, [$NaNO_2$] = 10 mM. Dose rate was 39.7 Gy/min. HPLC conditions as in Fig. 2. Inset: Dependence of fluorescence peak area on loss of **I** as determined by EPR.

Because these other oxidants are not O_2-reactive, while the formation of peroxyl radicals is O_2-dependent, the presence of oxidants other than peroxyl radicals should be readily identified by decreasing the $[O_2]$/[**I**] ratio (Scheme 2.1); a decrease in the yield of **II**, combined with a concomitant increase in alkoxylamine products would be predicted when peroxyl radicals contribute significantly to the total oxidant pool (Scheme 2.1).

To test this idea, solutions containing 1.5 mM DMSO, 20 mM $NaNO_2$ and N_2O/O_2 ratios ranging from pure N_2O to 80% N_2O/ 20% O_2 were subjected to gamma radiolysis in the presence of 30 μM **I** (Figure 2.17, see reactions. 2.1-2.6, 2.11-2.14). Because of the high N_2O concentrations employed, all $e^-_{(aq)}$ is converted quantitatively to •OH under all conditions (Rxns 2.1-2.2). •OH then reacts competitively with DMSO and NO_2^- to form $•CH_3$ and $•NO_2$ radicals, respectively (Rxns 2.3, 2.4). Based on the relative concentrations of DMSO and NO_2^- and their published rate constants for •OH reaction,[106] the yield of $•NO_2$ and $•CH_3$ is calculated to be 92% and 8%, respectively, independent of $[O_2]$. Under 20% O_2, the methyl radicals are converted to methyl peroxy radicals (~95%, Rxn 2.6), as calculated from the relative concentrations of O_2 and **I** and their published rate constants for reaction with methyl radicals;[106] **II** formation then represents the sum of $•NO_2$ and $•CH_3$ formation (Rxns 2.12-2.13; Figure 2.17A). With decreasing $[O_2]$, **II** formation decreases, while the methoxylamine (**VI**) formation increases due to greater reaction of **I** with the methyl radical (Rxn 2.11, Figure 2.17B; Scheme 2.1); under complete deoxygenation, **II** decreases by 10%, in good agreement with the calculated percentage of methyl radicals generated under these conditions (8%, see above). As

shown in the Appendix II, the decrease in the yield of **II** and the concomitant increase in the yield of **VI** with decreasing [O_2] are in good agreement with those calculated based on known rate constants (reactions 2.1-2.6, 2.11-2.19, Scheme 2.1).

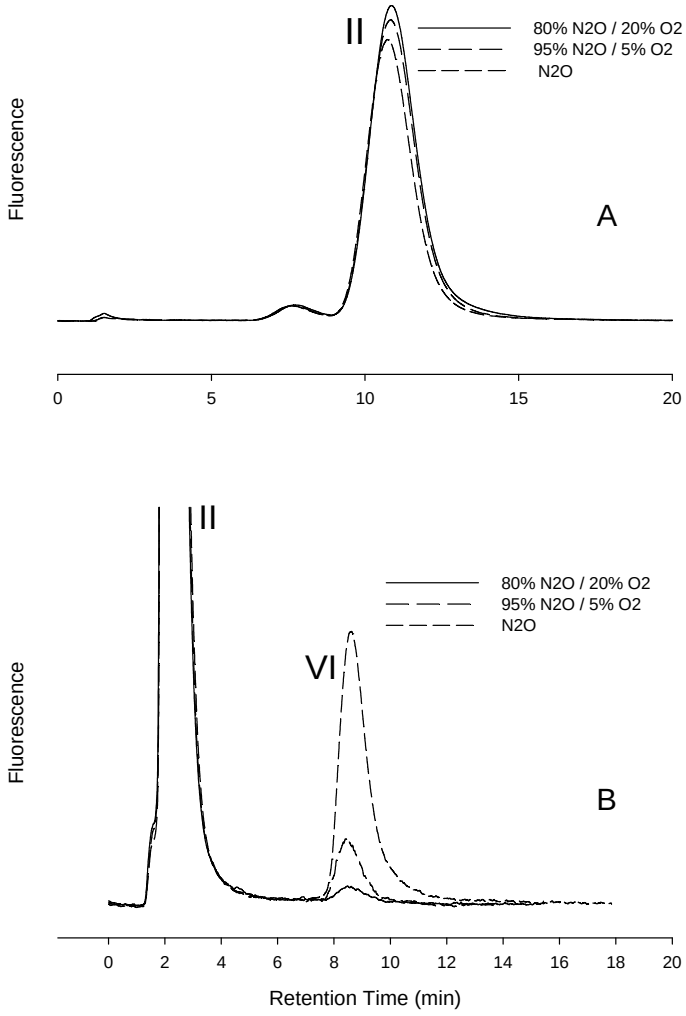

Figure 2.17 Determination of peroxyl radicals in the presence of •NO_2 by gamma radiolysis of a solution contains 30 μM **I**, 1.5 mM DMSO and 20 mM $NaNO_2$. Panel A: Decrease of **II** formation with decreasing [O_2]/[**I**] ratio. HPLC conditions were as in Figure 2.5. Panel B: Increase of methoxylamine product (**VI**) with decreasing [O_2]/[**I**] ratio. Mobile phase was 60% MeOH and 40% pH 4.0 acetate buffer. Other HPLC conditions were as in Figure 2.5.

Although the $[O_2]$/[**I**] ratio was altered by decreasing the $[O_2]$ in the above example, an increase in [**I**] could also have been employed. It should be further noted that this example is particularly challenging in that a small amount of peroxyl radical was detected over a very high background of $\bullet NO_2$.

2.3.4 Photo and thermal stability of I and II. Irradiation of **I** with high-intensity polychromatic light led to observable photo-degradation (15%) of **I** in 30 min**,** as determined by and HPLC with absorbance detection (Figure 2.18) and by UV/Vis spectroscopy (Figure 2.19). Significant photo-degradation and fluorescence loss (60%) of **II** was also observed over the course of 30-60 min by UV/Vis (Figure 2.20 Panel A, B) and fluorescence (Figure 2.20 Panel C). However, both **I** and **II** were stable for 12 or more hours in aqueous solution over a broad range of other conditions, including pH ranging from 4 to 10 and temperatures up to 50°C, as determined by UV/VIS spectroscopy (Figure 2.21).

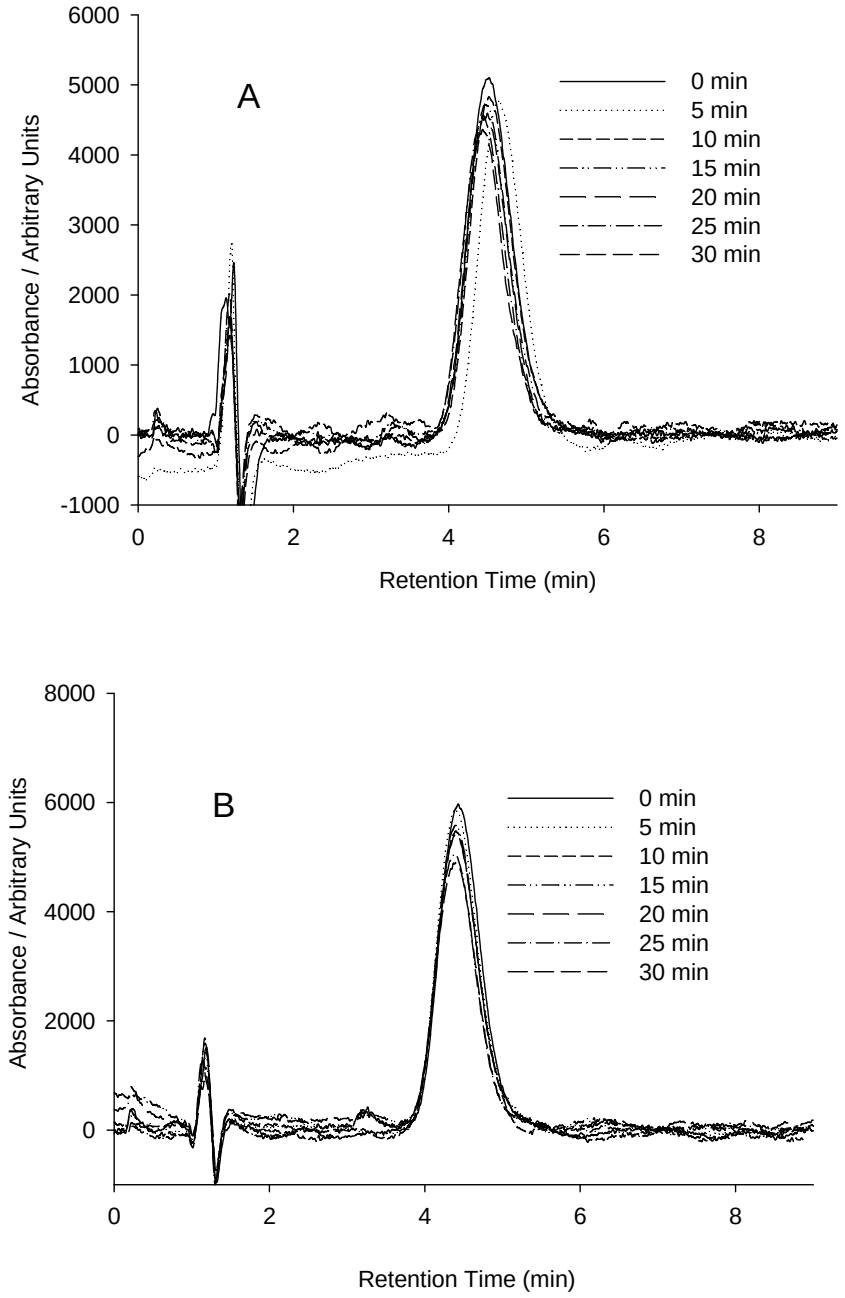

Figure 2.18. Stability of **I** under polychromatic irradiation. A, under N_2; B, under air.

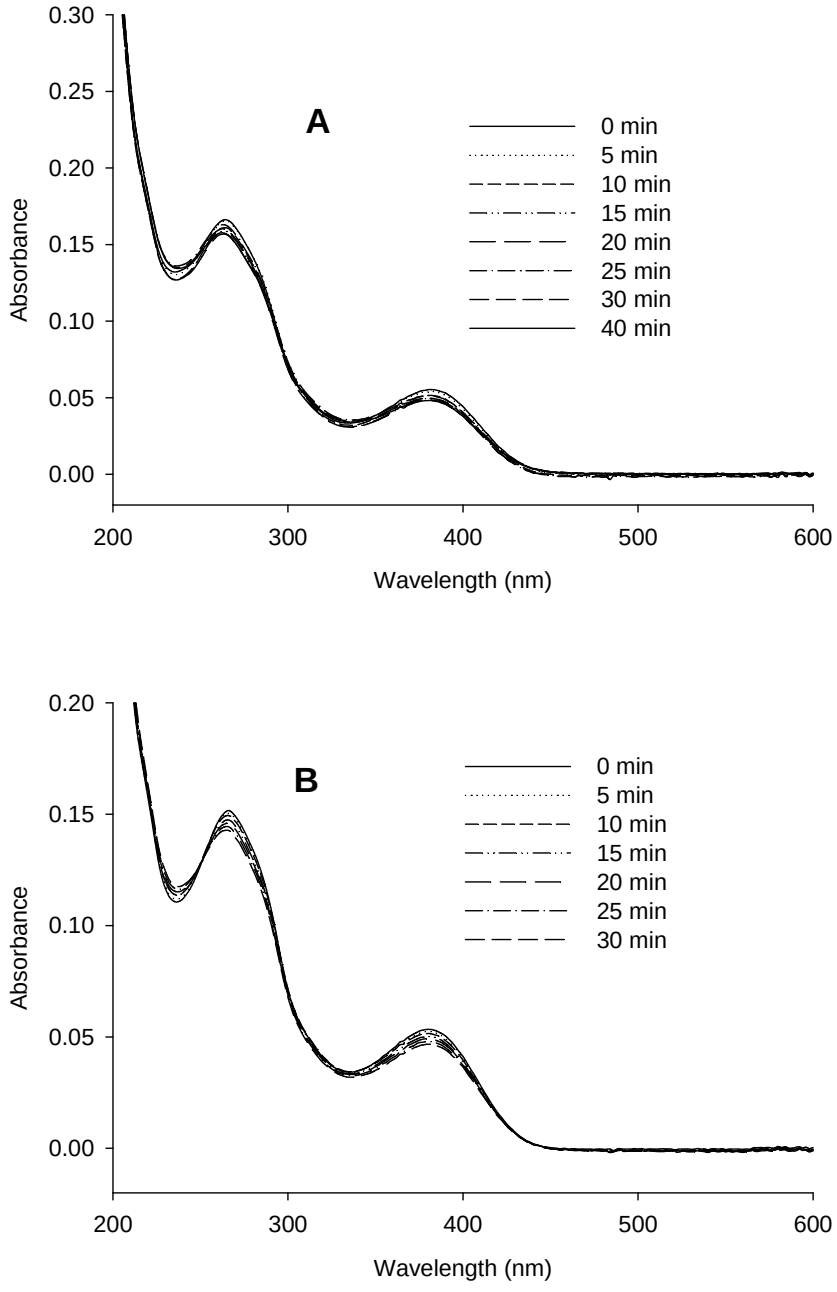

Figure 2.19 Stability of **I** under polychromatic irradiation A, under N_2; B, under air.

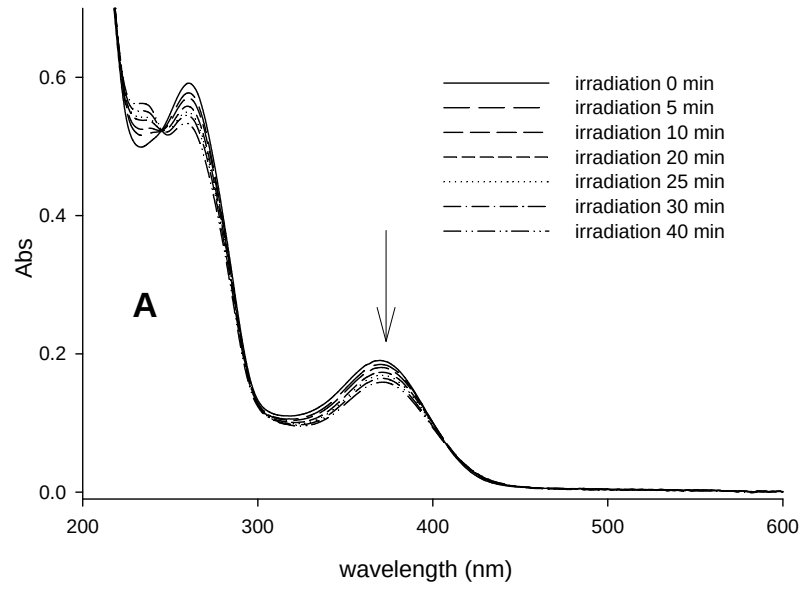
irradiation 0 min
irradiation 5 min
irradiation 10 min
irradiation 20 min
irradiation 25 min
irradiation 30 min
irradiation 40 min
A
Abs
wavelength (nm)
0.0
0.2
0.4
0.6
200
300
400
500
600

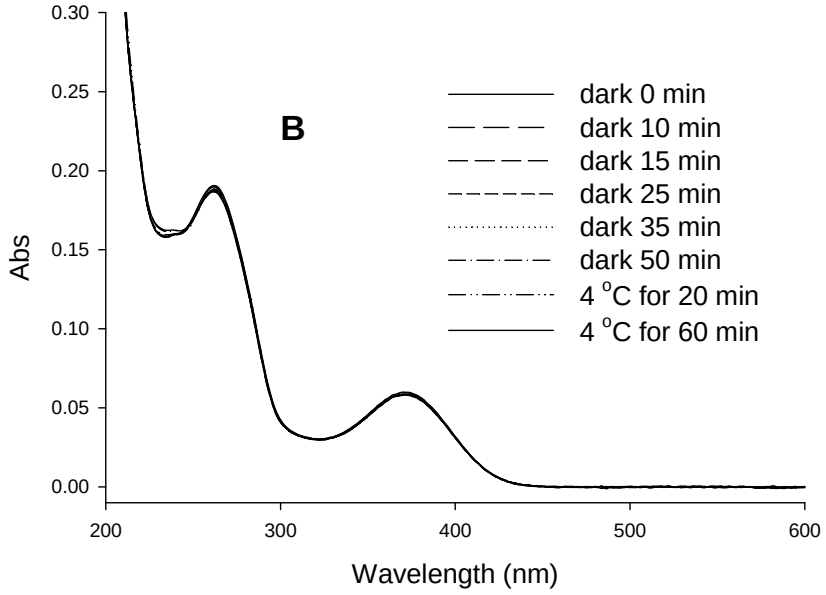
dark 0 min
dark 10 min
dark 15 min
dark 25 min
dark 35 min
dark 50 min
4 °C for 20 min
4 °C for 60 min
B
Abs
Wavelength (nm)
0.00
0.05
0.10
0.15
0.20
0.25
0.30
200
300
400
500
600

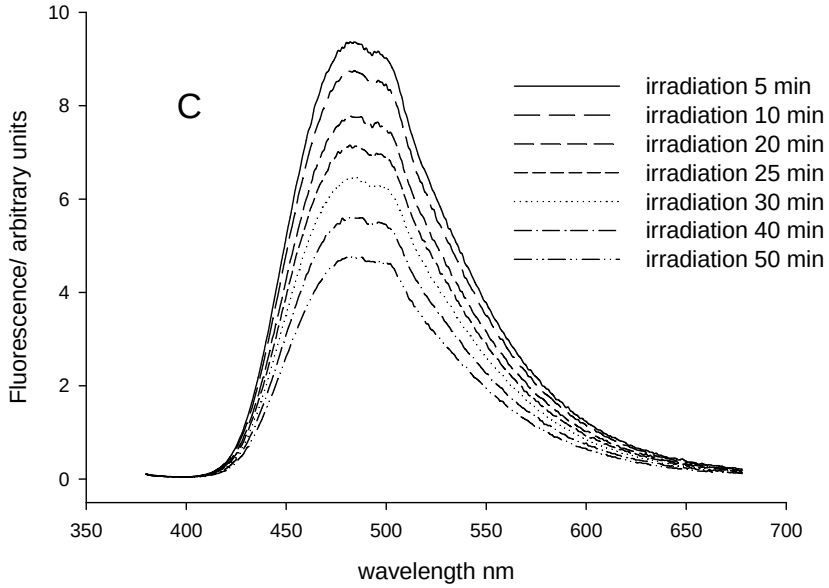

Figure 2.20 Stability of **II** under high intensity polychromatic irradiation. Panel A, polychromatic irradiation under air; Panel B, dark control; Panel C, fluorescence degradation monitored by steady state fluorometry.

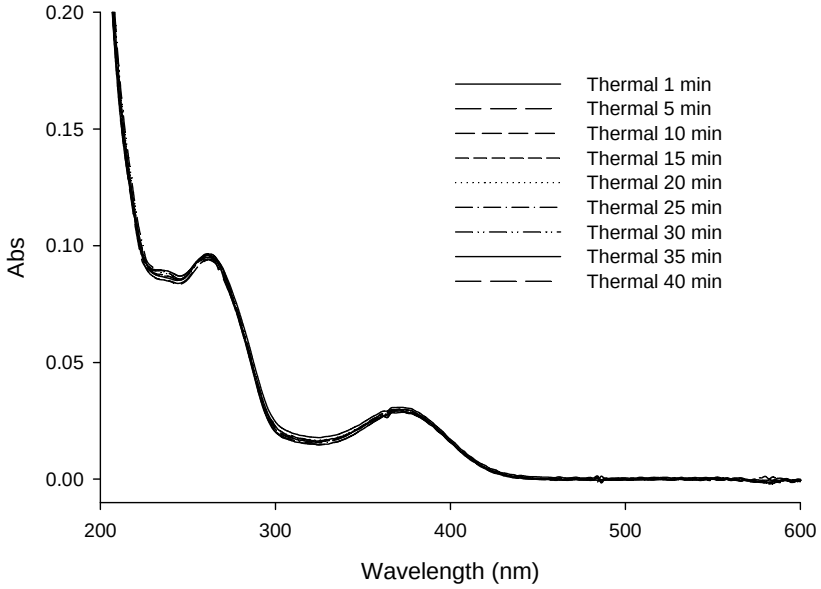

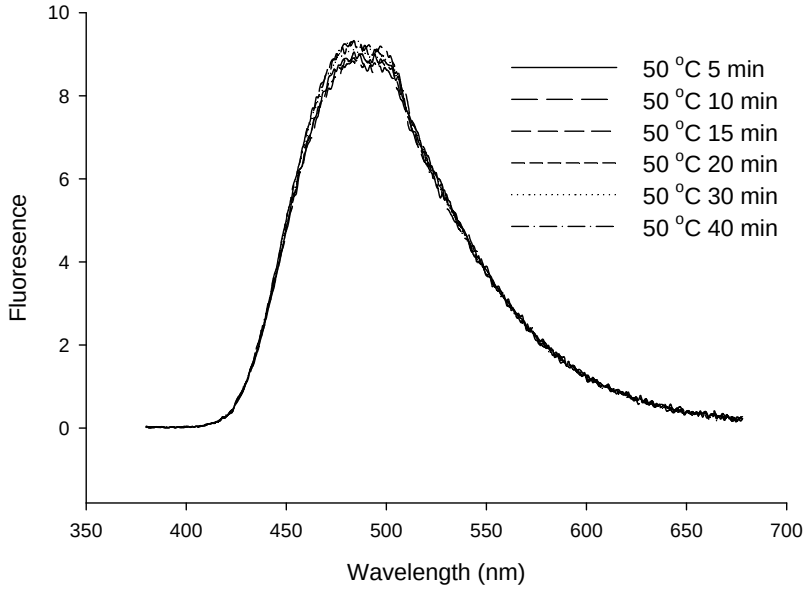

Figure 2.21 Thermal stability of II at 50°C in phosphate buffer, pH 7.4

These results indicate that while **I** can be employed in thermal systems, it will not be suitable generally for photochemical studies. The photo-stability of other fluorescamine-derivatized nitroxides such as 3-ampf and 4-atf, as well as a paramagnetic analogue methyl-fluorescamine (CH3-f, **VI**) is presented in Appendix III.

2.3.5 Linearity, Precision and Detection Limit. Employing the AAPH system, the concentration of **II** was calibrated by comparing the loss of nitroxide as measured by EPR with the increase in the fluorescence peak area in HPLC chromatograms (Figure 2.5 inset). Once product concentrations in micromolar range were established, a calibration curve in nanomolar range, where EPR determinations were not possible, was generated by serial dilution of **II**. Steady-state emission spectra were calibrated in the same fashion (Figure 2.5 inset). Chromatographic peak areas increased linearly over the concentration range of 5-7500 nM (n=9) with a R^2 value of 0.998 and the y intercept was not significantly different from zero.

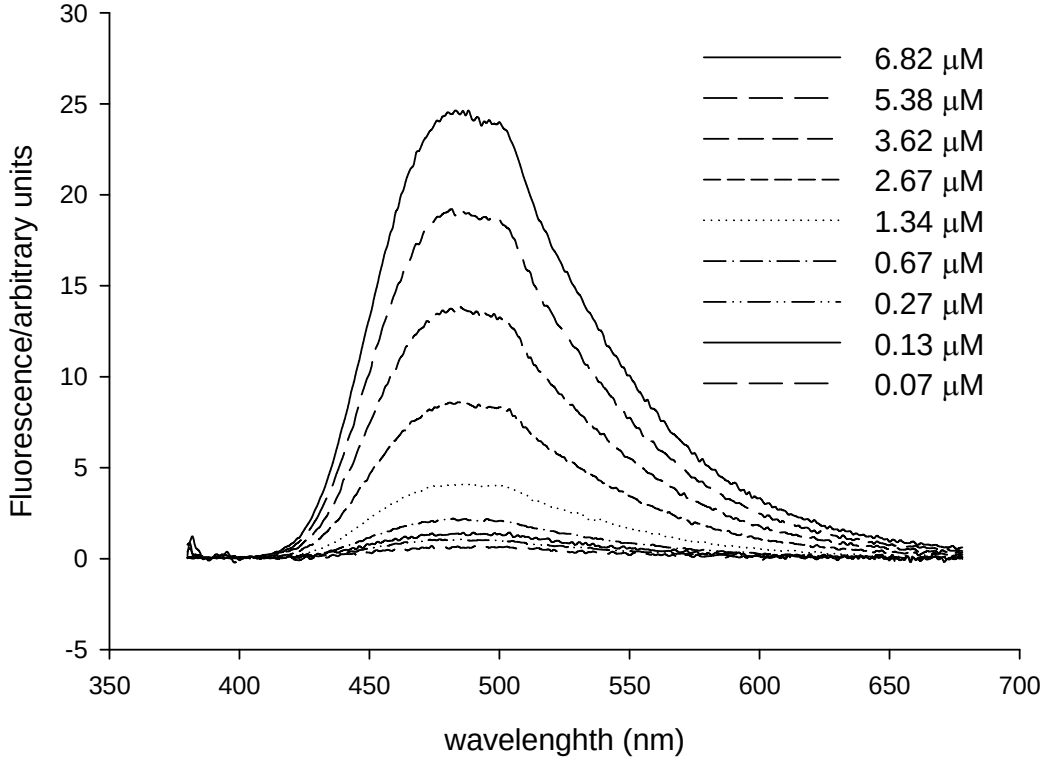

Figure 2.22 Direct fluorometric detection of the product **II** at different concentration range

Employing direct fluorometric detection (Figure 2.22), the linear range was from 0.66-6.2 μM with a R^2 value of 0.997. The precision of the HPLC analysis method was determined from the reproducibility of 5 HPLC injections of identical samples under the same experimental conditions over a period of 7 days at concentrations in the nM range (10-50 nM). The maximum RSD was 10.6% for HPLC separation with fluorescence detection. In a similar fashion, the maximum RSD for direct fluorometric detection method was 9.2%. Defining the detection limit as twice the standard error of the intercept obtained from linear regressions of calibration curves of **II**, with concentrations ranging from 5 to 240 nM (6 points; HPLC separation with fluorescence detection) and from 0.66-6.2 μM (6

points; direct fluorometry), we estimate values of ~3 nM for the HPLC analysis (125 μL injection volume) and ~0.35 μM for direct fluorometric detection.

2.3.6 Preliminary Applications. Employing **I**, peroxyl radical formation was detected in an aqueous dispersion of soybean PC lipsomes, a common model for cell membranes.[107-109] A water-insoluble azo compound, 2,2'-azo-bis-isobutyronitrile (AIBN), was used to initiate autoxidation of the polyunsaturated fatty acids within the PC liposomes via incubation at 50 °C under air. Analysis of the reaction mixture by HPLC showed that **II** increased with increasing incubation time (Figure 6A), from 2.9 μM at 20 min to 7.4 μM by 50 min. In the absence of the radical initiator (AIBN), **II** was not detected.

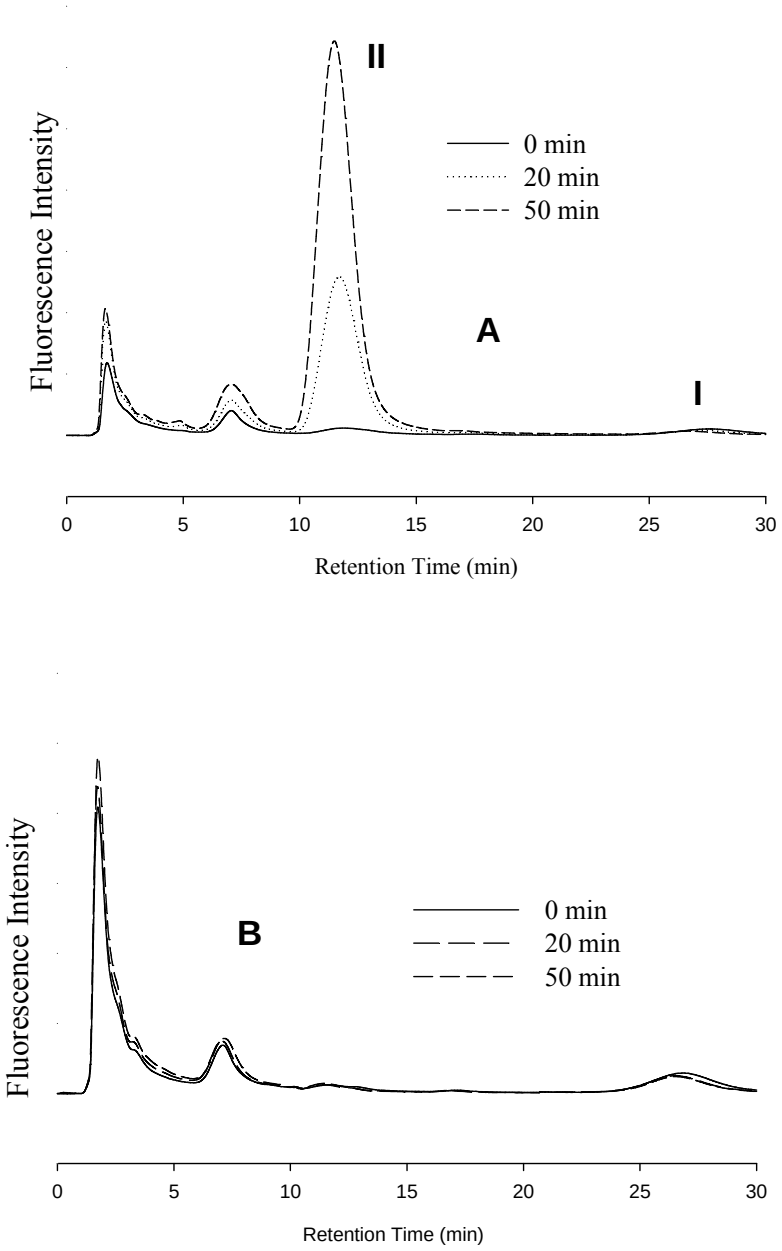

Figure 2.23 Application of **I**. Panel A: Formation of **II** in soybean PC liposome system incubated at 50 ˚C in the presence of 1 mM AIBN. $[O_2]$ = 180 μM, [**I**] = 28.4 μM and [PC] = 100 mM. HPLC conditions were as in Figure 2.5. Panel B: Control experiment performed under the same conditions, but in the absence of AIBN.

2.4 Discussion

The irreversible reaction of **I** with peroxyl radicals and other radical oxidants has two major consequences. First, because the reaction is stoichiometric (Figure 2.3A,B) and the product of these reactions (**II**) is reasonably stable, highly sensitive, quantitative measurements of the rates of oxidant formation can be obtained (Figures 2.3-2.5, 2.8, 2.17). Second, because the oxoammonium cation is not stable and rapidly decays to another species (Figure 2.5, 2.8), possible secondary oxidation reactions by the cation should be eliminated, thus precluding the formation of spurious secondary oxidation products.[53,110]

One disadvantage of this approach is that the peroxy radicals, unlike most carbon-centered radicals, do not form stable adducts with nitroxides (Scheme 2.1, Figures 2.3-2.5), and thus information on the structure of the peroxyl radical is lost. However, as shown here, lower concentrations of O_2 (or higher concentrations of **I**) can be employed to allow interception of the carbon-centered radicals by **I** prior to O_2 reaction, with the stable alkoxyamine products then generated providing information on structure (Scheme 2.1, Figure 2.17).[95-96] Further, changing the $[O_2]/[\mathbf{I}]$ ratio can allow discrimination between peroxyl radicals and other one-electron oxidants (Figure 2.17).

Another potential problem is the reduction of **I** to the hydroxylamine by certain compounds[95-96] and by cells[95-96] that also results in enhanced fluorescence. Although this problem should be alleviated to some extent by the use of low concentrations of **I**, it will likely limit the direct fluorometric detection in some cases. However, even in these cases,

HPLC analysis will still allow a clear discrimination among products (Figure 2.17),[78] and thus the selective detection of these radicals.

Due to its photo-bleaching by high intensity polychromatic light, **I** may not be applicable to the detection of radicals in many photochemical experiments. This potential drawback can be overcome by the use of 3-ap itself, following by derivatization with fluorescamine to form **II**, as will be discussed in Chapter III.

Chapter III Trace Determination of Peroxyl Radicals Employing 3-ap Followed by Fluorescamine derivatization

Abstract

Previously, 3-amino-2,2,5,5,-tetramethyl-1-pyrrolidinyloxy (3-ap) was shown to undergo an irreversible one-electron oxidation reaction by cyclic voltammetry (Chapter II). Here, it is also shown that unlike other amino-nitroxides, 3-ap undergoes a stoichiometric reaction with peroxyl radicals to generate a diamagnetic product. UV/Vis and mass spectrometric analysis suggests that following the formation of the oxoammonium cation of 3-ap, a proton is lost with concomitant nitroxide ring cleavage to form possibly a nitroso compound. It is further established that derivatization with fluorescamine of the electrochemical oxidation product of 3-ap, as well as the product of 3-ap reaction with peroxyl radicals leads to the formation of **II** (Figure 2.8). As 3-ap and its oxidation product are stable to high intensity polychromatic irradiation, 3-ap could be employed to determine the photochemical formation of peroxyl radicals upon irradiation of tap water with polychromatic light.

3.1 Introduction

Peroxyl radicals, formed by the rapid addition of molecular oxygen to carbon-centered radicals, not only play an important role in many pathological processes, chronic diseases

and aging by also serve as key intermediates in thermal and photochemical degradation of both natural and man-made materials in environmental systems.[9-20,54]

As discussed in Chapter I and II, quantitative detection of peroxyl radicals at low concentration level is challenging due to the lack of highly sensitive detection methods. Some of the recently developed prefluorescence probes,[74-75,95-96] including 3-apf (**I**), appear to be photo-sensitive and may not be applicable for detecting peroxyl radicals under high intensity polychromatic irradiation (>275 nm).

In Chapter II, we demonstrated that the photo-stable cyclic nitroxide, 3-amino-2,2,5,5,-tetramethyl-1-pyrrolidinyloxy (3-ap), undergoes a unique, irreversible electrochemical oxidation reaction by cyclic voltammetry. The initial oxidation product, when followed by immediate derivatization with fluorescamine, formed the same product (**II**) as the reaction of **I** reaction with peroxyl radicals. Thus it should prove possible to employ 3-ap to detect and quantify peroxyl radicals optically by HPLC analysis with fluorescence detection, as shown in Scheme 3.1:

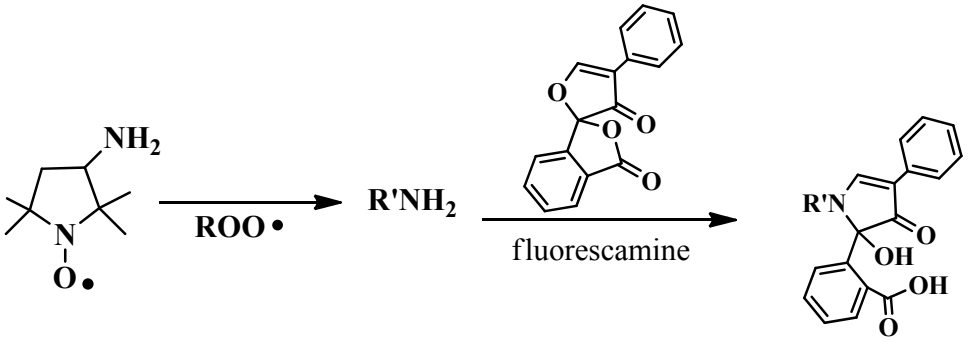

Scheme 3.1 Detection of photo generated peroxyl radicals using 3-ap as a probe.

Tang[111] performed preliminary work on the kinetics of nitroxide reaction with photo-generated peroxyl radicals in several model systems, including irradiation of sodium pyruvate and sodium nitrite/DMSO solutions (Scheme 3.2). Here we use thermolysis (Scheme 3.3) and radiolysis (reactions 3.1-3.4) to produce peroxyl radicals for study of the reaction with nitroxides. Analysis of the initial product of 3-ap oxidation was performed by UV/Vis spectroscopy and mass spectrometry. Finally, the preliminary application of 3-ap for the detection of peroxyl radicals generated by photo-irradiation of a natural water system is shown.

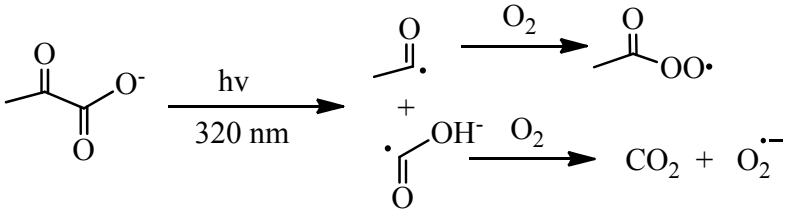

Photolysis of Pyruvate

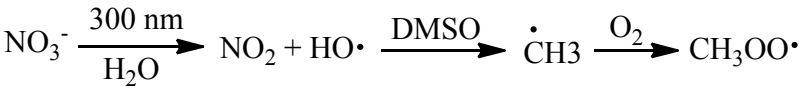

Photolysis of Nitrate

Scheme 3.2 Peroxyl radicals generated by photolysis

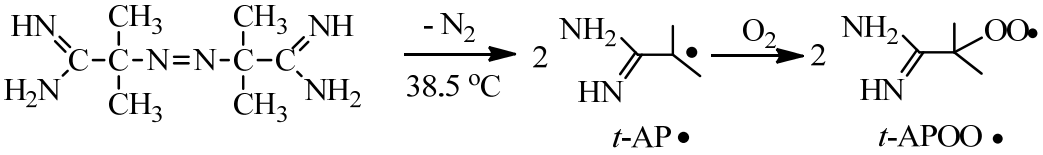

t-APOO generation: Thermolysis of 2,2'-azo-bis-(2-amidinopropane) dihydrochloride

Scheme 3.3 t-APOO radical generation by thermolysis of AAPH

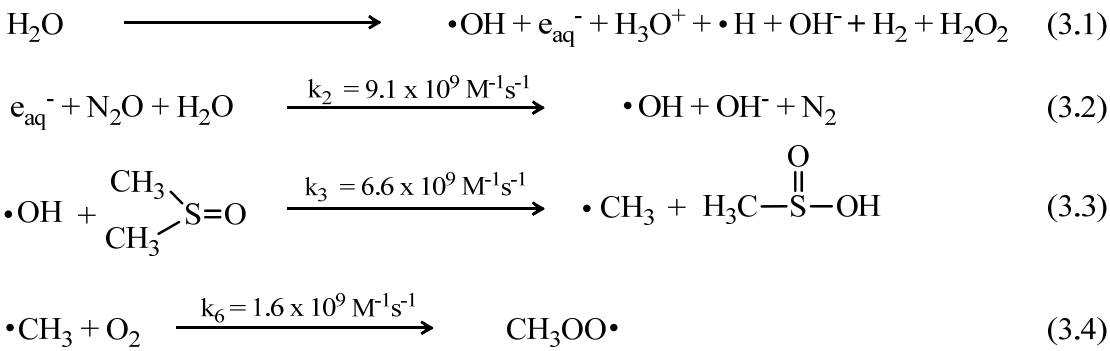

$$H_2O \longrightarrow \bullet OH + e_{aq}^- + H_3O^+ + \bullet H + OH^- + H_2 + H_2O_2 \quad (3.1)$$

$$e_{aq}^- + N_2O + H_2O \xrightarrow{k_2 = 9.1 \times 10^9\ M^{-1}s^{-1}} \bullet OH + OH^- + N_2 \quad (3.2)$$

$$\bullet OH + (CH_3)_2S{=}O \xrightarrow{k_3 = 6.6 \times 10^9\ M^{-1}s^{-1}} \bullet CH_3 + H_3C{-}S(=O){-}OH \quad (3.3)$$

$$\bullet CH_3 + O_2 \xrightarrow{k_6 = 1.6 \times 10^9\ M^{-1}s^{-1}} CH_3OO\bullet \quad (3.4)$$

3.2 Materials and Methods

3.2.1 Chemicals

Nitroxides (3-ap, 3-aminomethyl-2,2,5,5-tetramethyl-1-pyrrolydinyloxy (3-amp), 3-carbamoyl-2,2,5,5-tetramethyl-1-pyrrolidineoxy (3-cp) and 4-amino-2,2,6,6-tetramethylpiperidinyloxy (4-at)) and fluorescamine were purchased from Acros and Sigma Aldrich, respectively. 2,2'-Azo-bis-(2-amidinopropane) dihydrochloride (AAPH) was purchased from Cyman Chemical Co. Sodium phosphate (99.999%), sodium hydroxide were obtained from Aldrich. Sodium carbonate and sodium nitrite (99.99+%) was purchased from Sigma Aldrich. DMSO, HPLC grade methanol, acetonitrile and glacial acetic acid were all purchased from Fisher. Acetone was obtained from Sigma Aldrich. Nitrogen, air, oxygen and nitrous oxide were all from Airgas. All chemicals were used without further purification. Pure water for all experiments was obtained from a Millipore MilliQ system.

3.2.2 Thermolysis Thermolysis of AAPH was carried out in a 4 mL quartz cuvette in pH 7.4, 50 mM sodium phosphate buffer in a thermostated water bath at 38.5 ± 0.5 °C. The

stock AAPH solution (80 mM) was prepared daily and stored in an ice bath prior to thermolysis. Reactions were initiated by immersion of the reaction vessel in the water bath. Reactions were terminated by placing aliquots of the reaction mixture in a -20°C freezer for minimally 10 min. For anaerobic experiments, samples were purged for 20 min with N_2, with the headspace of the cuvette continuously purged with N_2 during thermolysis.

3.2.3 Steady State Radiolysis Steady state radiolysis was performed using a ^{60}Co source at room temperature. The dose rate was determined in each experiment using a Fricke dosimeter. 20 mM DMSO in 10 mM pH 7.4 phosphate buffer was saturated either with N_2O alone (to generate carbon centered radical) or with 80% N_2O/ 20% O_2 (to generate methyl peroxyl radical) in a Wheaton 5 ml serum vial. The vials were immediately sealed (while still purging) with a Wheaton rubber plug stoppers, which were then fastened by aluminum crimping tool.

3.2.4 Photolysis In polychromatic irradiation, samples were placed in a 1-cm cuvette and irradiated with a 300 W xenon lamp. The actinic light was first filtered through 22 cm MilliQ water and then through a 275 nm long pass filter to provide a light intensity of 150 mW/cm^2. In monochromatic irradiation experiments, a 1000 W xenon arc lamp was employed as light source. A Spectral Energy GM252 monochrometer was used to select irradiation light wavelength, with a bandpass of 10 nm. The irradiation intensity was determined with an IL 1700 radiometer. Samples were purged with N2 or oxygen for 10 min before irradiation while the headspace of the cuvette was continuously flushed during irradiation.

3.2.5 HPLC The reversed-phase HPLC system is consisted of a Gilson Model 811B dynamic mixer, an Eldex Model B-100S single piston pump, a 0-5000 psi pressure gauge, a Valco Model C10W injection valve. A 4 μm reversed phase C18 packing Nova-Pack column in a RCM 8×10 cm Waters radial compression module was employed for separation. The column temperature was maintained at 29 ^{0}C by a Buchi B-481 thermostat water bath. In most cases, the mobile phase was 65% sodium acetate buffer (50 mM, pH 4.0) and 35% methanol (v/v), with a flow rate of 1.0 ml/min. A Perkin Elmer 785A UV-Vis detector set at 390nm was employed. The fluorescence detector was a Hitachi Model L4870 set at 390 nm (excitation) and 490 nm (emission). A 125 μL sample loop was employed. OMS Tech Elab software was used for data acquisition and post run processing.

3.2.6 UV/Vis spectrophotometer A Hewlet-Packard 8452A diode array spectrophotometer was employed for all optical absorption measurements. All measurements were performed at room temperature except the AAPH thermolysis experiment.

3.2.7 Electron Paramagnetic Resonance A Bruker ESP300E EPR spectrometer was used to follow the nitroxide spin loss. Samples were drawn into 50 μL capillary tubes, sealed top and bottom with Critoseal, and placed within standard 3 mm ID quartz EPR tubes. Standard instrument settings were frequency 9.8 GHz; microwave power 9.4 mW; modulation amplitude 1.0 G. Spin levels were determined from areas obtained by double integration of the EPR spectra, as compared with the area obtained from known concentrations of 3-cp.

3.2.8 Derivatization with Fluorescamine

Bulk electrolysis of ~2 mM 3-ap, 3-amp and 4-at was performed with a 3-electrode system on a BAS CV-50W voltammetric analyzer in neutral pH buffer saturated with K_2SO_4. The voltage was 750 mV vs. Ag/AgCl and the electrolysis time was 90 min. A 10 mM fluorescamine solution in acetonitrile was added to the reaction mixture in a 1 ml centrifuge tube and vortexed for 1 min at room temperature. The pH of the solution was adjusted to 8.1 and fluorescamine was added in 5 to 10-fold molar excess relative to the product. **II** was then separated and purified by HPLC, followed by extraction with chloroform. **II** was dried under N_2 flow and stored in the freezer at -20°C until use.

3.2.9 Product Analysis by Mass Spectrometry The electrochemical oxidation product of 3-ap, together with the unreacted 3-ap, was extracted by chloroform at alkaline pH (~10) and was dried by flushing with N_2. It was stored at -20°C before subject to analysis. A JEOL AccuTOF-CS ESI-TOF mass spectrometer coupled with an Agilent 1100 HPLC module at the University of Maryland was also employed for part of the product analysis. The ESI spray voltage was 2.2 kV for positive ion mode and 2.0 kV for negative ion mode. Capillary temperature was 250°C. Mobile phase for the HPLC was 50/50 v/v ACN/water with a flow rate of 100 μL/min. The accurate mass data were determined by single ion mass drift correction of an internal standard compound.

3.3 Results

3.3.1 Reaction Stoichiometry and Kinetics

Two alkyl radicals (t-AP• and •CH_3) were produced by thermolysis of 1 mM AAPH under anaerobic conditions and gamma radiolysis of 20 mM DMSO solution saturated with N_2O, respectively (Scheme 2.2, reaction 2.1-2.3). Under aerobic conditions, these alkyl radicals were converted quantitatively to peroxyl radicals (t-APOO•; ~95%, reaction 2.6), owing to the high $[O_2]/[3\text{-ap}]$ ratios employed (varying from ~5 to 20), as well as to the higher reaction rates of carbon-centered radicals with O_2 (~2-4×10^9 $M^{-1}s^{-1}$) [102] as compared with the nitroxides (~1-8×10^8 $M^{-1}s^{-1}$).[43,94] EPR was then used to follow the spin loss of 3-ap under anaerobic and aerobic conditions to compare the reactivity of 3-ap with carbon centered and peroxyl radicals, respectively (Scheme 3.4).

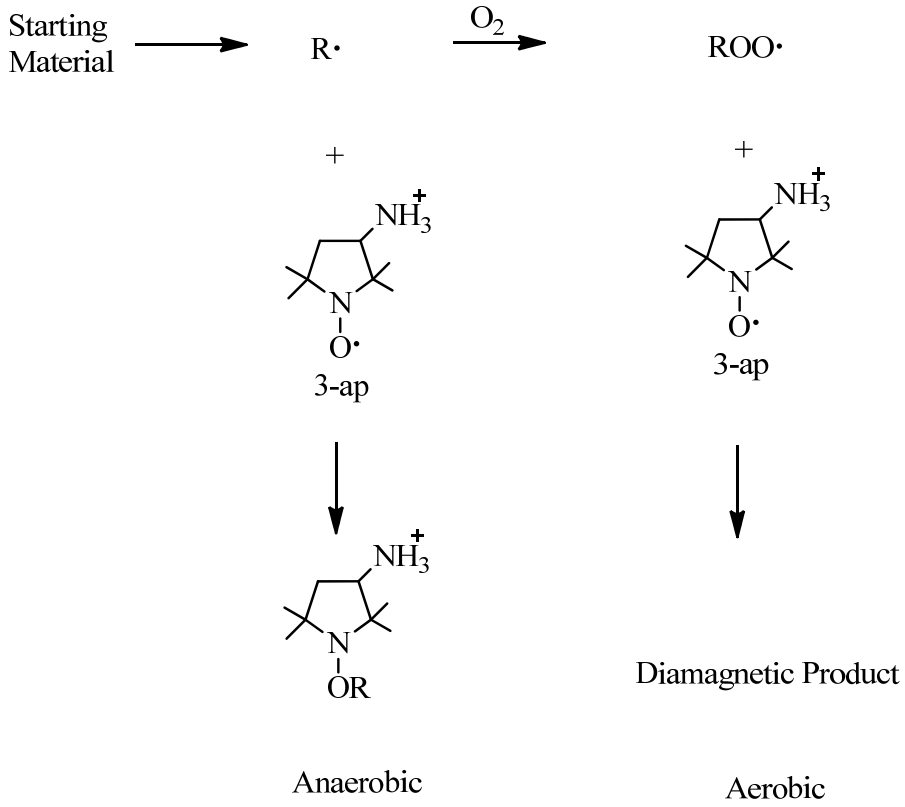

Scheme 3.4 Reaction of 3-ap with carbon-centered radicals to form the alkoxylamine product under anaerobic conditions and with peroxyl radicals to form diamagnetic product under aerobic conditions.

Similar to 3-apf (**I**), identical rates of spin loss were observed for 3-ap under N_2 and air during the thermolysis of AAPH (Figure 3.1A) and radiolysis of DMSO (Figure 3.1B), indicating that peroxyl radicals (t-APOO•, CH_3OO•) reacted with 3-ap to the same extent as their corresponding carbon centered radicals (t-AP•, CH_3•). We also observed that these rates were independent of [3-ap], showing that both carbon centered radicals (under N_2) and peroxyl radicals (under air) were reacting quantitatively with 3-ap. Because nitroxides are known to react irreversibly with carbon-centered radicals to produce stable alkoxylamine products at room temperature, [43,76-80,94] it can be concluded that 3-ap also reacts irreversibly with peroxyl radicals.

Other amino-nitroxides (3-amp and 4-at), like their fluorescamine-derivatized counterparts, exhibited much lower rates of spin loss in the presence than in the absence of air (Figure 3.1C, D), indicating a partially reversible reaction with peroxyl radicals. The lower rates of spin loss in air suggest partial regeneration of the nitroxyl moiety through reduction of the oxoammonium cation.[36-37,39,53] These results are consistent with the cyclic voltammetry results reported in Chapter II, Figure 2.8, and show further that the 1:1 stoichiometric reaction of 3-ap with peroxyl radicals (Figure 3.1) was unique among the amino-nitroxides examined.

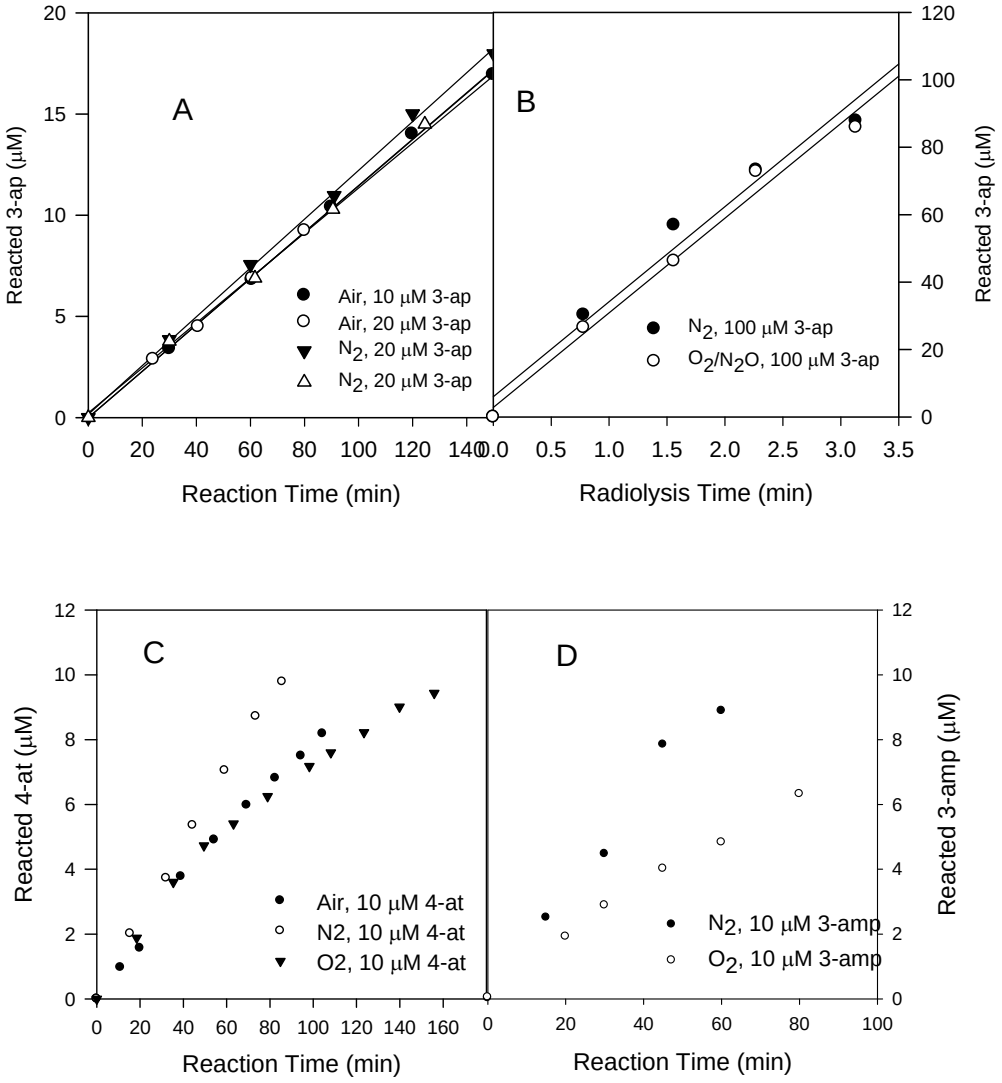

Figure 3.1. Time course for reaction of 3-ap, 3-amp and 4-at reaction with carbon-centered as companied with peroxyl radicals. Panel A: Time course for the reaction of 3-ap with t-AP• (under N_2) and t-APOO• (under air) generated by thermolysis of AAPH (1 mM) in 50 mM phosphate buffer, pH 7.4 at 38.5 ± 0.5 ˚C. $[O_2]$ = 210 μM at this temperature. Panel B: Time course for the reaction of 3-ap with CH_3• (under N_2O) and CH_3OO• (80% N_2O/ 20% O_2) generated by gamma radiolysis in 10 mM phosphate buffer, pH 7.4 contains [DMSO] = 20 mM, $[O_2]$ = 250 μM. Dose rate was 56.9 Gy/min. Panel C: Time course for the reaction of 4-at with t-AP• (under N_2) and t-APOO• (under air) in 50 mM phosphate buffer, pH 7.4. [4-at] = 10 μM. Panel D: Time course for the reaction of 3-amp with t-AP• (under N_2) and t-APOO• (under air) in 50 mM phosphate buffer, pH 7.4. [3-amp] = 10 μM. Other reaction conditions as in Panel A.

3.3.2 Product Analysis by UV/Vis and HPLC.

The bulk electrolysis products of several piperidinyl and pyrolidinyl nitroxides were analyzed by UV/Vis spectroscopy. A unique absorption pattern for 3-ap oxidation product was observed. The product, generated either by electrochemical oxidation or by reaction with radiolytically generated CH_3OO radical, showed increased absorption at 250 nm (Figure 3.2, Panel C and D). In constrast, the absorption at this wavelength decreased for the oxidation products of all other nitroxides such as 3-amp, 3-cp and 3-cap (Figure 3.2, Panel A, E and F), consistent with the formation of an oxoammonium cation for these nitroxides. For 4-at oxidation product, the absorption at 250 nm also decreased with a new absorption peak appeared at 300 nm, indicating that there is new species generated. In general, these results agree with the cyclic voltammetry results that neither bulk electrolysis nor reaction with peroxy radical give rise to a stable 3-ap oxoammonium cation, unlike other nitroxides. Rather, these results points to the possible formation of a nitroso compound (**IIIa** or **IIIb**) based on the absorption increase.[36] **IIIa** or **IIIb** is also consistent with the m/z 157 peak observed in mass spectrometry experiments (Figure 3.4).

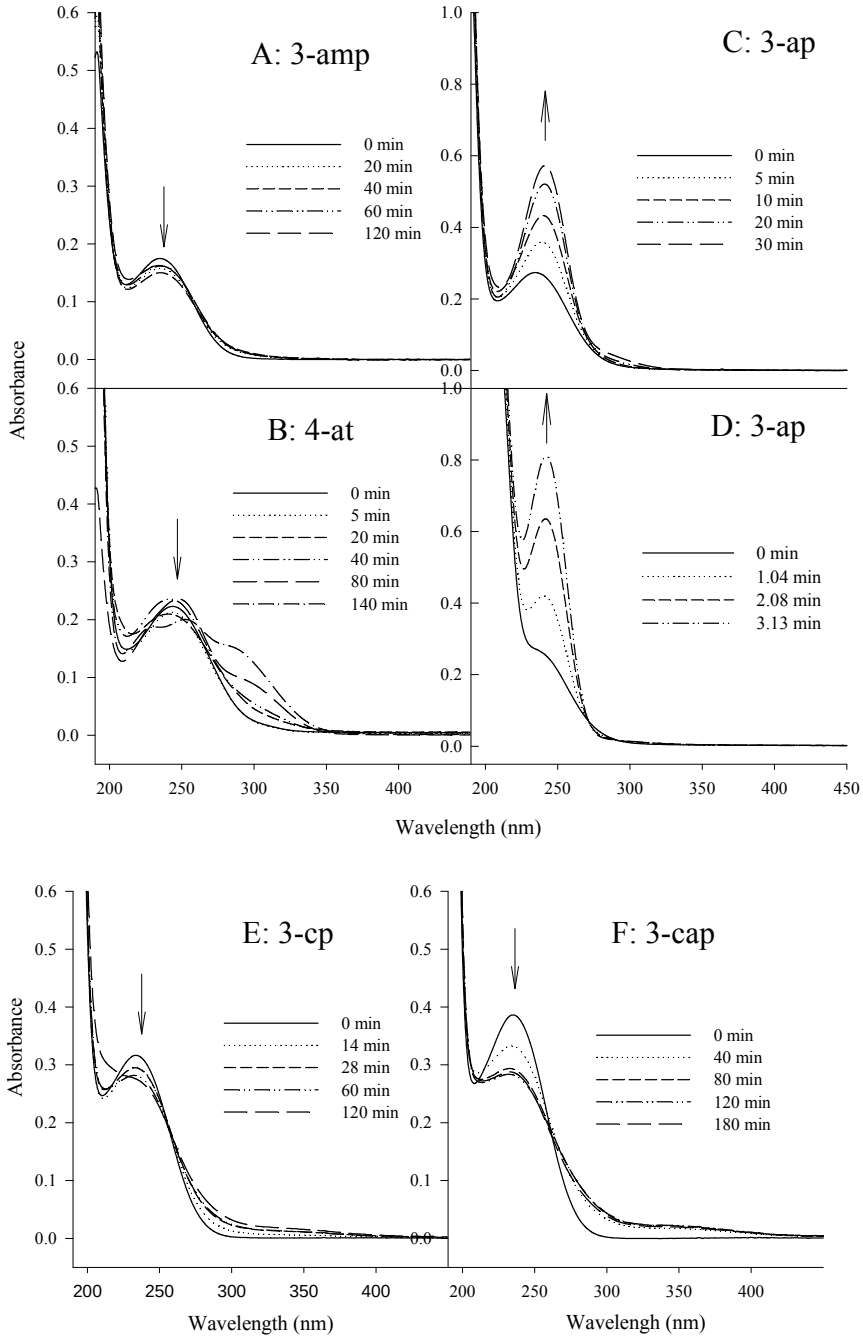

Figure 3.2. UV/Vis spectroscopy of oxidation products of 3-amp, 4-at, 3-ap (A-C); 3-cp, 3-cap (E-F) and the product of 3-ap reaction with methyl peroxy radical generated by radiolysis (D). The time in the inset indicates the electrolysis time (A-C, E-F) and irradiation time (D). Concentrations of the nitroxides are 1.5 mM in electrolysis. 3-ap reaction with methyl peroxyl radical ([3-ap]=100 μM, [DMSO]=1 mM) with the solution saturated with 80% N2O/20% O2 (v/v). Dose rate: 56.9 Gy/min.

The initial 3-ap electrochemical oxidation product, or the product of 3-ap reaction with peroxyl radicals, when followed by immediate derivatization with fluorescamine, formed product (**II**) (Figure 2.8). Although **II** was stable in aqueous solutions under neutral or alkaline pH for 12 h, it was observed that the initial 3-ap oxidation product (before derivatization), as detected chromatographically following fluorescamine derivatization to form **II**, was not completely stable in aqueous solution, but very slowly converted to a more polar, less fluorescent species as the time between formation and derivatization was increased (Figure 3.3).

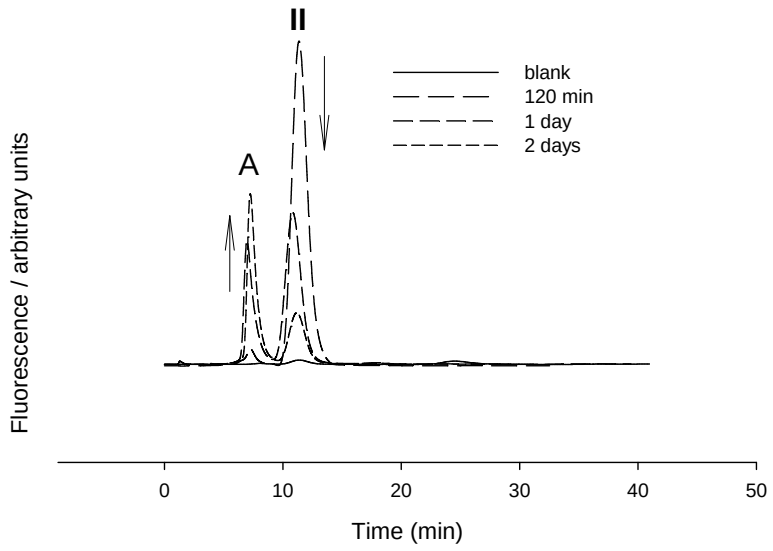

Figure 3.3 Time course for the conversion of the initial 3-ap oxidation product to its secondary product in pH 8.2 borate buffer at 4 ^{0}C. Samples were derivatized with fluorescamine immediately before HPLC analysis. The HPLC mobile phase was 65% sodium acetate buffer / 35% MeOH v/v. Excitation wavelength 390 nm, emission wavelength 490 nm. Injection volume was 125 µL.

3.3.3 Product Analysis by Mass Spectrometry

Analysis of the 3-ap electrochemical oxidation product by AccuTOF ESI MS revealed two major peaks at 157.134 and 118.083 after extraction with chloroform at pH 9, but only one major peak (m/z 118.083) after extraction at pH 12 (Figure 3.4).

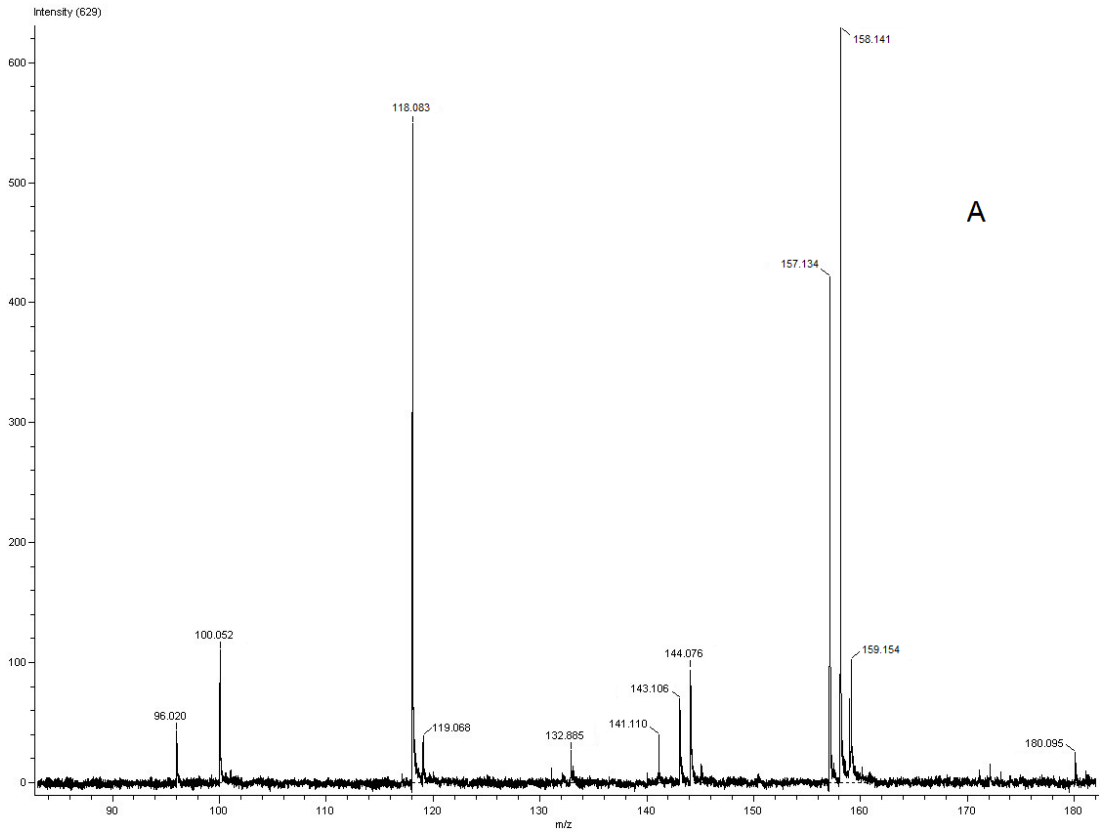
Intensity (629)
600
500
400
300
200
100
0
158.141
118.083
157.134
A
100.052
144.076
159.154
143.106
96.020
119.068
141.110
132.885
180.095
90
100
110
120
130
140
150
160
170
180
m/z

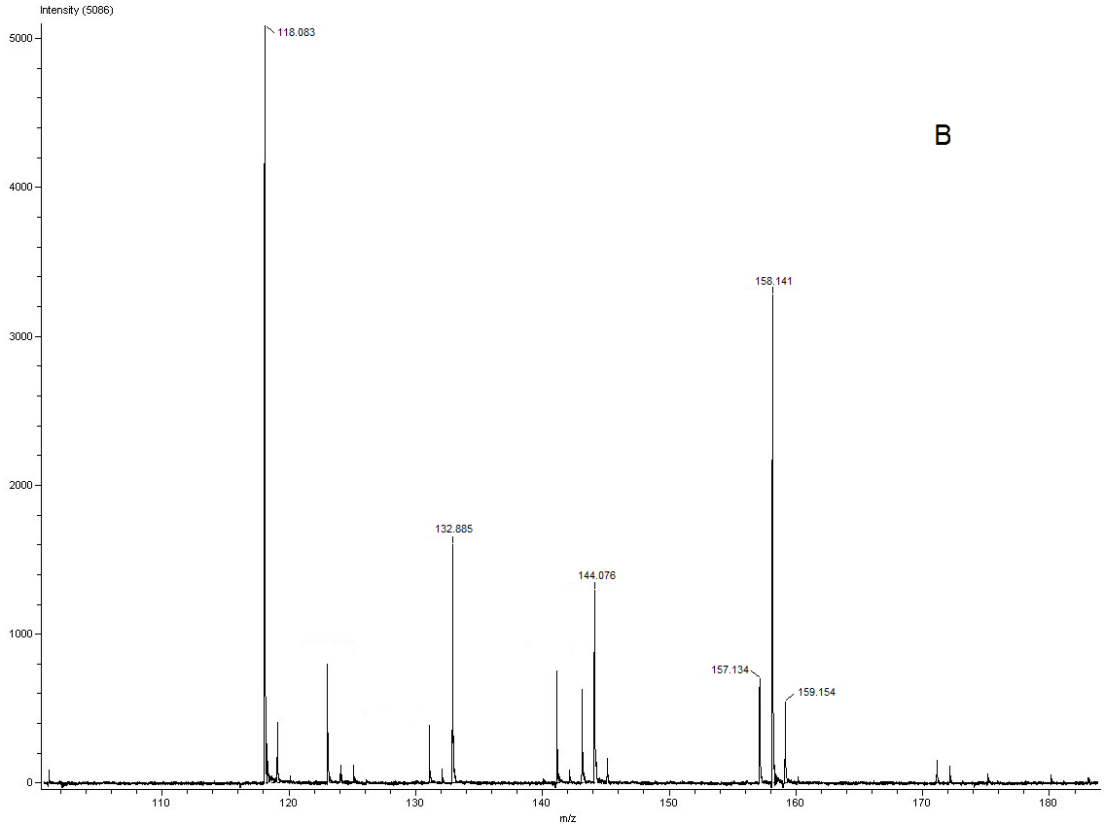

Figure 3.4. AccuTOF-CS ESI-TOF spectrum of the oxidation product of 3-ap alone after ~ 3h in solution at pH 9 (A) and pH 12 (B). 3-ap was oxidized by bulk electrolysis as described in materials and methods. Sample was extracted by chloroform and dissolved in 50/50 MeOH/H_2O before injected into MS. Needle voltage 2kV, orifice 1 voltage 15V, orifice 2 voltage 7V.

Ultra-high resolution FT-ICR mass spectrometry of the products of 3-ap extracted at pH 9 provided the molecular formula of these two species, $C_8H_{17}N_2O$ (M+H, 157.1335) and $C_5H_{12}NO_2$ (M+H, 118.0862). These results suggest that the oxoammonium cation of 3-ap first undergoes rapid ring cleavage and proton loss to form an initial product, either **IIIa** or **IIIb** (M+H, 157.1335) (Scheme 3.4), which subsequently converts at higher pH to a

secondary product in the absence of derivatization with fluorescamine; this product was tentatively identified as **IV** (M+H: 118.0862, $C_5H_{12}NO_2$; see Scheme 3.5).

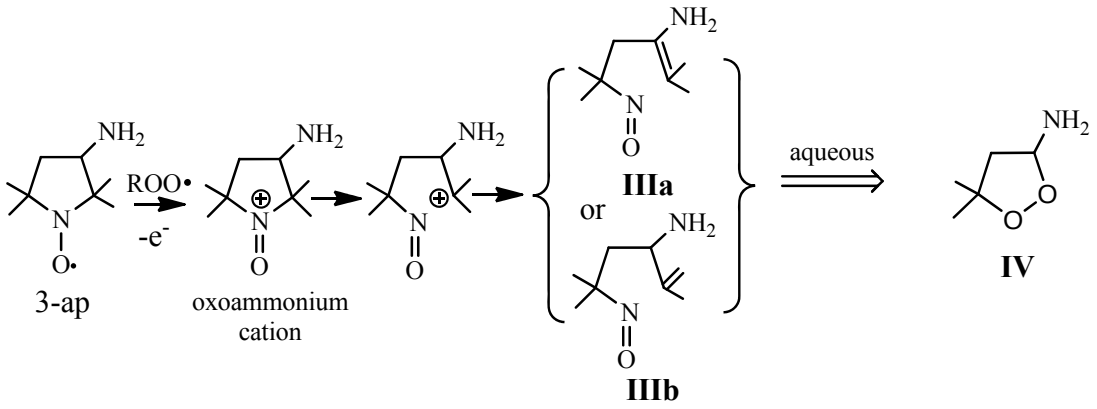

Scheme 3.5 Proposed reaction mechanism of 3-ap oxidation reaction

Although the exact mechanism of **IV** formation is not presently obvious to us, the structure of **IV** is consistent with the ring structure proposed for **V** (Scheme 2.4, Chapter II), based on high resolution mass spectrometry and extensive NMR analysis.

3.3.4 Thermal and Photo Stability. The photo-stability of 3-ap and its initial electrochemical oxidation product was tested under polychromatic photo-irradiation. It was found that both 3-ap and its oxidation product were stable within the experimental time scale (60 min) as shown in Figure 3.5. The thermal stability of both species was tested under 50 °C with no observable loss by UV/Vis spectroscopy (Figure 3.6).

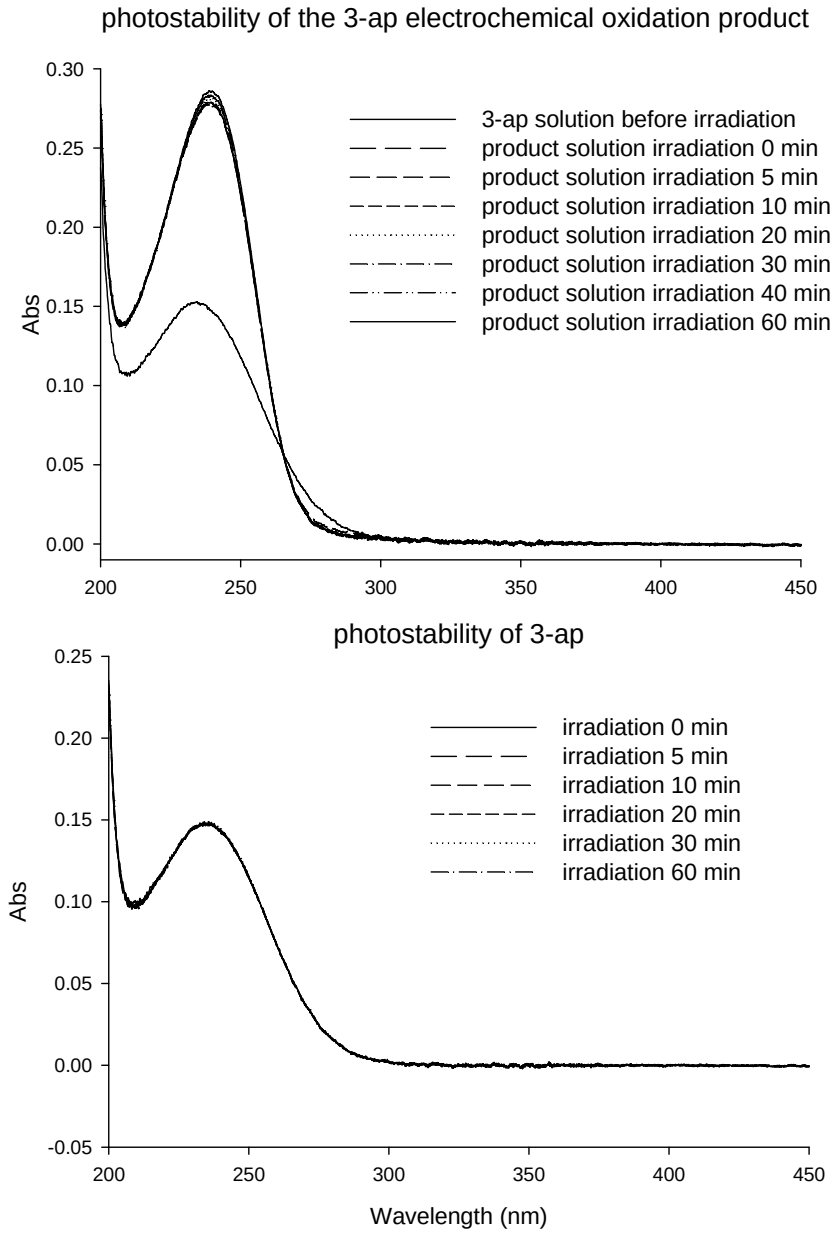

Figure 3.5 Photo-stability of 3-ap and its electrochemical oxidation product under polychromatic irradiation. The actinic light from a 300 W Xe Arc lamp was first filtered through 22 cm MilliQ water and then through a 275 nm long pass filter.

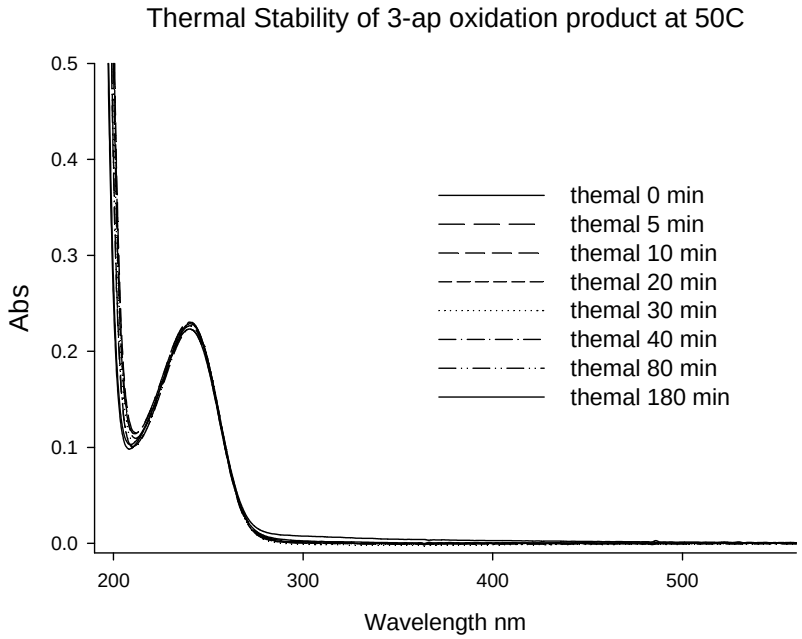

Figure 3.6 thermal stability of 3-ap electrochemical oxidation product under 50℃ in phosphate buffer, pH 7.4.

3.3.5 Preliminary Applications.

It has been established that 3-ap undergoes stoichiometric reaction with peroxyl radicals to form a product that converts to **II** upon derivatization with fluorescamine. Photochemical formation of peroxyl radicals was observed upon irradiation of tap water with polychromatic light. Since **I** was not stable under these conditions, 3-ap was used to detect the generation of peroxyl radicals, with the product immediately derivatized with fluorescamine at pH 8.1 (Scheme 3.1). Formation of **II** increased with increasing irradiation time from 180 nM at 60 min to 250 nM at 90 min (Figure 3.7A). **II** was not formed when Milli-Q water was irradiated in the presence of 3-ap (Figure 3.7B) nor when tap water was irradiated in the absence of 3-ap (Figure 3.7C). To test for the presence of

other oxidants, tap water was irradiated under anaerobic conditions and the generation of alkoxylamine products was determined chromatographically. Consistent with prior work[24], acetyl and methyl alkoxylamines were identified as the major products, with their total concentration increasing from 130 nM at 60 min to 200 nM at 90 min. This significantly lower yield of the alkoxylamine products relative to **II** suggests the presence of additional oxidant or oxidants.

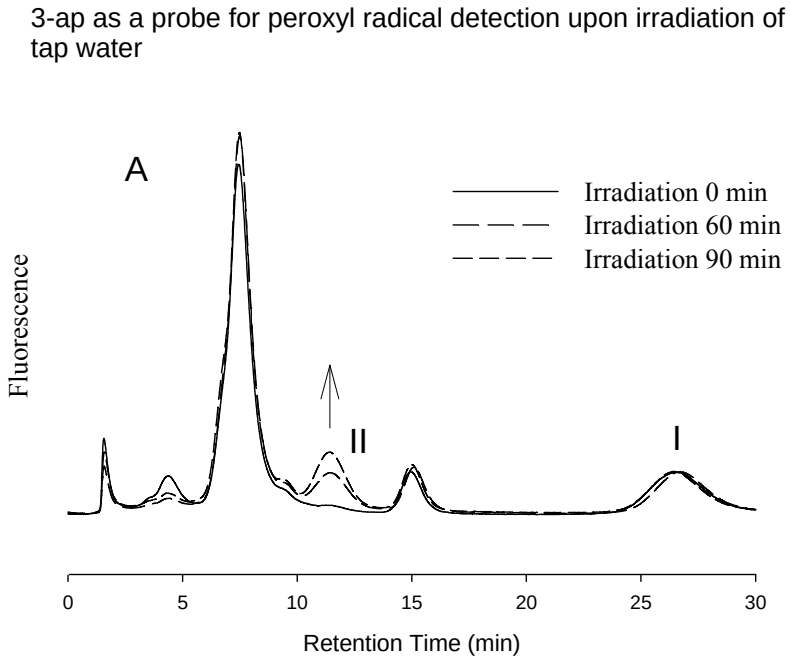

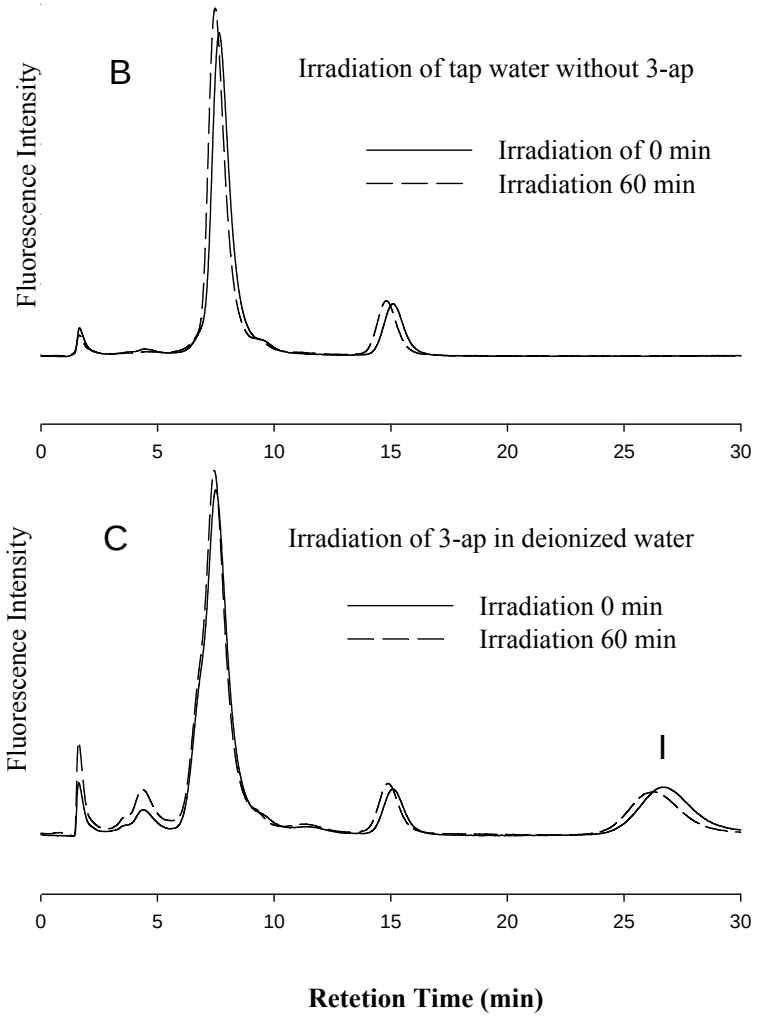

Figure 3.7 Panel A: Peroxyl radical detection in irradiated tap water using 3-ap as a fluorescence probe. Peak A is the product and peak B is 3-apf. 3-apf concentration: 10 μM. Irradiation conditions as described in methods section. The HPLC mobile phase was 65% sodium acetate buffer / 35% MeOH v/v. Excitation wavelength 390 nm, emission wavelength 490 nm. Injection volume was 125 μL. Panel B is irradiation of tap water in the absence of 3-ap; Panel C is irradiation of 3-ap in deionized water. HPLC conditions are the same as in Panel A. In all panels, **I** refers to fluorescamine-derivatized 3-ap and **II** refers to fluorescamine-derivatized 3-ap oxidation product.

3.4 Concluding Remarks

It has been established in this chapter that 3-ap reacts stoichiometrically with peroxyl radicals. Similar to **I**, oxoammonium cation of 3-ap is not stable and rapidly decays to a product that is relatively stable. Mass spectrometric analysis indicated that 3-ap reaction with peroxyl radicals give rise to an initial product that is consistent with **IIIa** or **IIIb** (Figure 3.4), which, upon derivatization with fluorescamine produces **II**, the same product observed upon direct reaction with **I** (Chapter II). Due to the formation of **II** by immediate derivatization of 3-ap oxidation product, highly sensitive determination of peroxyl and other oxidants formation can be obtained. Unlike **I**, 3-ap can be employed in high intensity polychromatic irradiation experiments because both 3-ap and its oxidation product are stable toward photo-irradiation.

Chapter IV Summary and Future Work

Summary

A novel and highly sensitive method for the quantitative determination of low concentrations of peroxyl and other radical oxidants produced in biological and environmental model systems was presented in this thesis. This approach utilizes stable nitroxide radicals as optical switches. By covalently coupling a nitroxide at a short distance from a chromophore, fluorescence emission from the chromophore can be largely quenched. Upon reaction of the nitroxide moiety with radicals to form diamagnetic products, the intramolecular quenching pathway is eliminated and fluorescence emission is greatly enhanced, thereby allowing radicals to be detected and quantified.

To obtain quantitative information of the generation of peroxyl radicals, an ideal probe has to react with peroxyl radicals stoichiometrically. In this research, the stoichiometry of peroxyl radicals with several pre-fluorescent nitroxide probes, synthesized by reaction of amino nitroxides (3-amino-2,2,5,5,-tetramethyl-1-pyrrolidinyloxy (3-ap) 3-aminomethyl-2,2,5,5-tetramethyl-1-pyrrolydinyloxy (3-amp), and 4-amino-2,2,6,6-tetramethylpiperidinyloxy (4-at)) with fluorescamine, was studied. All these probes undergo partially reversible reactions with peroxyl radicals except 3-ap-fluorescamine (**I**). Upon **I** reaction with peroxyl radicals, a more highly fluorescent diamagnetic product (**II**) was generated, which is stable in aqueous solutions at neutral or

alkaline pH. Therefore, **I** was selected as a potentially highly sensitive and versatile probe to determine oxidant production optically (Chapter II). 3-ap alone was also shown to react with peroxyl radicals stoichiometrically while other nitroxides undergo partially reversible reaction with peroxyl radicals (Chapter III).

The structure of **II** was analyzed in order to elucidate the possible reaction mechanism. Synthesized by derivatization of the electrochemical oxidation product of 3-ap with fluorescamine, **II** was first characterized by FT-ICR MS following HPLC purification. Dominant peaks at m/z 395.16013 and 393.14564 were observed in positive and negative ion mode, respectively, corresponding to a molecular formula of $C_{22}H_{22}N_2O_5$ (predicted masses: 395.16015 in positive mode and 393.14560 in negative mode). NMR analysis of **II** was not successful due to its instability in organic solvents. To resolve this issue, the electrochemical oxidation product of 3-ap was reacted with benzoyl chloride to form the stable amide (Scheme 4.1). Following HPLC purification, this product was identified as the cyclic peroxide **V** (Scheme 4.1) as established by FT-ICR MS (Figure 2.12) and extensive NMR analyses (Chapter II, Appendix I). Analysis by AccuTOF ESI MS of the electrochemical oxidation product of 3-ap revealed two major peaks at 157.134 and 118.083 after extraction with chloroform at pH 9 (Figure 3.4). Based on these results, we proposed the reaction pathways as in Scheme 4.1 below:

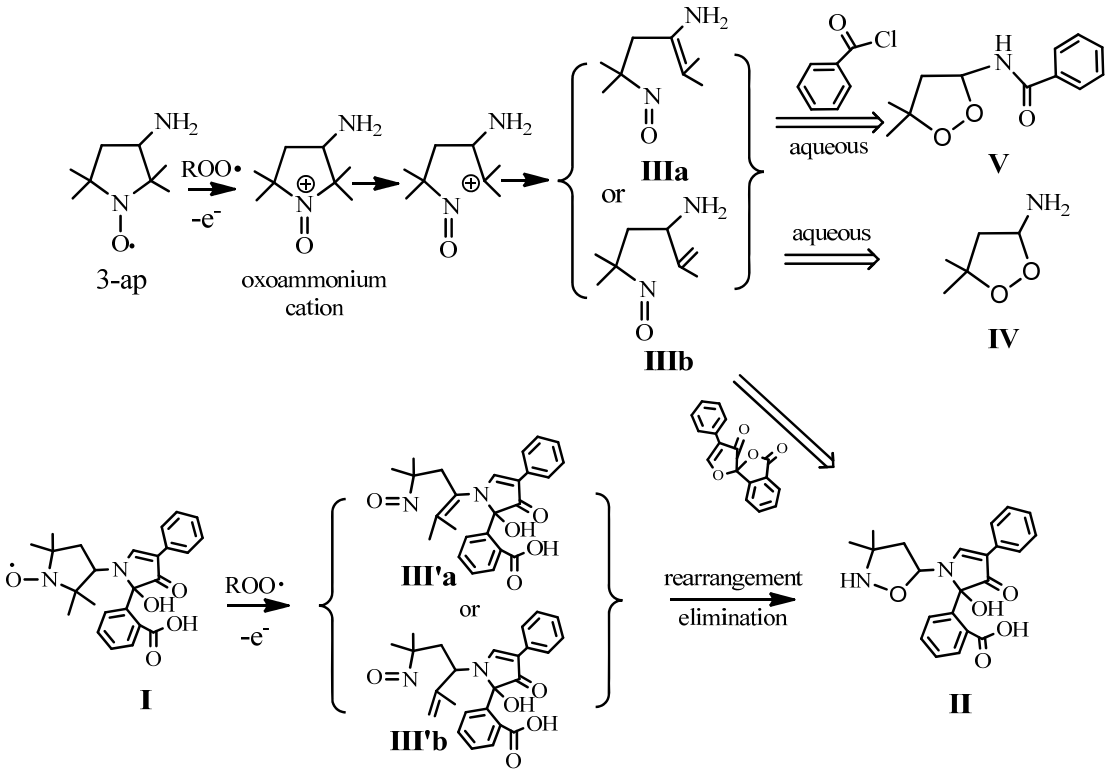

Scheme 4.1 Proposed reaction mechanisms for 3-ap/**I** oxidation reaction, either by reaction with peroxyl radicals or by electrochemical oxidation.

Our results indicate that other radicals capable of oxidizing **I** to the oxoammonium cation will also generate **II** (Figure 2.16) and thus will also be detected. However, by changing the $[O_2]$/[nitroxide] ratio, we showed that peroxyl radicals can be detected and quantified preferentially in the presence of other radical oxidants, such as $\bullet NO_2$ and $CO_3^{\bullet-}$.

To achieve reliable quantitative detection of peroxyl radicals, stability of the pre-fluorescent probes and the product was tested under a range of experimental conditions. **I** and **II** were stable for 12 or more hours in aqueous solution over a broad range of conditions, including pH ranging from 4 to 10 and temperatures up to 50°C. Although **I**

was stable under monochromatic photo-irradiation, significant photo-degradation was observed for **I** and **II** under polychromatic irradiation. These results indicate that while **I** can be employed in thermal systems, it will not be suitable generally for photochemical studies (Chapter II). In contrast, 3-ap and the 3-ap oxidation product were stable at pH 6-8 under either thermal (up to 38.5 ˚C) or irradiation conditions over time scales extending to 90 min (Chapter III).

The use of **I** to quantitatively determine the formation rate of peroxyl radicals generated by thermolysis and radiolysis of simple model systems was demonstrated (Chapter II). Since both **I** and **II** were stable in these systems, the production of **II** should provide a reliable measure of peroxyl radical accumulation. Concentrations of **II** as low as 3 nM was detected by HPLC analysis with fluorescence detection using a 125 μL injection loop, while a detection limit of ~0.35 μM for direct fluorometric detection was achieved. The sensitivity for HPLC analysis could be easily improved by using a larger injection volume. For the detection of photochemically generated peroxyl radicals, 3-ap was employed.

This approach has been employed in preliminary applications to determine the thermal production of peroxyl radicals in an aqueous dispersion of soybean phosphatidylcholine (PC) liposomes (Chapter II). A water-insoluble azo compound, 2,2'-azo-bis-isobutyronitrile (AIBN), was used to initiate autoxidation of the

polyunsaturated fatty acids within the PC liposomes via incubation at 50 ^{0}C under air. Analysis of the reaction mixture by HPLC showed that **II** increased with increasing incubation time from 2.9 μM at 20 min to 7.4 μM by 50 min. Detection of photochemically produced peroxyl radicals was achieved by employing 3-amino-2,2,5,5,-tetramethyl-1-pyrrolidinyloxy (3-ap) alone, followed by derivatization with fluorescamine. Formation of **II** increased with increasing irradiation time from 180 nM at 60 min to 250 nM at 90 min. Under anaerobic conditions, significantly lower yield of the alkoxylamine products relative to **II** was obtained, suggests the presence of additional oxidant or oxidants.

Future Work

Based on this work, the method described in this thesis should be broadly applicable to the determination of the formation of peroxyl and other radical oxidants in other biologically or environmentally related systems. The unequivocal direct structural identification of **II** would provide key information about the mechanisms of 3-ap reaction with peroxyl radicals and deserves further study. The reaction of other amino nitroxides with peroxyl radicals is also worth futher investigation. Another interesting topic to continue is study of the photochemical degradation of 4-atf and 3-ampf under anaerobic and aerobic conditions.

Determination of production of peroxyl radicals in cell culture.

I has been shown to be able to determine the peroxyl radical generation in aqueous dispersion of soybean phosphatidylcholine (PC) liposomes, a commonly adopted model for cell membrane. Due to the relatively high rate constant for **I**/3-ap reaction with peroxyl radicals, low concentrations of **I**/3-ap could be used for peroxyl radical detection. This will help preclude reaction of **I**/3ap with highly reactive radicals such as OH and RO radical. The bioreduction of **I**/3-ap could be a potential problem in cell culture; however, by employing HPLC separation, the formation of **II** can still be determined without interference from the hydroxylamine derivatives.

Unequivocal Structure Identification of II.

Due to the instability of **II** in organic solvents examined, and its low solubility in D_2O, the direct NMR analysis of **II** was not possible. Benzoyl chloride was used to derivatize the 3-ap oxidation product to form a stable amide (**V**) which was successfully characterized by 1D and 2D NMR. However, the structure of the nitroxide moiety in **V** is not consistent with the structure in **II** which was analyzed by high resolution mass spectrometry. To resolve this inconsistency, its vital that the direct structure analysis of **II** be performed, either by finding a suitable solvent, or by using a different reagent to derivatize 3-ap oxidation product.

Reactions of other nitroxides with peroxyl radicals.

Although previous research has been conducted regarding the reaction mechanisms of peroxyl radical reaction with nitroxides, it is still not completely resolved as to why **I**/3-ap

undergoes different reaction schoichiometry from that of other nitroxides, considering the similarity of the structures of these nitroxides. It could be insightful to study how different ring substitutes will affect the reaction, and/or investigate the redox potentials for these nitroxides. These studies would hopefully provide useful information regarding the different reaction mechanisms of nitroxide-peroxyl radical reactions.

Photo induced reduction or oxidation of fluorescamine-derivatized nitroxides.

The photo induced redox reaction of fluorescamine-derivatized nitroxides under both anaerobic and aerobic conditions appears to be a very interesting research topic based on the preliminary studies on **I**, 3-ampf, 4atf and a non-radical analogue, CH_3-fluorescamine (**VI**), as shown in Appendix III. It appears that depending on the structure of the nitroxide moiety, fluorescamine-derivatized nitroxides were observed to form different photo-degradation products, based on the UV/Vis absorbance spectra of these products. At the presence of nitroxides, the photo-bleaching of CH_3-fluorescamine was precluded until the nitroxide was consumed. Further investigation of the possible mechanisms of these photodegradation reactions should provide valuable information regarding the electron or charge transfer processes in these molecules.

Appendix I

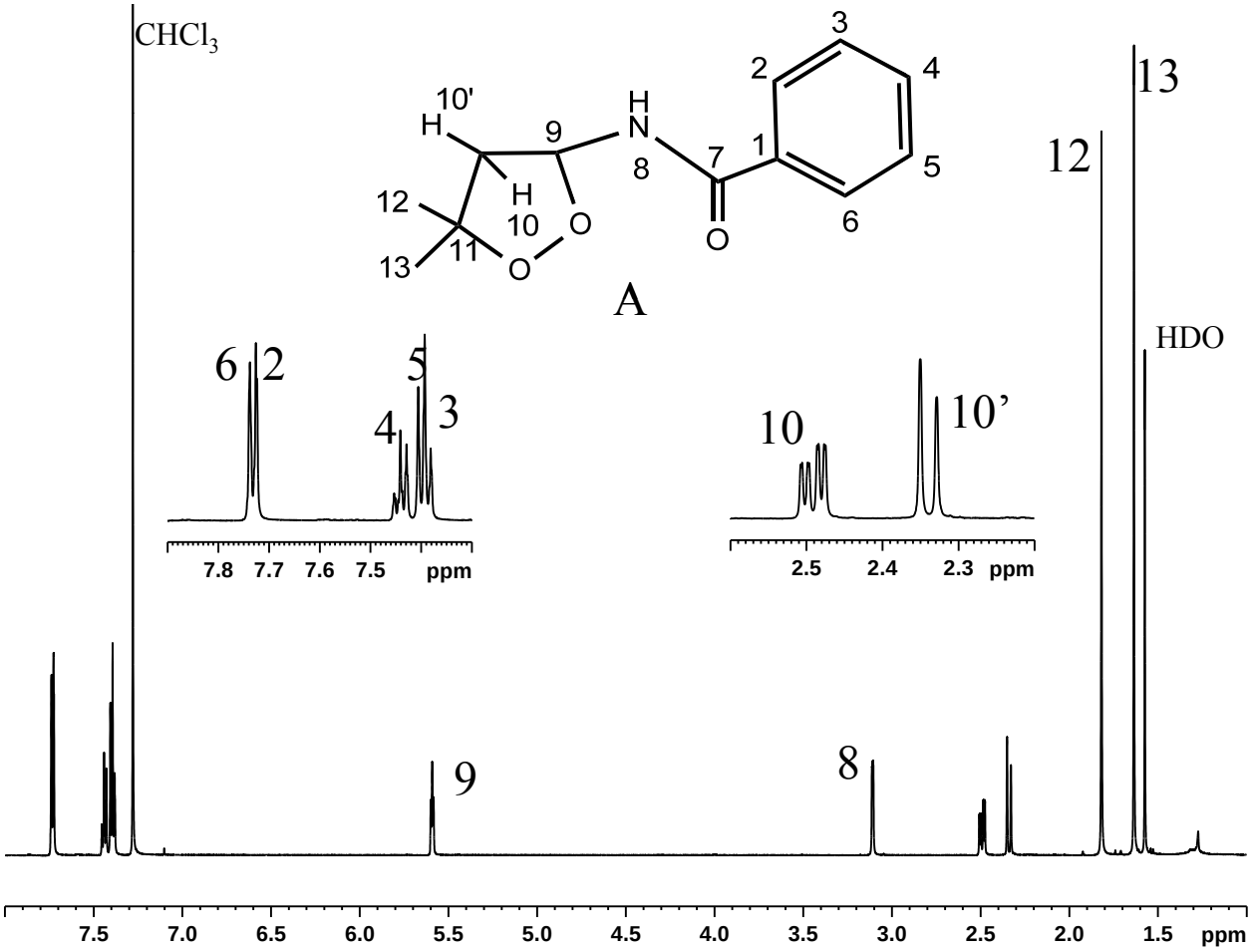

Fig. A1. 1D H-1 at 600MHz. NMR signal assignments shown in structure A.

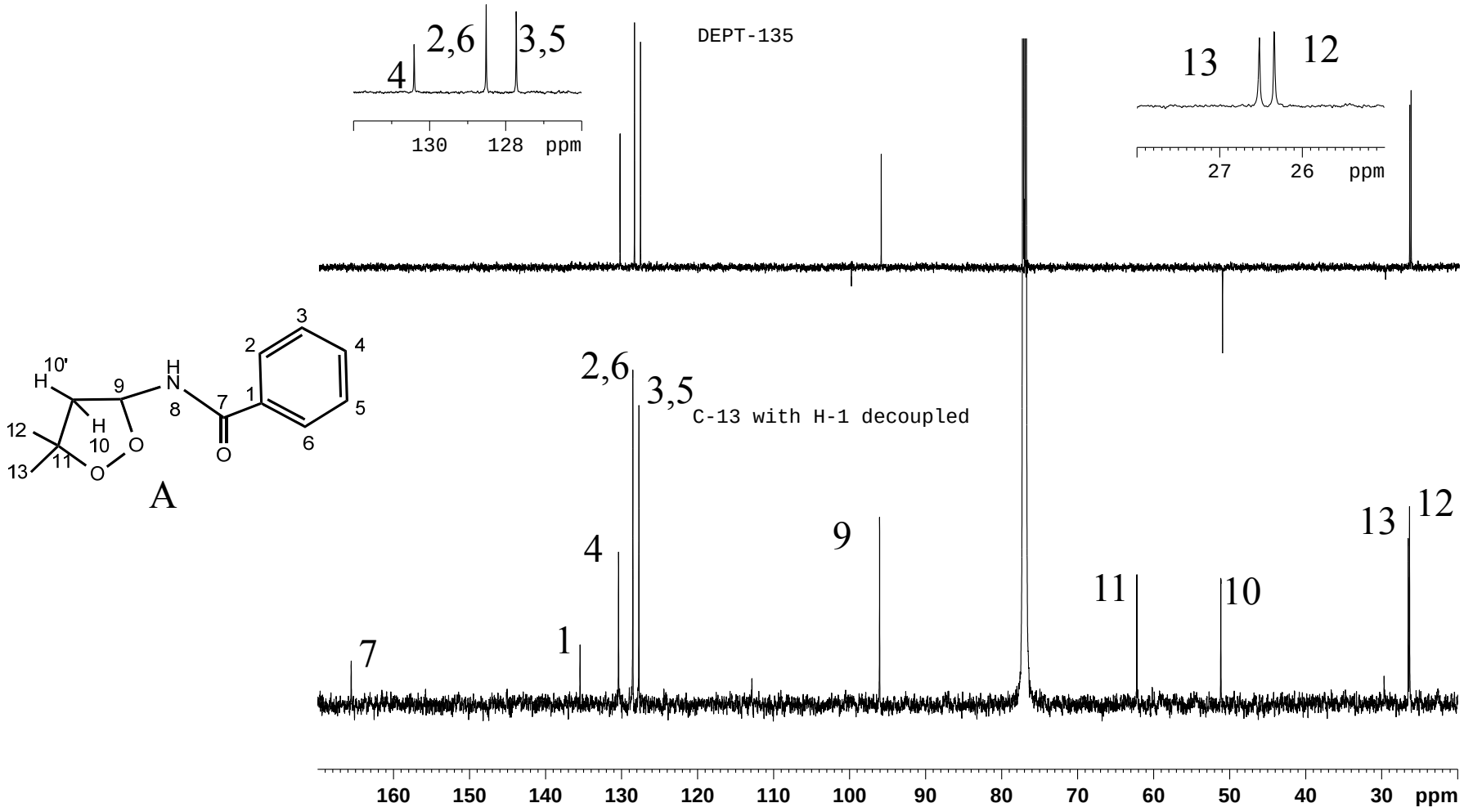

Fig. A2. C-13 with H-1 decoupled (lower trace) and C13-DEPT-135 (top trace) at 150MHz C-13 of Structure A.

gs-DQ-COSY

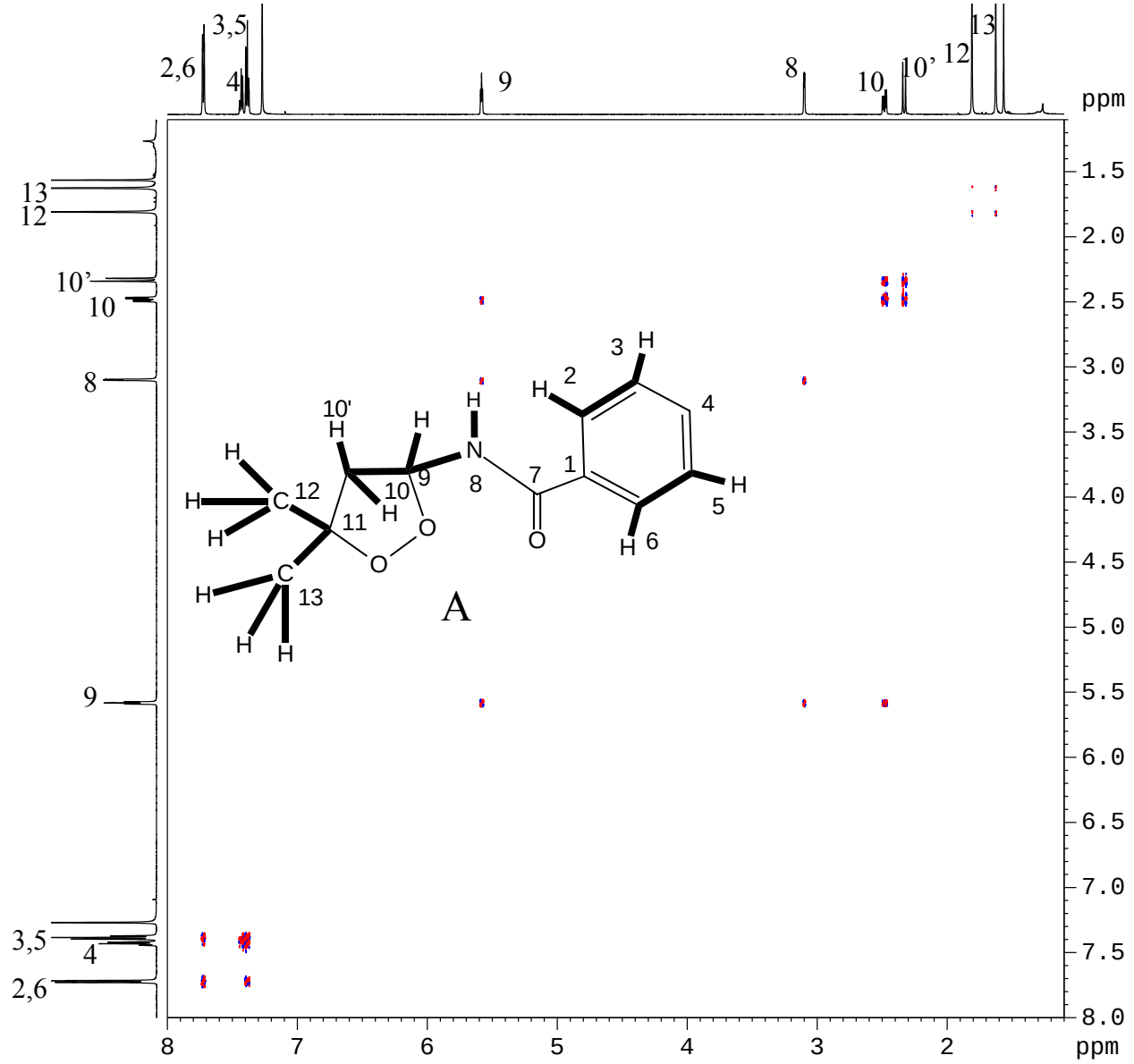

Fig. S11. 600MHz Double quantum filtered H-1 COSY with gradient selection. Bold lines in Structure A indicates the observed correlations.

gs-DQ-COSY

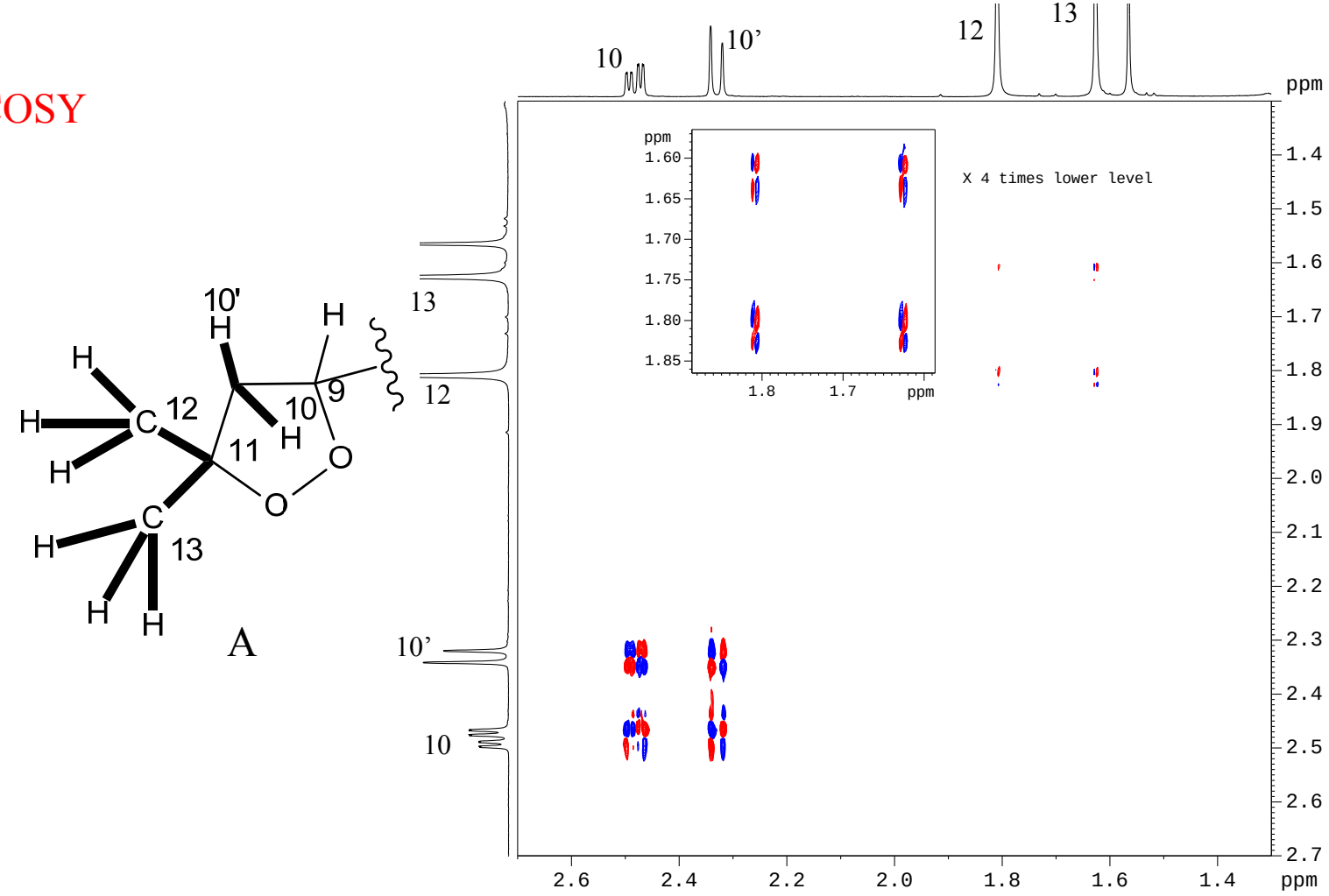

Fig. A4. Aliphatic region, expansion of 600MHz Double quantum filtered H-1 COSY with gradient selection. Bold lines in Structure A indicates the observed correlations.

NOESY

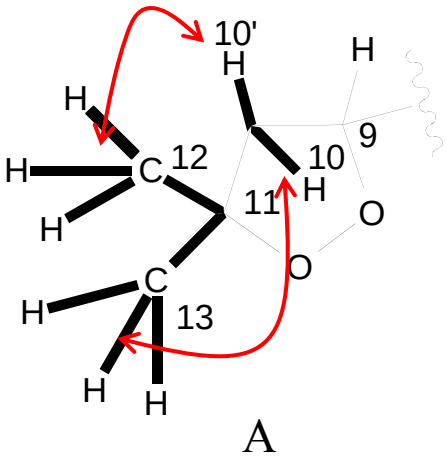

A

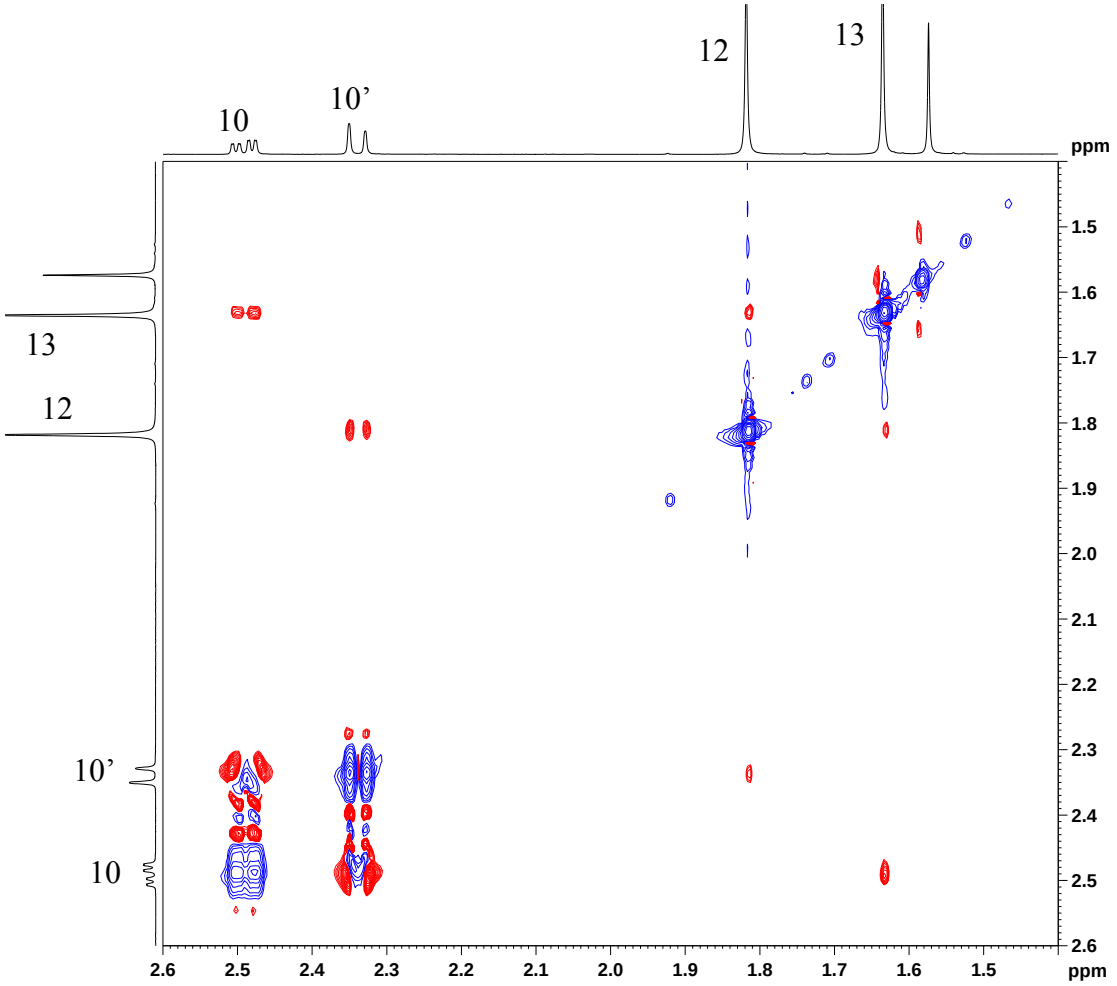

Fig. A5. Aliphatic region, expansion of 600MHz f H-1 NOESY with gradient selection. Red correlation peaks are positive phased NOE, blue contours are negatively phased for auto-correlation peaks.
Red arrow in Structure A indicates the observed NOE.

gs-DQ-COSY

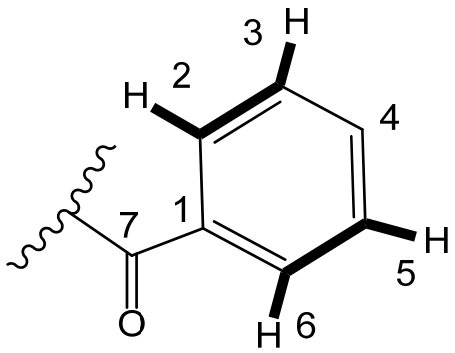

A

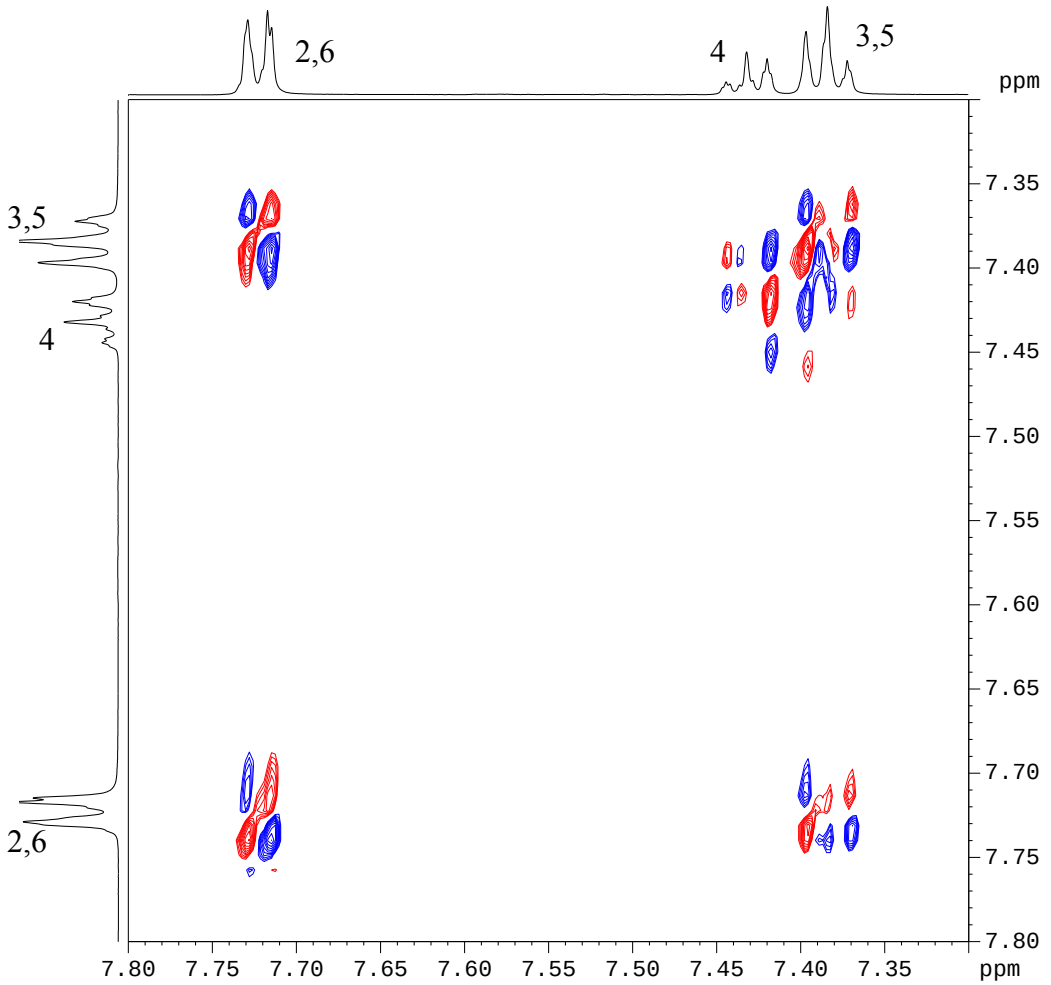

Fig. A6. Aromatic proton region, expansion of 600MHz Double quantum filtered H-1 COSY with gradient selection. Bold lines in Structure A indicates the observed correlations.

gs-
HSQC

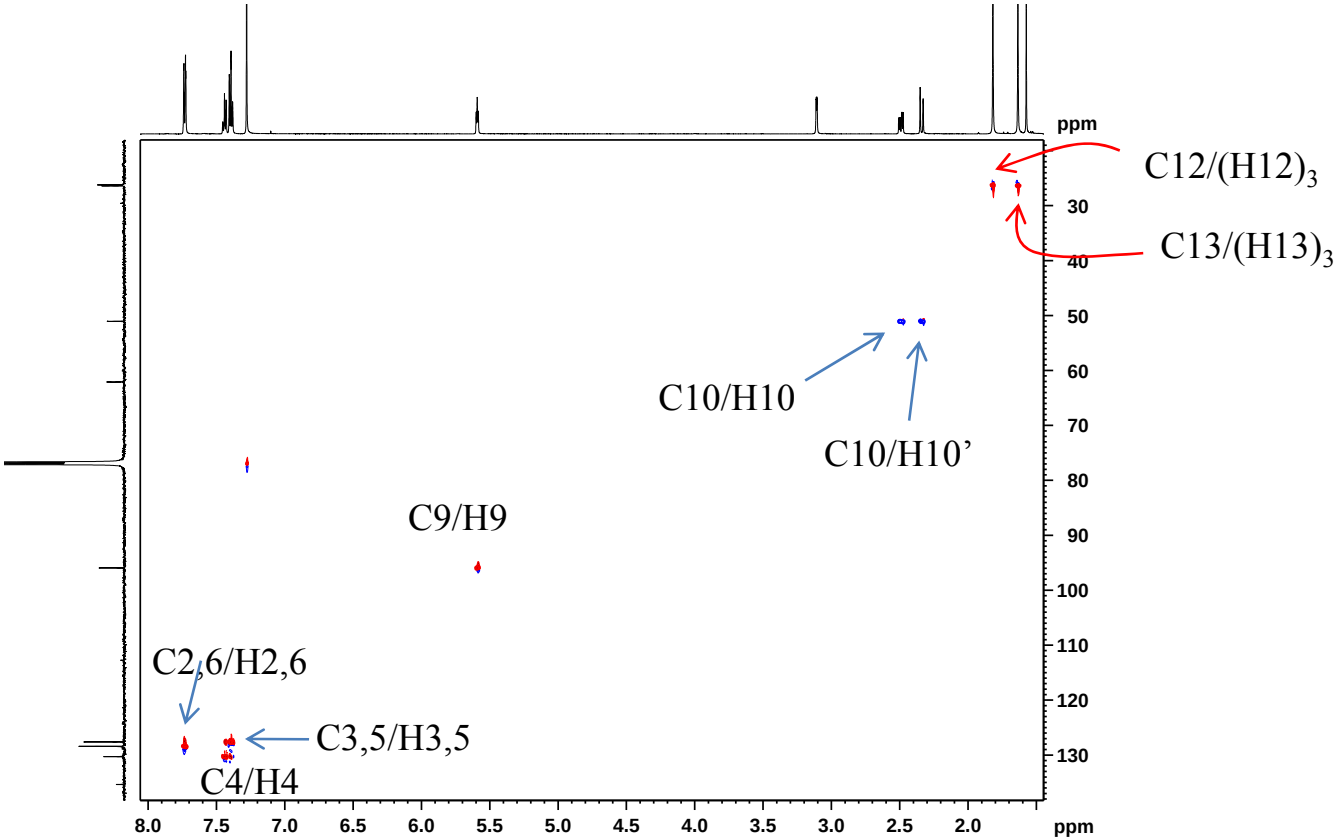

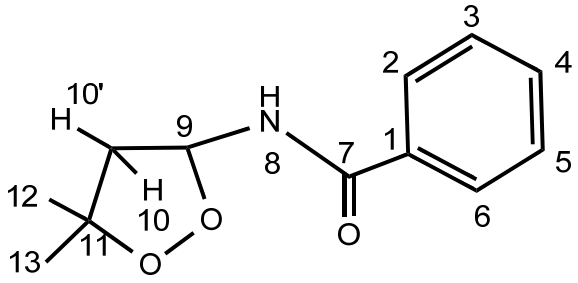

Fig.A7. Full range contour plot of gs-HSQC of structure A, region expansions and signal assignments are shown in the following figures 16 & 17.

gs-
HSQC

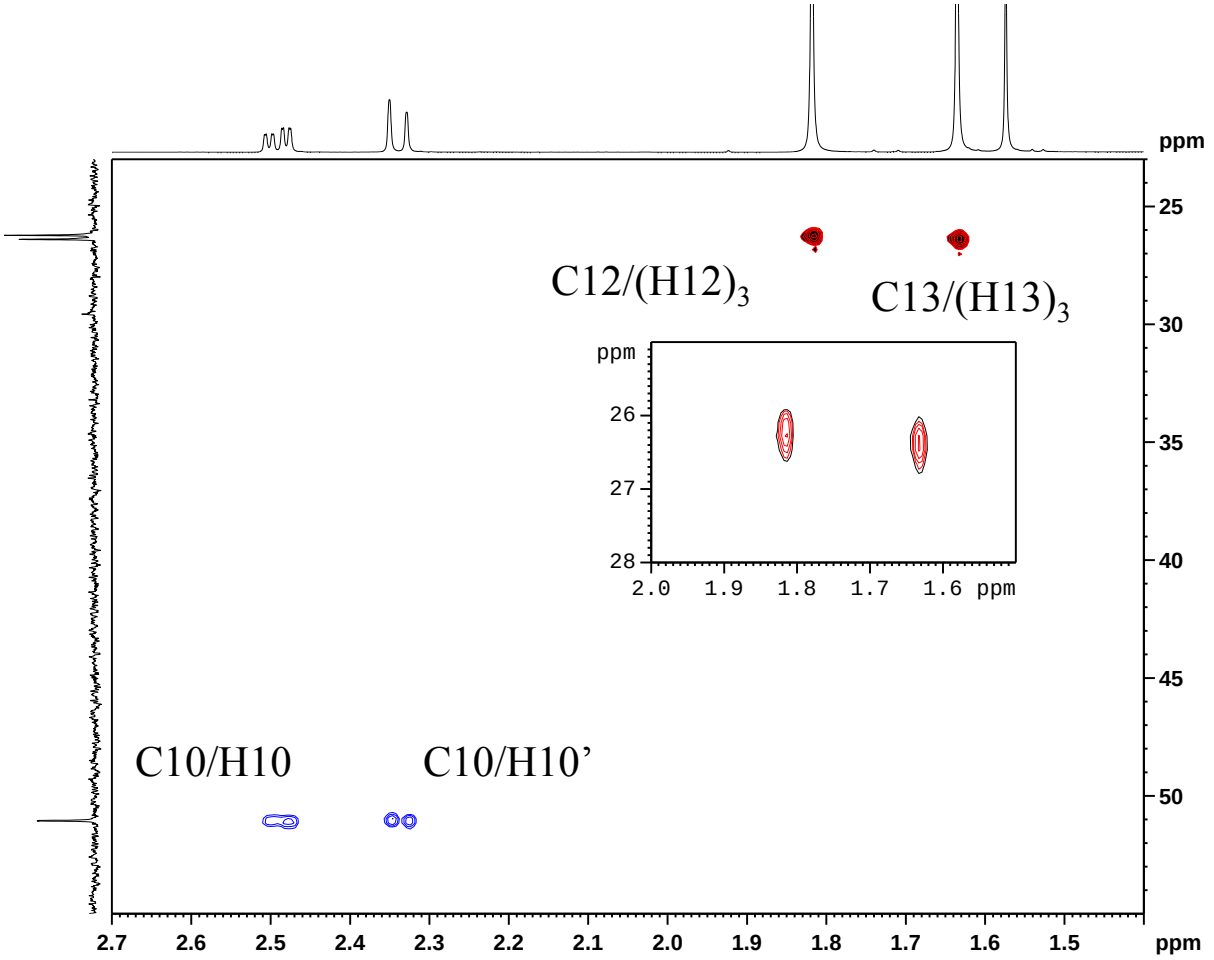

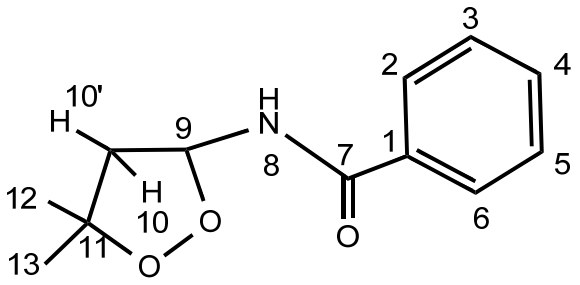

Fig.A8. Aliphatic H-1/C-13 regional plot of gs-HSQC of structure A, showing the C12-H12 and C13-H13 assignments.

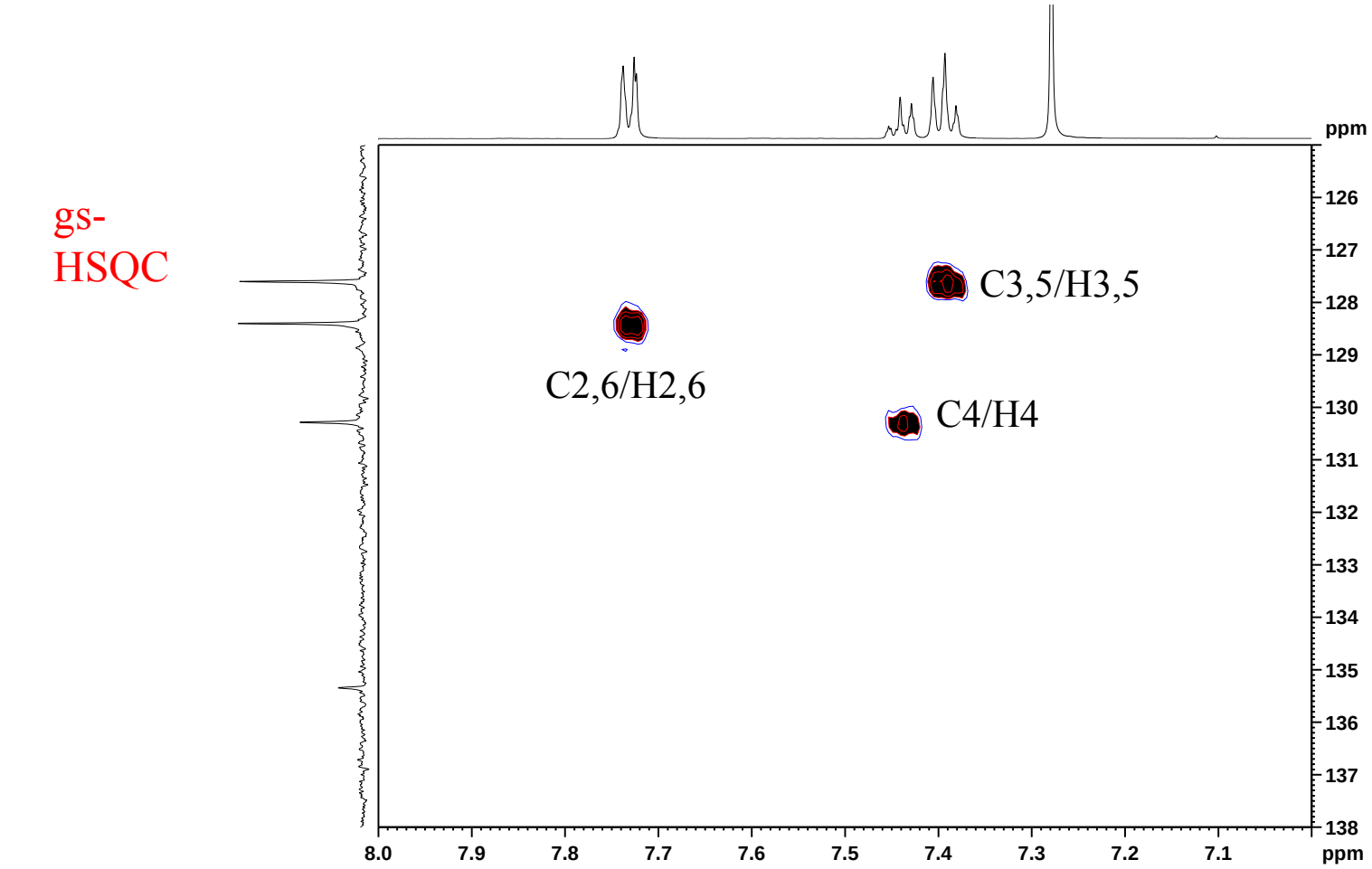

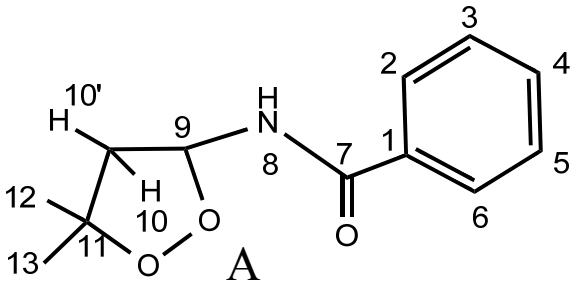

Fig.A9. Aromatic H-1/C-13 regional plot of gs-HSQC of structure A.

gs-HMBC

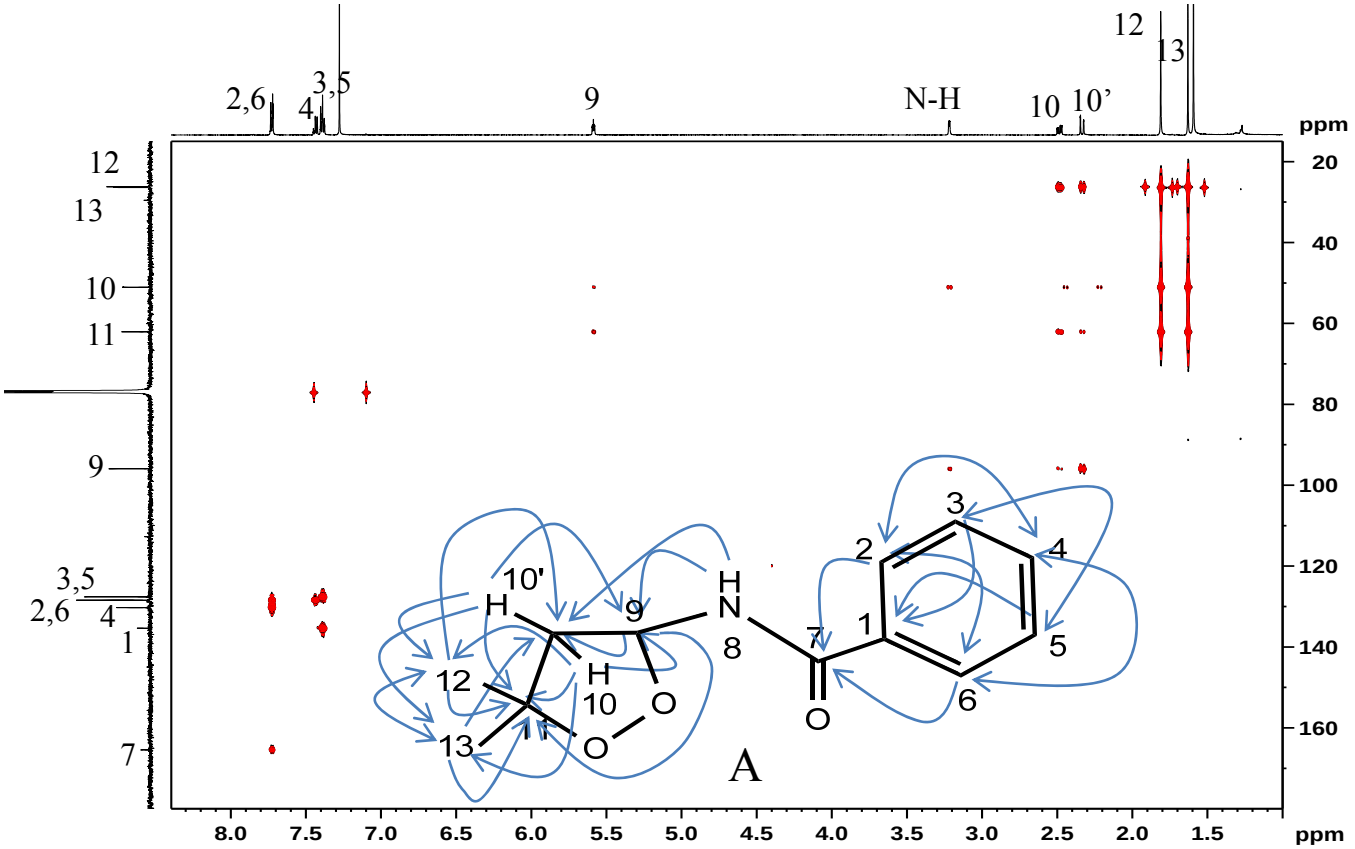

Fig.A10. Full range contour plot of gs-HMBC of structure A. Expansion plots in the following figures 19-21. Arrows in Structure A show the observed 3 bonds H-1/C-13 correlations.

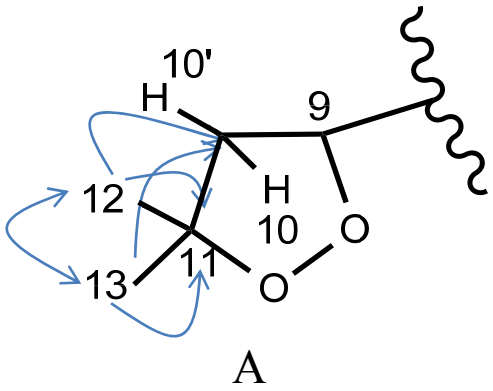

A

gs-HMBC

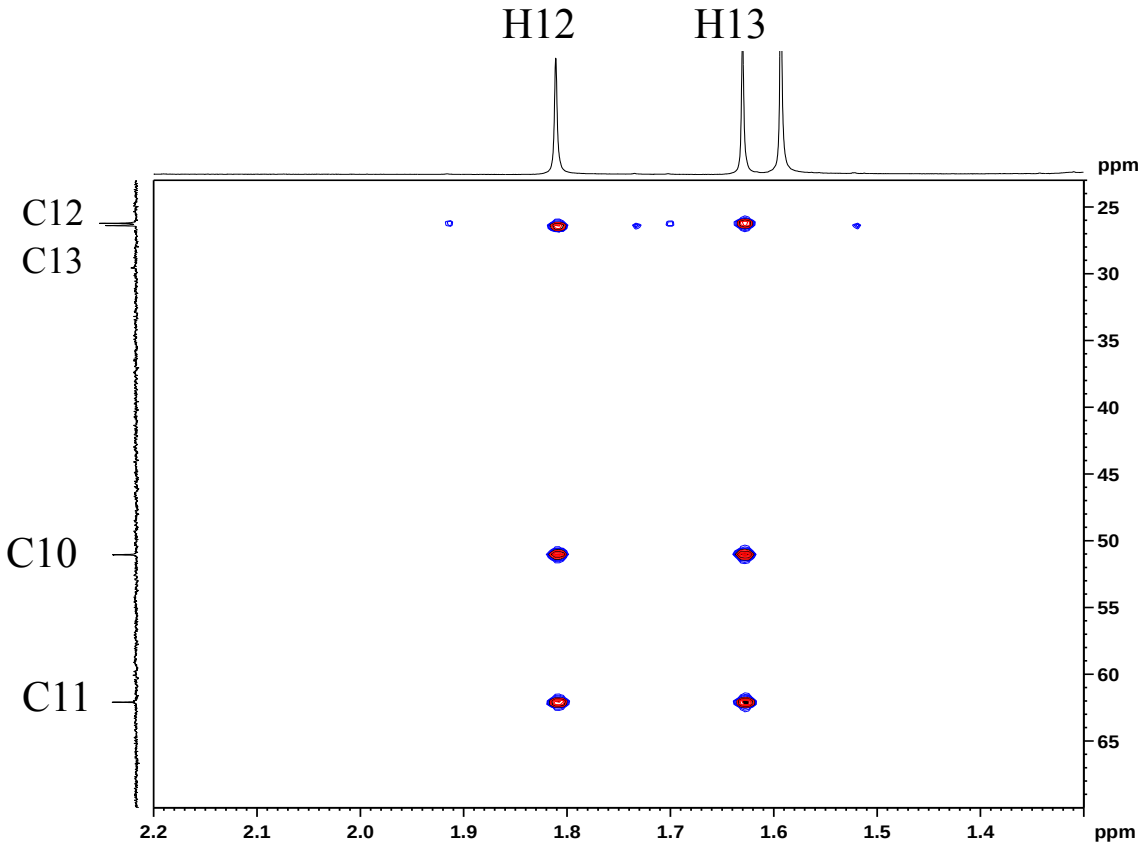

Fig.A11. C-12 and C-13 region contour plot of gs-HMBC of structure A. Arrows in Structure A (portion shown) represent the observed 3 and 4 bonds H-1/C-13 correlations.

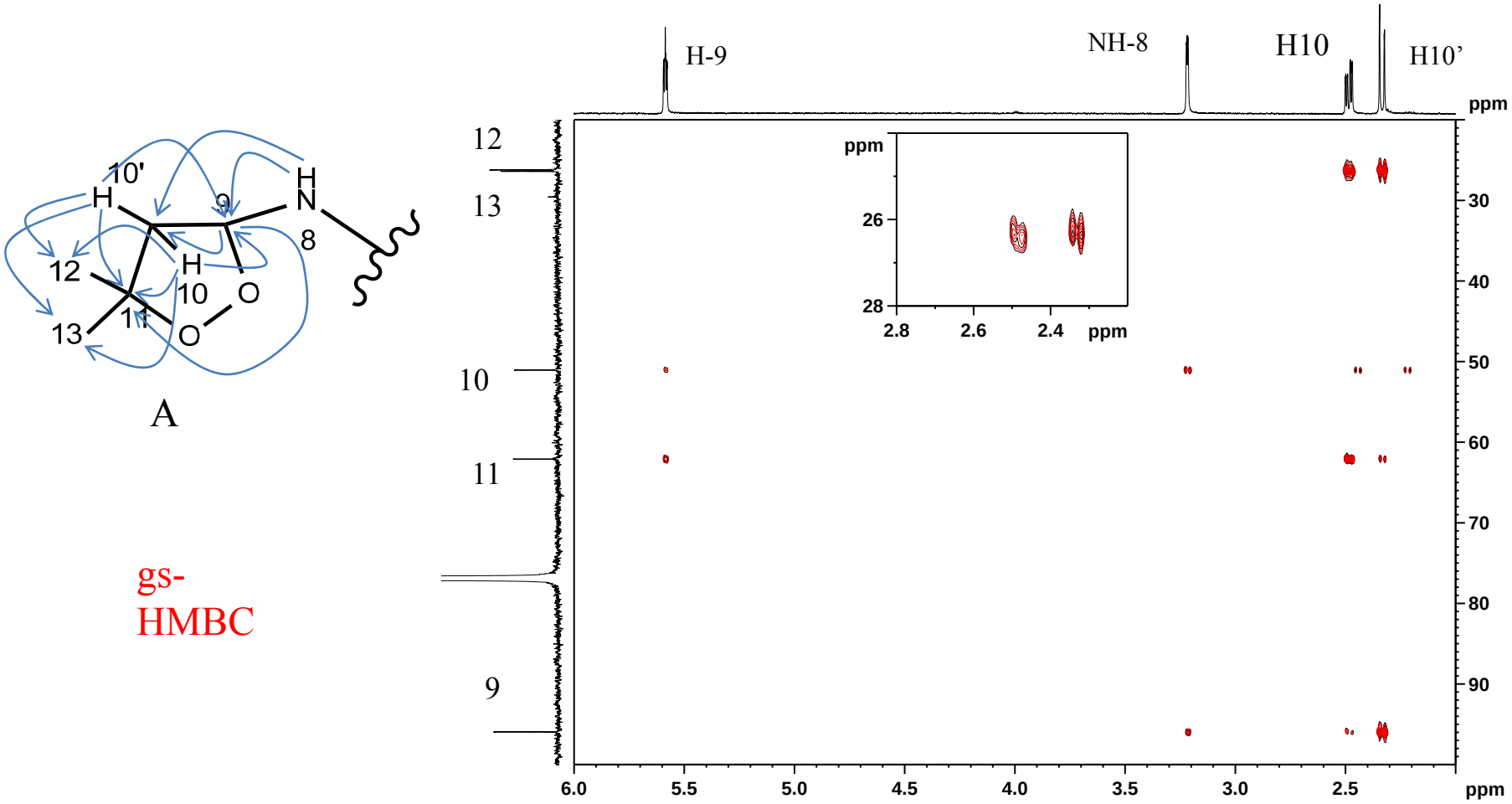

Fig. A12. Aliphatic region contour plot of gs-HMBC of structure A. Arrows in Structure A show the observed 3 to 4 bonds H-1/C-13 correlations.

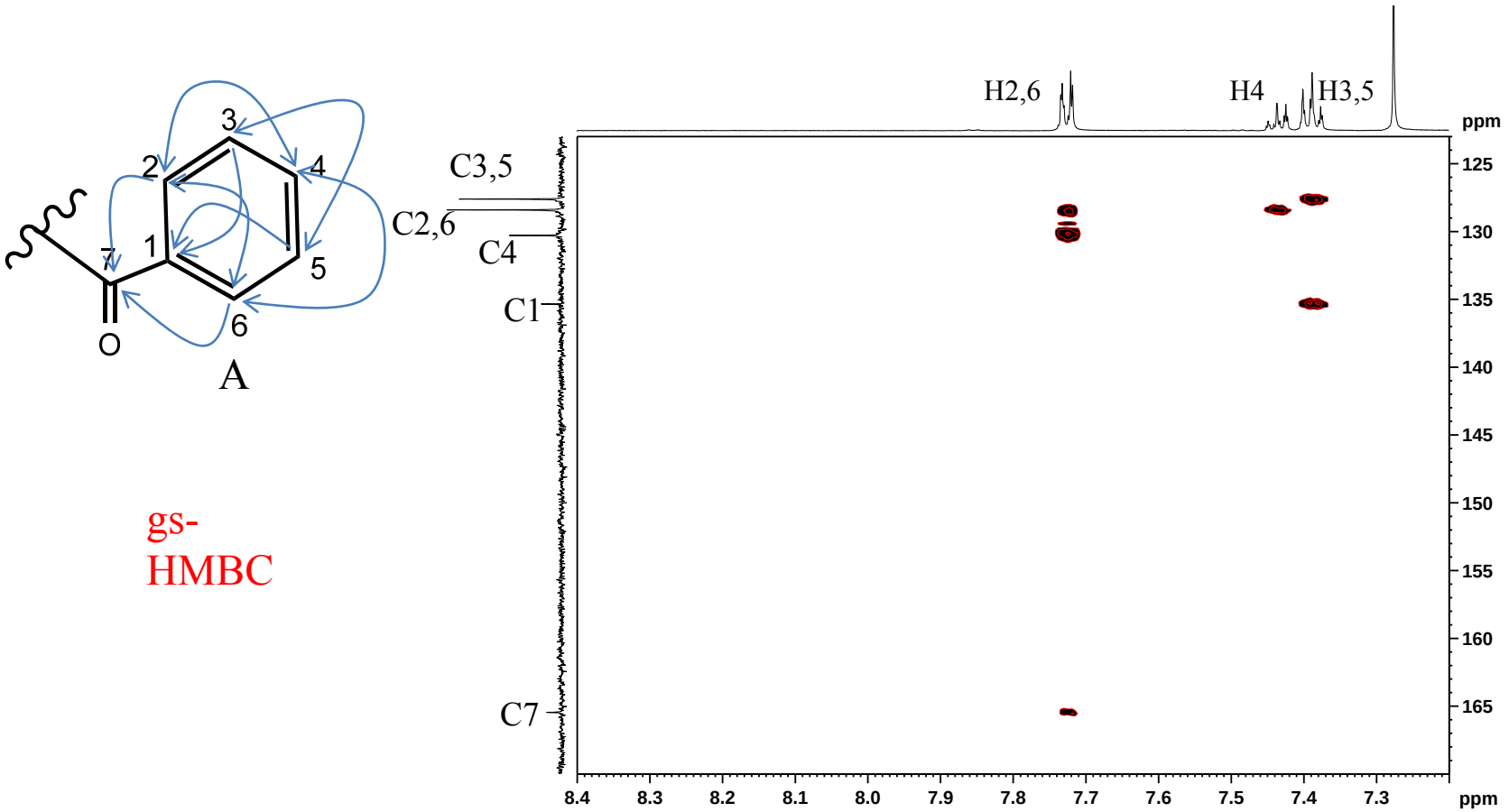

Fig.A13. Aromatic region contour plot of gs-HMBC of structure A.. Arrows in Structure A show the observed 3 to 4 bonds H-1/C-13 correlations.

HMQC-COSY,
H2BC

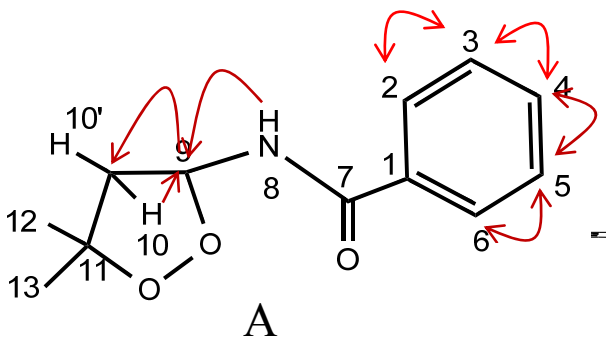

A

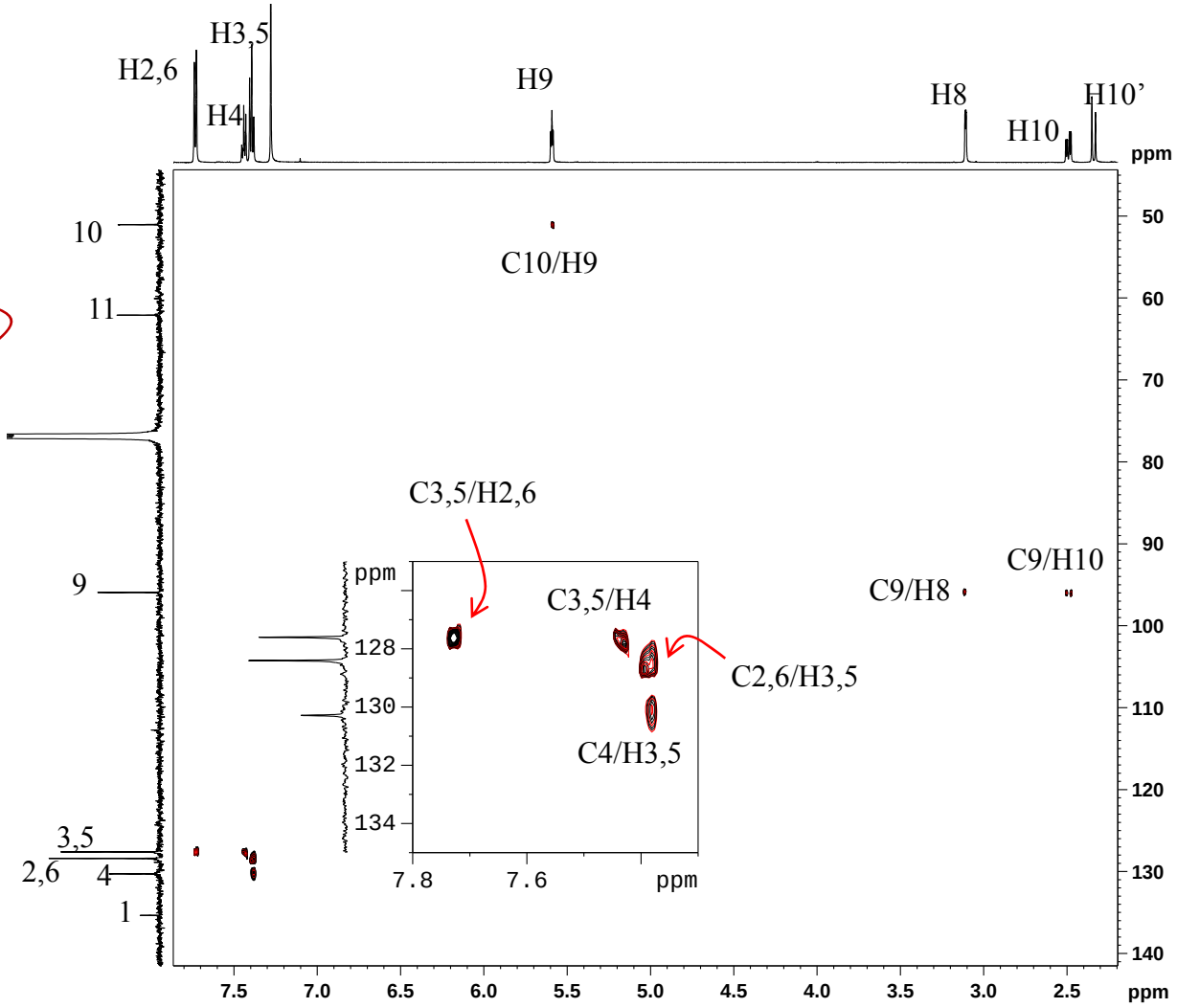

Fig.A14. gs-H2BC [HMQC-COSY] plot of structure A. Correlation shows Carbons with adjacent protons, typically J2 bonds coupling.

Appendix II

Calculation of the yields of II and VI under varying O_2 concentrations.

The table below listed the respective peak areas under varying O_2 concentrations (peak areas of **VI** were normalized to **II** based on the quantum yield difference of **II** and **VI** (see Chapter II)).

N_2O/O_2 Peak Area	80%/20%	95%/5%	100%/0%
II decrease	1.20×10^7	1.17×10^7	1.08×10^7
VI increase (corrected)	3.15×10^4	1.24×10^5	7.1×10^5

Under the condition of Figure 5 (1.5 mM DMSO, 20 mM $NaNO_2$), the fraction of •OH reacting to produce •CH_3 (f_{CH3}) and •NO_2 (f_{NO2}) radicals, respectively, are:

$$f_{CH3} = \frac{k_3[DMOSO]}{k_3[DMSO] + k_4[NO_2^-]} = \frac{6.6\times10^9\times1.5\ mM}{6.6\times10^9\times1.5\ mM + 6\times10^9\times20\ mM} = 0.08 \quad (a)$$

$$f_{NO2} = 1 - 0.08 = 0.92 \quad (b)$$

At 80% N_2O/20% O_2 at room temperature, [O_2] = 0.25 mM and [**I**] = 0.03 mM. The fraction of •CH_3 reacting with O_2 to generate CH_3OO• (f'_{CH3OO}) is given by:

$$f'_{CH3OO} = \frac{k_6[O_2]}{k_6[O_2] + k_7[I]} = \frac{1.6\times10^9\times0.25\ mM}{1.6\times10^9\times0.25\ mM + 7.8\times10^8\times0.03\ mM} = 0.95 \quad (c)$$

while the fraction of •CH_3 reacting with **I** to generate **VI** (f'_{CH3}) is given by,

$$f'_{CH3} = 1 - f_{CH3OO} = 1 - 0.95 = 0.05 \quad (d)$$

At 95%N_2O/5%O_2, [O_2] = 62.5 μM, the fraction of •CH_3 reacting with O_2 to generate CH_3OO• (f'_{CH3OO}) is given by,

$$f'_{CH3OO} = \frac{k_6[O_2]}{k_6[O_2] + k_7[I]} = \frac{1.6\times10^9\times0.06\ mM}{1.6\times10^9\times0.06\ mM + 7.8\times10^8\times0.03\ mM} = 0.81 \qquad (e)$$

while the fraction of •CH_3 reacting with **I** to generate **VI** (f'_{CH3}) is given by,

$$f'_{CH3} = 1 - f_{CH3OO} = 1 - 0.81 = 0.19 \qquad (f)$$

At 100% N_2O, all •CH_3 produced by OH reaction with DMSO reacted with **I** to generate **VI**.

Taking the total **II** formation under 80% N_2O/20% O_2 to be 100%, then under this condition, the contribution of [**II**] by peroxyl radical is 0.08 × 95% ~ 8%, while the [**VI**] formation will be 0.08 × 5% = 0. 4% (0.3% based on **VI** peak area). At 95% N_2O/5% O_2, contribution of **II** by peroxyl radical is 0.08 × 81% = 7% while the [**VI**] formation will be 8% – 7% = 1% (1% based on **VI** peak area); the decrease of **II** is 2% based on **II** peak area decrease. At 100% N_2O, all the •CH_3 radical will react with **I** to form **VI**. The theoretical increase of the yield of [**VI**] should therefore be 8% of the total [**II**] formation (under 80% N_2O and 20% O_2). The actually observed increase of [**VI**] was 6% based on the peak area calculation. The decrease of **II** was 10% based on **II** peak area calculation. The quantum yield difference of **II** and **VI** (see main text) was taken in to account in all calculations.

Taking the total formation of [**VI**] under 100% N_2O as 100%, then the [**VI**] at 95% N_2O/5% O_2 will be 19% (equation f, 17% based on peak area); at 80% N_2O/20% O_2 will be 5% (equation d, 4% based on peak area).

Appendix III

Photochemical stability of other fluorescamine derivatized nitroxides.

The photostability of the fluorescamine derivatized amino nitroxides, **I**, 3-ampf and 4-atf was also tested under momochromatic photo irradiation conditions. 2 major absorbance peaks, observed at 390 (± 4) nm (ε=5225 $M^{-1}cm^{-1}$) and 270 (± 4) nm (ε=13900 $M^{-1}cm^{-1}$), were due to the fluorescamine moiety. A small peak at 248 nm, which is buried by the 270 nm fluorescamine peak, is due to the nitroxide moiety. Contrary to the conclusion under polychromatic irradiation, **I** was rather stable under monochromatic irradiation at 390 nm, probably because of the absence of low wavelengths light that causes its photo bleaching in polychromatic irradiation. On the other hand, under both anaerobic and aerobic conditions, significant photo degradation was observed for 3-amf and 4-atf, especially 4-atf. Isosbestic points were also observed during the process of photo irradiation for 3-ampf and 4-atf, indicating the formation of new chemical species. A structurally similar diamagnetic compound, methyl-fluorescamine (**VI**), was also studied as a reference.

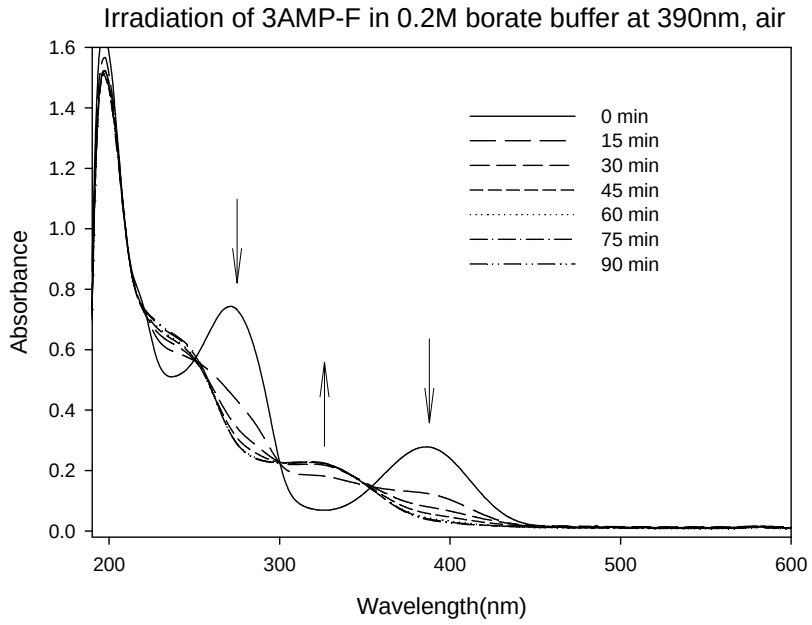

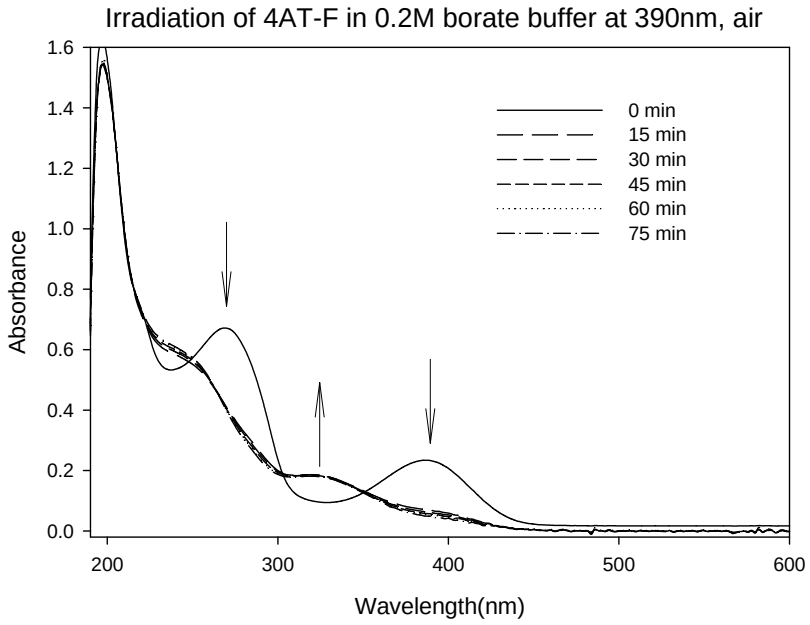

Figure A15a Photostability of 3-ampf and 4-atf under aerobic conditions

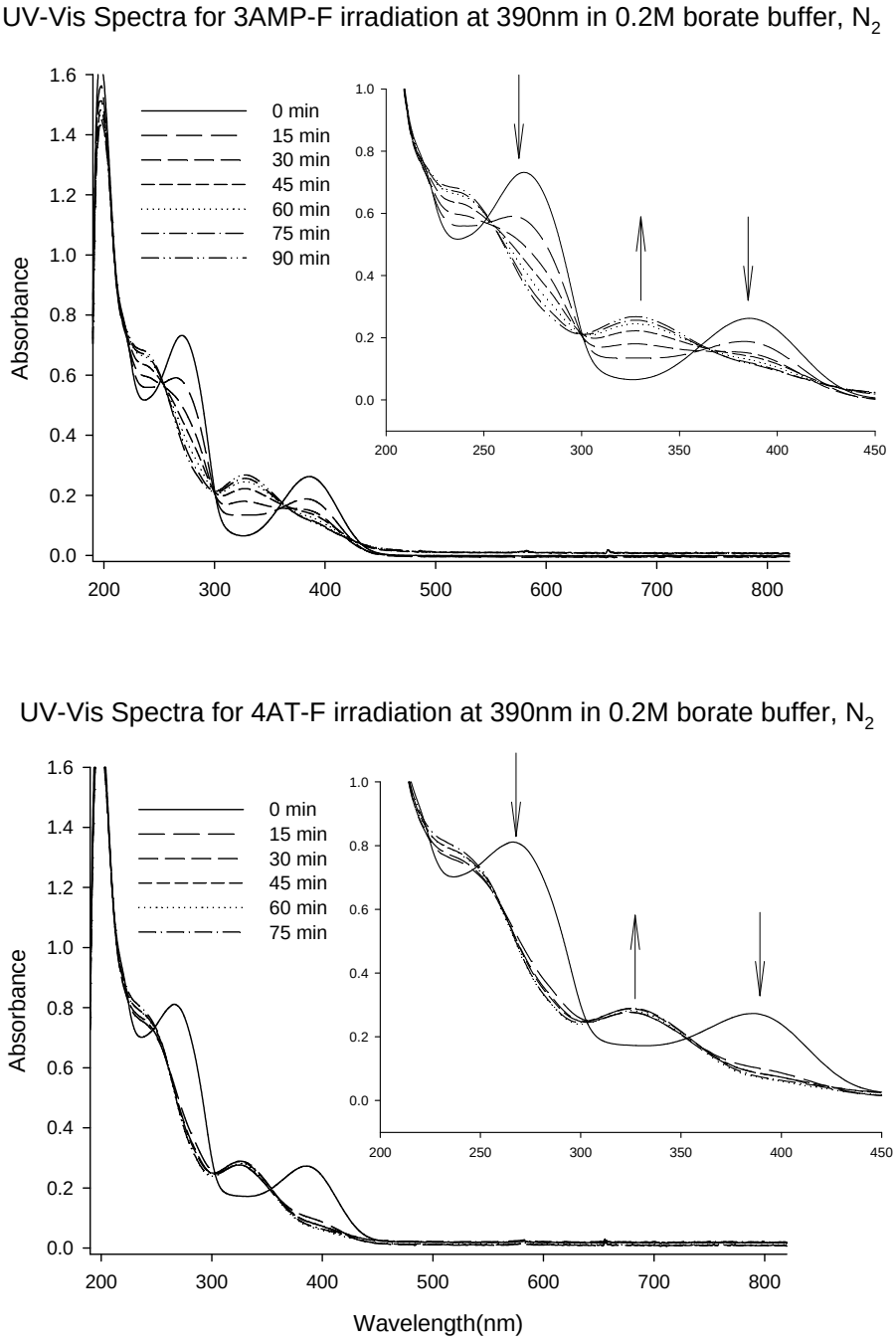

Figure A15b Photostability of 3-ampf and 4-atf at 390nm under anaerobic conditions

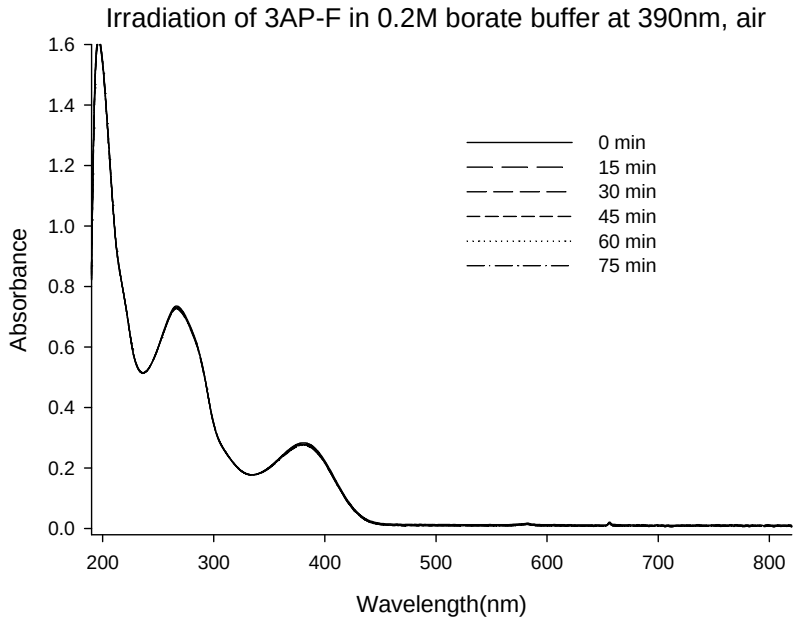

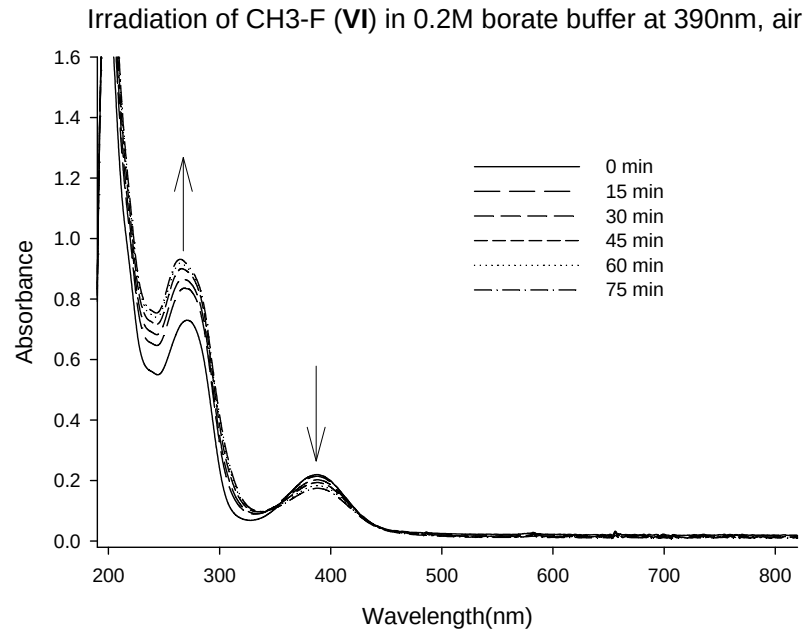

Figure A15c Photostability of 3-apf and CH_3-f (product **VI**) at 390nm under air

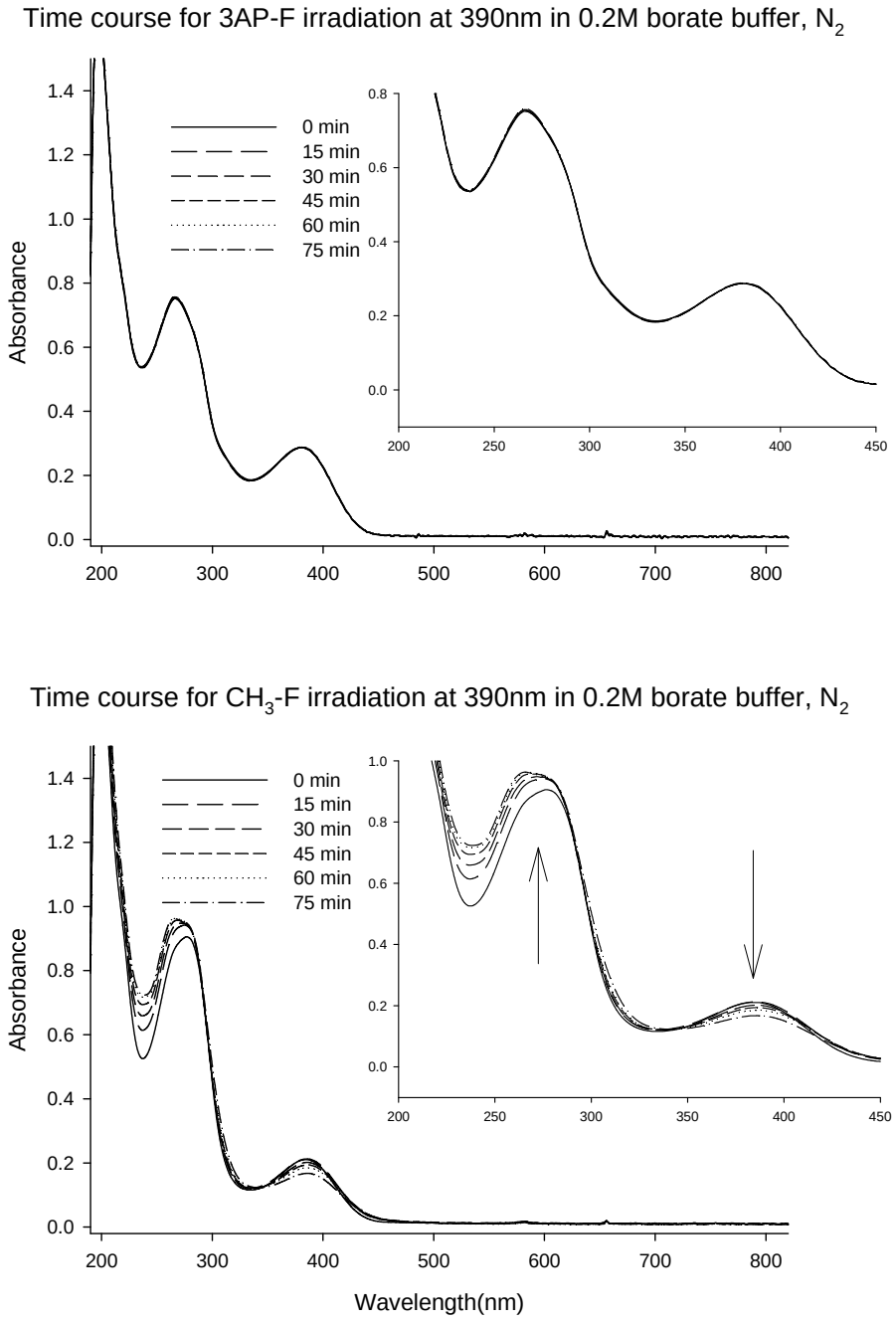

Figure A15d Photostability of 3-apf and CH_3-f (product **VI**) at 390nm under air

For 3-ampf, the photodegradation process was slower under anaerobic conditions than under aerobic conditions, indicating that the photodegradation was facilitated by oxygen, as shown in Figure A16 below.

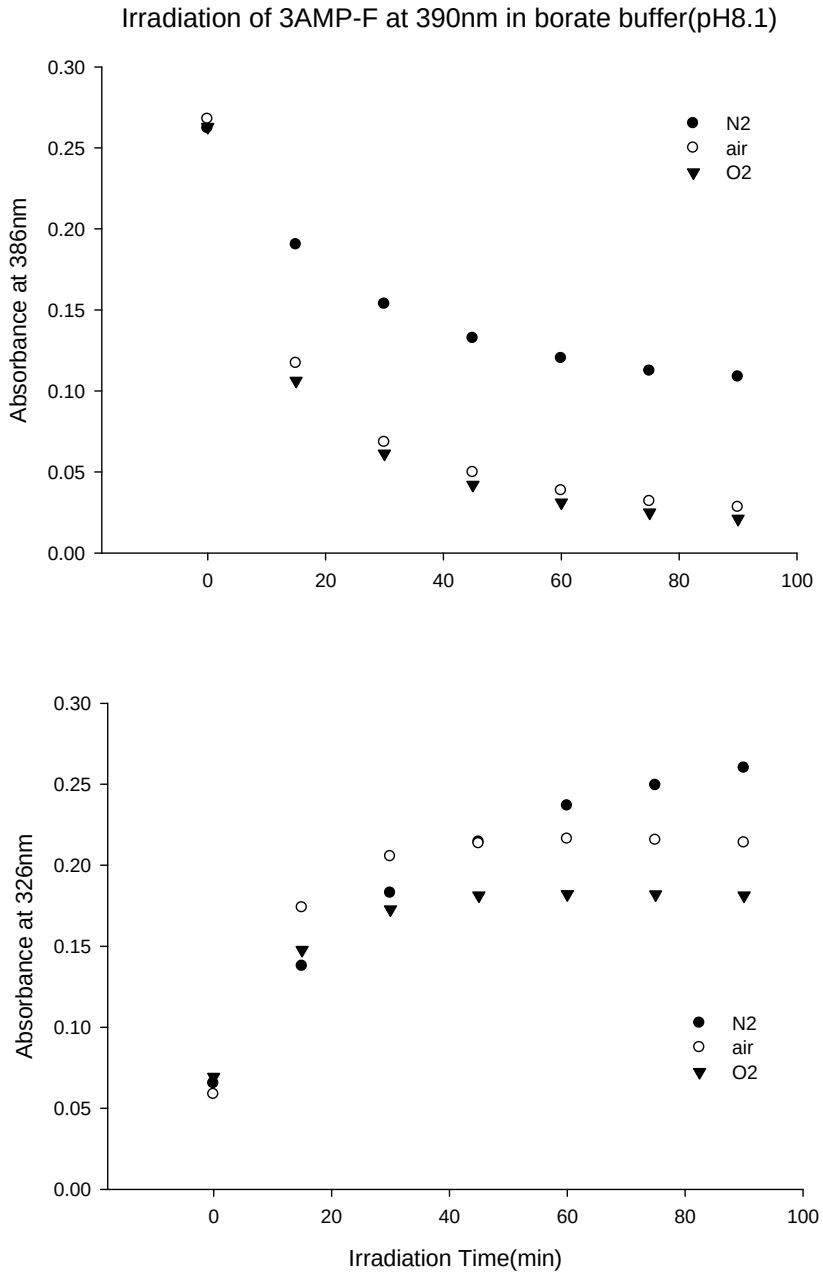

Figure A16. Time course of the absorbance for 3-ampf in borate buffer, pH 8.2, under monochromatic photo irradiation at 390nm.

The concentration of the nitroxide moiety was followed by EPR. Under anaerobic condition, the decrease of nitroxide concentration indicates that the nitroxide moiety was either reduced or oxidized during the photo degradation of the fluorescamine moiety, but finally reached equilibrium. Under aerobic condition, while the photo degradation process was faster than under anaerobic condition, the nitroxide moiety concentration did not decrease as indicated by a constant EPR signal in Figure A17 below:

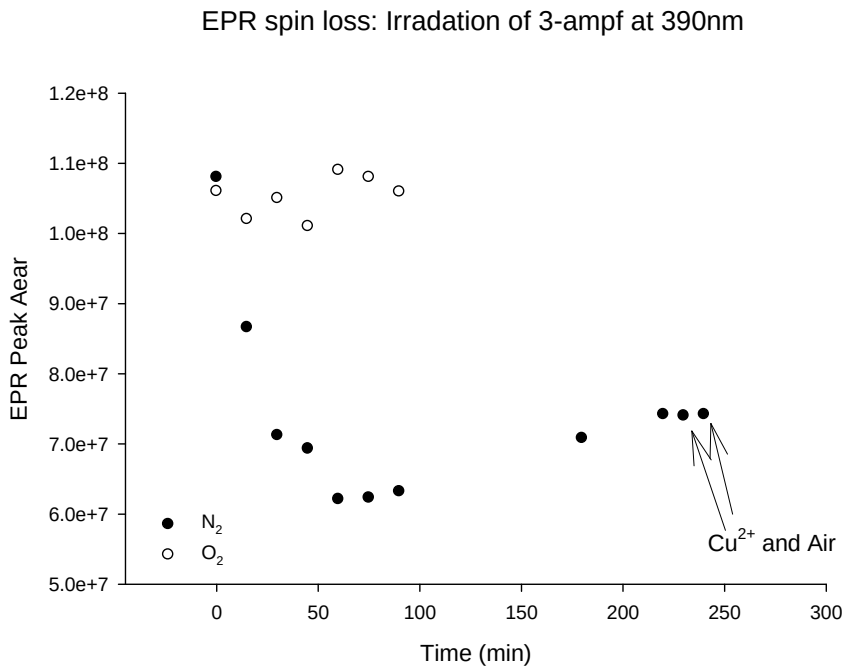

Figure A17 Time course of the spin loss for photo irradiation of 3-ampf at 390 nm under both anaerobic and aerobic conditions

Addition of Cu^{2+} and exposure to air at the end of anaerobic irradiation at 220 min did not result in noticeable increase in EPR signal. This evidence indicates the absence of hydroxylamine product, rather, photo induced oxidation reaction is more likely to occur and

that an oxoammonium cation intermediate is most likely to be present under aerobic condition. The proposed mechanism was shown below:

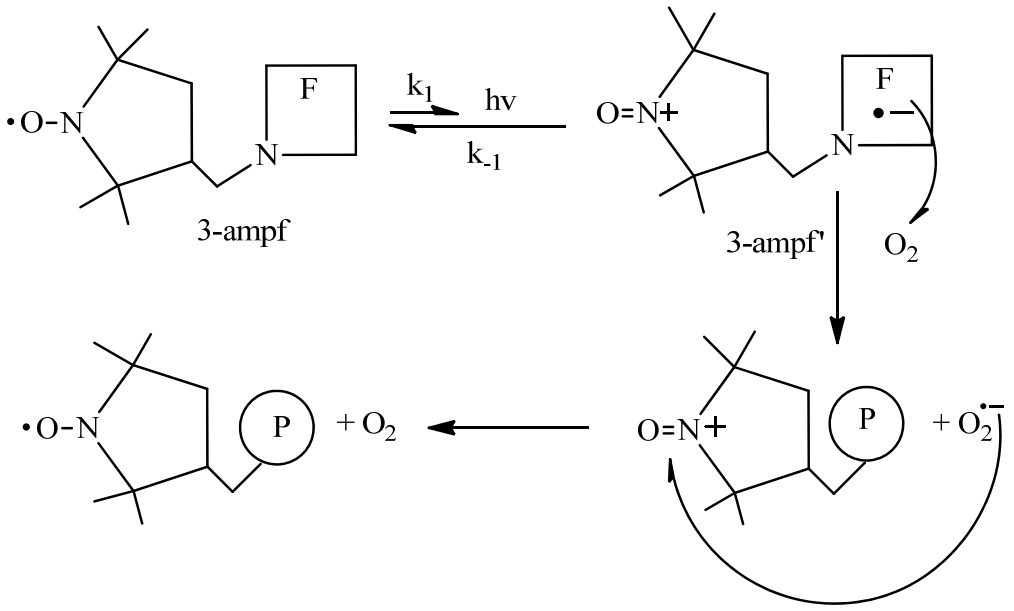

where F stands for fluorescamine moiety while P stands for the degradation product. The first step should be a reversible reaction, as indicated by CV and kinetics study of 3-amp. Once the nitroxide moiety lost one electron to form oxoammmonium cation, the electron can either be captured by oxygen to form superoxide radical; or regained by the oxoammonium cation to form the original nitroxide. Either way, the fluorescamine moiety will be photo bleached during the electron shuttling process to lose absorbance at 390 and 270 nm. Oxygen acts as a catalyst to accelerate the degradation of the fluorescamine moiety while the nitroxide was not consumed in the reaction. The 2nd possible mechanism is that the fluorescamine moiety may undergo Norrish Type II photo reaction to generate singlet oxygen, which then attack the fluorescamine to cause photo bleaching of 3-ampf under

aerobic condition; or undergo Norrish Type I reaction under anaerobic condition to cause photo degradation. However, this mechanism is less likely since 1. 3-apf showed no noticeable photo degradation; 2. a diamagnetic product CH_3-f (**VI**) showed different photo degradation product and 3. the decrease in EPR spin level indicates redox reaction of the nitroxides moiety, which must involve electron transfer.

For the photo irradiation of 3-ampf under anaerobic condition, once the nitroxide moiety lost electron to fluorescamine moiety, the electron can only go back to the oxoammonium cation, which results in the formation of the original nitroxide. The reaction reached equilibrium when k_1[3-ampf]eq = k_{-1}[3-ampf']eq, when the spin level keeps constant.

For 4-atf, the photodegradation process was almost equal under either anaerobic conditions or under aerobic conditions, indicating that the photodegradation was not affected by oxygen, as shown in Figure A18 below.

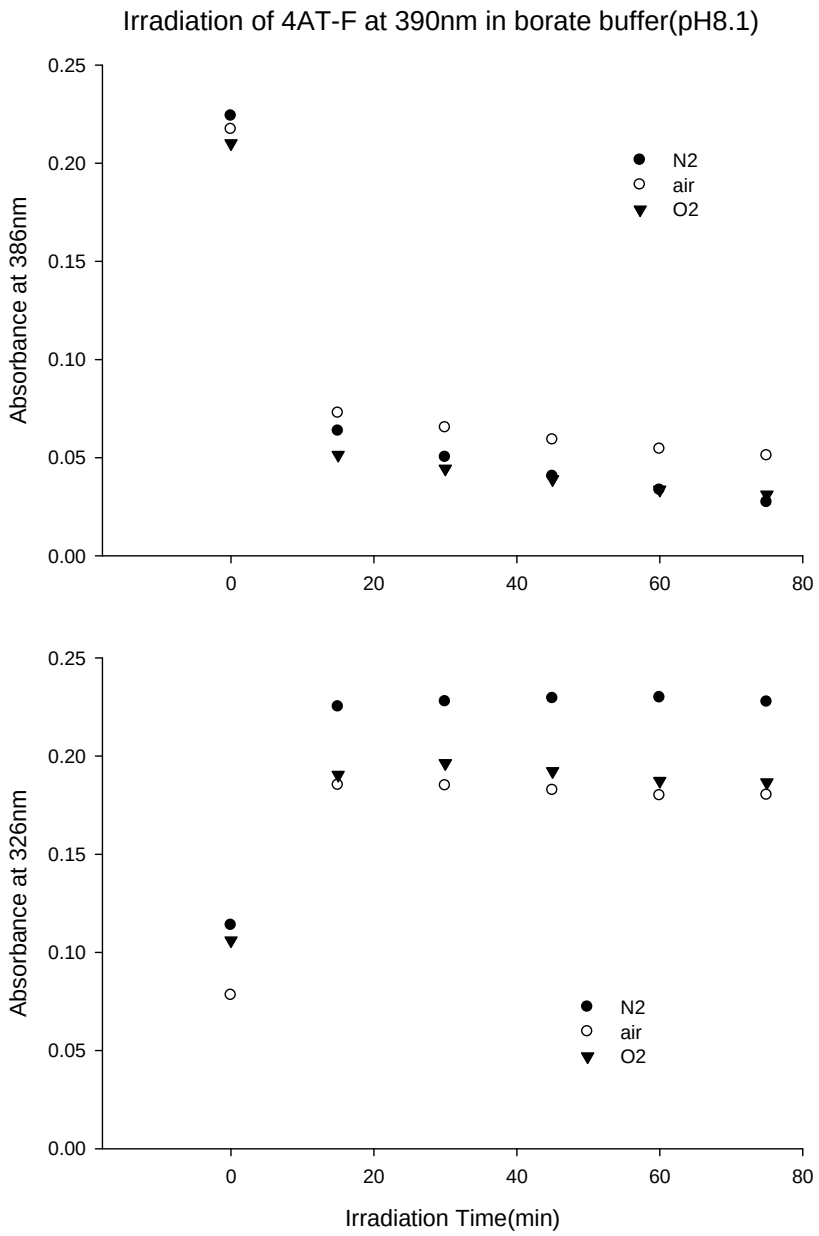

Figure A18. Time course of the absorbance for 4-atf in borate buffer, pH 8.2, under monochromatic photo irradiation at 390nm.

Decrease in spin loss was observed for both anaerobic and aerobic conditions during 4-atf photo irradiation process (Figure A19). The photo reaction reached equilibrium in about 30min under aerobic condition while it took longer time under anaerobic condition. Electron transfer appears to be involved in both conditions. Addition of Cu^{2+} or exposure to air at the

end of anaerobic irradiation brings the spin level to about the same level as in aerobic irradiations. These observations indicate that photo induced reduction reaction is most likely to be involved. It has been reported that nitroxides can be photo reduced to its hydroxylamine in the presence of electron in aqueous solutions.

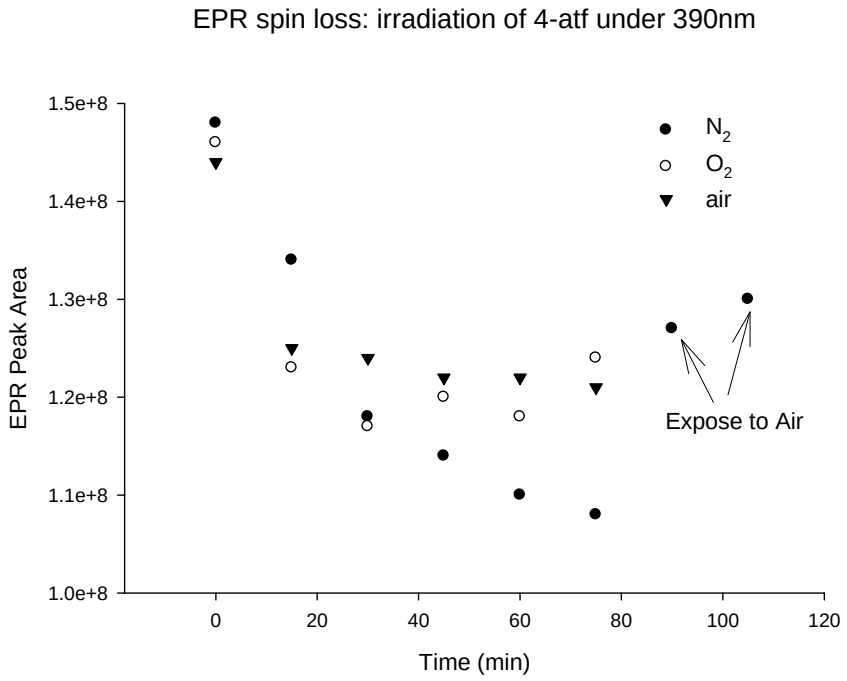

Figure A19 Time course of the spin loss for photo irradiation of 3-ampf at 390 nm under both anaerobic and aerobic conditions

The proposed mechanism for 4-atf photo reduction reaction, involving a hydroxylamine product, is shown below:

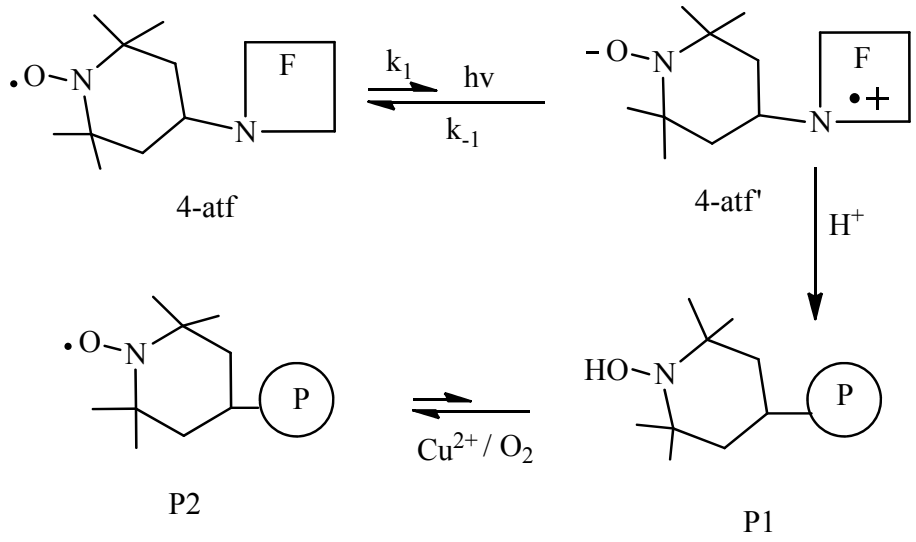

Under anaerobic condition, P1 is the final product and the path way from P1 (diamagnetic) to P2 (paramagnetic) was eliminated. As a result, the final equilibrium concentration for nitroxide moiety is lower. Under aerobic condition, part of the diamagnetic P1 will be oxidized back to nitroxide and equilibrium will be established between P1 and P2. Therefore, final P1 concentration is higher than that under anaerobic condition.

For **I**, it is not clear at this moment as why it is so stable under monochromatic photo irradiation at 390 nm. One possible explanation is that the nitroxide N-O moiety is closer to fluorescamine moiety, which facilitates the electron delocalization during electron transfer process and may help stabilize the excited fluorescamine moiety. The spin level of **I** was constant during the monochromatic photo irradation processes. The photo degradation of CH_3-f is more likely a photosensitization reaction, either by Norrish Type I (anaerobic) or Type II (aerobic) mechianism.

References

(1) Halliwell, B.; Gutteridge, J.M.C. *Free Radicals in Biology and Medicine, 4th ed.*, Oxford University Press, Oxford, **2007**.

(2) Halliwell, B.; Gutteridge, J.M.C., *Meth. Enzymol.* **1990**, 186, 1.

(3) Wessling-Resnick, M., *Am.J.Physiol.*, **2006**, 290, G1.

(4) Hentze, M.W., *Cell*, **2004**, 117, 285.

(5) Liu, X.; Theil, E.C. J. *Acc.Chem.Res.*, **2005**, 38, 167.

(6) Gutteridge, J.M.C.; Stocks, J. *Crc.Critc.Rev.Clin.Lab.Sci.* **1981**, 14, 257.

(7) Park, Y.S. *FEBS.Lett.* **1999**, 458, 133.

(8) Earnster, L.; Dallner, G. *Biochim.Biophys.Acta.* **1995**, 1271, 195.

(9) Marnett, L. J. *Adv in Exp. Med. and Bio*l. **1991**, 283, 65-70.

(10) Venkataraman, S.; Schafer, F. Q.; Buettner, G. R. *Antioxid. Redox. Sign.* **2004**, 6, 631-638.

(11) Rodriguez, H.; Valentine, M. R.; Holmquist, G. P.; Akman, S. A.; Termini, *J. Biochem*. **1999**, 38, 16578-16588.

(12) Termini, J. *Critc. Rev. Oxid. Stress. Aging.* **2003**, 1, 39-53.

(13) Adam, W.; Kurz, A.; Saha-Moeller, C. R. *Chem. Res. Toxicol*. **2000**, 13, 1199-1207.

(14) Kanazawa, A.; Sawa, T.; Akaik, T.; Maeda, H. *Cancer Lett. (Shannon, Ireland)* **2000**, 156, 51-55.

(15) Schuchmann, M. N.; Zegota, H.; Von Sonntag, C. *Oxyg. Rad. Chem. Biol., Proc., Int. Conf., 3rd* **1984**, 629-635.

(16) Aejmelaeus, R. T.; Holm, P.; Kaukinen, U.; Metsa-Ketela, T. J. A.; Laippala, P.; Hervonen, A. L. J.; Alho, H. E. R. *Free Rad. Biol. & Med.* **1997**, 23, 69-75.

(17) Afanas'ev, I. B. *Biogerontol*. **2005**, 6, 283-290.

(18) Strong, R.; Mattamal, M. B.; Andorn, A. C. *Free Rad. Aging* **1993**, 223-246.

(19) Spiteller, G. *Free Rad. Biol. & Med*. **2006**, 41, 362-387.

(20) Tappel, A.; Tappel, A. *Med. Hypoth*. **2004**, 63, 98-99.

(21) Van-Sonntag, C. *The Chemical Basis of Radiation Biology.* Taylor and Francis, London, **1987**.

(22) DiGuiseppi, J.; Fridovich, I. *Crit. Rev. Toxicol*. **1984**, 12, 315-342.

(23) Rush, J.D.; Bielski, B.H.J., *J. Phys. Chem*., **1985**, 89, 5062.

(24) Cabelli, D.E.; Bielski, B.H.J., *J. Phys. Chem*., **1983**, 87, 1809.

(25) Koppenol, W.H., FEBS Lett., 1990, 264(2), 165-167.

(26) Kanofsky, J.R., *J. Org. Chem.,* **1986**, 51, 3386.

(27) Augusto, O. *Free.Rad.Biol.Med*. **2002**, 32, 841.

(28) Foote, C.S. *Active O2 in Chemistry*.Blackie, London, **1995**.

(29) Rozantsev, E.G., *Pure Appl. Chem.*, **1989**, 62, 311.

(30) Kocherginsky, N.; Swartz, H.M., Nitroxide Spin labels (Reactions in biology and Chemistry), CRC press, 1995.

(31) Krishna, C.M.; Grahame, D.A.; Samuni, A.; Mitchell, J.B.; Russo, A., *Proc. Natl. Acad. Sci.*, **1992**, 89, 5537-5541.

(32) Weil, J.T.; Van Der Veen, J.; Olcott, H.S., *Nature*, **1968**,219,168.

(33) Antosiewicz, J.; Bertoli, E.; Damiani, E.; Greci, L.; Popinigis,J.; Przybylski,S.; Tanfani, F.; Wozniak, M., *Free rad. Biol. Med*., **1993**, 15, 203-208.

(34) Voest, E.E.; Van Faassen, E.; Marx, J.J.M., *Free rad. Biol. Med*., **1993**, 15, 589.

(35) Samuni, A. M.; DeGraff, W.; Krishna, M. C.; Mitchell, J. B. *Mol. Cell. Bio*., **2002**, 234, 327-333.

(36) Goldstein, S.; Samuni, A.; Russo, A. *J. Am. Chem. Soc*. **2003**, 125, 8364- 8370.

(37) Goldstein, S.; Merenyi, G.; Russo, A.; Samuni, A. *J. Am. Chem. Soc*. **2003**, 125, 789-795.

(38) Offer, T.; Samuni, A., *Free Rad. Bio. Med*. **2002**, 32, 872- 881.

(39) Samuni, A.; Goldstein, S.; Russo, A.; Mitchell, J. B.; Krishna, M. C.; Neta, P. *J. Am. Chem. Soc.*, **2002**, 124, 8719-8724.

(40) Samuni, A.; Krishna, C.M.; Riesz, P.; Finkelstein, E.; Russo, A.J., *J. Bio. Chem*. **1988**, 263, 17921-17924.

(41) Samuni, A.; Krishna, C.M.; Riesz, P.; Finkelstein, E.; Russo, A.J., *Free rad. Biol. Med.*, **1989**, 6, 141.

(42) Mitchell, J.B.; Samuni, A.; Krishna, C.M.; Degraff, W.G.; Ahn, M.S.; Samuni, U.; Russo, A., *Biochem.*, **1990**, 29, 2802-2807.

(43) Beckwith, A.L.J.; Bowry, V.W.; Ingold, K.U., *J. Am. Chem. Soc*., **1992**, 114, 4983-4992.

(44) Bowry, V.W.; Ingold, K.U., *J. Am. Chem. Soc*., **1992**, 114, 4992-4996.

(45) Brede, O.; Beckert, D.; Windolph, C.; Gottinger, H.A., *J. Phys. Chem.*, **1998**, 102, 1457-1464.

(46) Antosiewicz, J.; Popinigis, J.; Wozniak, M.; Damiani, E.; Carloni, P.; Greci, L. *Free Rad. Biol. Med.* **1995**, 18, 913-917.

(47) Damiani, E.; Paganga, G.; Greci, L. *Biochem. Pharmacol*. **1994**, 48, 1155-1161

(48) Damiani, E.; Carloni, P.; Biondi, C.; Greci, L. *Free Rad. Biol. Med*. **2000**, 28, 193-201.

(49) Gabbianelli, R.; Falcioni, G.; Santroni, A.; Caulini, G.; Greci, L.; Damiani, E. *Free Rad. Biol. Med*. **1997**, 23, 278-284.

(50) Damiani, E.; Kalinska, E.; Canapa, A.; Canestrari, S.; Wozniak, M.; Greci, L. *Free Rad. Biol. Med.* **2000**, 28, 1257-1265.

(51) Cardellini, L.; Carloni, P.; Greci, L.; Stipa, P.; Faucitano, A. Gazz. *Chim. Ital*. **1989**, 119, 621-625.

(52) Barton, D. H.; Le, Gloahec, V. N.; Smith, J. *Tetrahedron Lett*. **1998**, 39, 7483-7486.

(53) Goldstein, S.; Samuni, A. *J. Phys. Chem. A* **2007**, 111, 1066-1072.

(54) Micallef, A.S.; Blinco, J.P.; George, G.A.; Reid, D.A.; Rizzardo, E.; Huang, S.H.; Bottle, S.E. *Polyr.Degr.Stability* **2005**, 89, 427-435.

(55) Bersohn, M.; Thomas, J. R. *J. Am.Chem.Soc*. **1964**, 86, 959.

(56) Chiba, T.; Kaneda, T. *Agricultural and Biol. Chem*. **1984**, 48, 2593-2594.

(57) Kitaguchi, H.; Ohkubo, K.; Ogo, S.; Fukuzumi, S. *J. Am.Chem.Soc*. **2005**, 127, 6605-6609.

(58) Davies, M. J. *Free Rad. Res. Comm*. **1989**, 7, 27-32.

(59) Davies, M. J. *Biochem. J.* **1989**, 257, 603-606.

(60) Qian, S. Y.; Wang, H. P.; Schafer, F. Q.; Buettner, G. R. *Free Rad. Biol. & Med*. **2000**, 29, 568-579.

(61) Jones, C. M.; Burkitt, M. J. *J.Chem.Soc, Perkin Transactions 2* **2002**, 2044-2051.

(62) Janzen, E. G. *Methods Enzymol*. **1984**, 105, 188-198.

(63) Sumini, A. Y.; Sumui, A.; Swartz, S. M. *Free Rad. Bio. Med*. **1989**, 6, 179-183.

(64) Finkelstein, E.; Rosen, G. M.; Rauckman, E. J. *J. Am. Chem. Soc*. **1980**, 102, 4994-4999.

(65) Janzen, E. G. *Acc. Chem. Res*. **1971**, 4, 31-40.

(66) Sugata, R.; Iwahashi, H.; Ishii, T.; Kido, R. *J. Chromatog*. **1989**, 487, 9-16.

(67) Iwahashi, H. *J. Chromatog, A* **2000**, 904, 197-202.

(68) Yamauchi, R.; Hara, Y.; Murase, H.; Kato, K. *Lipids* **2000**, 35, 1405-1410.

(69) DeLange, R. J.; Glazer, A. N. *Anal. Biochem*. **1989**, 177, 300-306.

(70) Makrigiorgos, G. M.; Kassis, A. I.; Mahmood, A.; Bump, E. A.; Savvides, P. *Free Rad. Biol. & Med.* **1996**, 22, 93-100.

(71) Iuliano, L.; Piccheri, C.; Coppola, I.; Pratico, D.; Micheletta, F.; Violi, F. *Biochimica et Biophysica Acta* **2000**, 1474, 177-182.

(72) Maulik, G.; Salgia, R.; Makrigiorgos, G. M. *Methods in Enzymol*. **2002**, 352, 80-91.

(73) Pino, E.; Aspee, A.; Lopez-Alarcon, C.; Lissi, E. *J. Phys. Org. Chem*. **2006**, 19, 867-873.

(74) Setsukinai, K.; Urano, Y.; Kakinuma, K.; Majima Hideyuki, J.; Nagano, T. *J.Biol.Chem*. **2003**, 278, 3170-3175.

(75) Heyne, B.; Beddie, C.; Scaiano, J. C. *Org. & biomol. Chem*. **2007**, 5, 1454-1458.

(76) Blough, N.V.; Simpson, D.J. *J. Am.Chem.Soc* **1988**, 110, 1915-1917.

(77) Green, S.A.; Simpson, D.J.; Zhou, G.; Ho, P.S.; Blough, N.V. *J.Am.Chem.Soc*, **1990**, 112, 7337-7346.

(78) Kieber, D.J.; Blough, N.V. *Anal.Chem*. **1990**, 62, 2275-2283.

(79) Kieber, D.J.; Blough, N.V. *Free Rad Res.Comm*. **1990**, 10, 109-117.

(80) Gerlock, J.L.; Zacmanidis, P.L.; Bauer, D.R.; Simpson, D.J.; Blough, N.V.; Salmeen, I.T. *Free.Rad.Res.Comm*. **1990**, 10, 119-121.

(81) A term originally coined by Scaiano and co-workers and employed herein: Ballesteros, O.G.; Maretti, L.; Sastre, R.; Scaiano, J.C. *Macromolecules*, **2001**, 34, 6184-6187.

(82) Zhu, Q.; Lian, Y.; Thyagarajan, S.; Rokita, S.E.; Karlin, K.D.; Blough, N.V. *J.Am.Chem.Soc*. **2008**, 130, 6304-6305.

(83) Gan, D.; Jia, M.; Vaughan, P.P.; Falvey, D.E.; Blough, N.V. *J.Phys. Chem.A*. **2008**, 112, 2803-2812.

(84) Alaghmand, M.; Blough, N.V. *Environ. Sci. Technol*. **2007**, 41, 2364-2370.

(85) Fairfull-Smith, K.E.; Blinco, J.P.; Keddie, D.J.; George, G.A.; Bottle, S.E. *Macromolecules*, **2008**, 41, 1577-1580.

(86) Coenjarts, C.; Garcia, O.; Llauger, L.; Palfreyman, J.; Vinette, A.L.; Scaiano, J.C. *J.Am.Chem.Sco*. **2003**, 125, 620-621.

(87) Aliaga, C.; Juarez-Ruiz, J.M.; Scaiano, J.C.; Aspee, A. *Org.Lett*. **2008**, 10, 2147-2150.

(88) Flicker, T.M.; Green, S.A. *Environmental Health Perspectives*, **2001**, 109, 765-771.

(89) Chen, W.; Wang, X.; Tu, X.; Pei, D.; Zhao, Y.; Guo, X. *Small*, **2008**, 6, 759-764.

(90) Kalai, T.; Schindler, J.; Balog, M.; Fogassy, E.; Hideg, K. *Tetrahedron*, **2008**, 64, 1094-1100.

(91) Borisenko, G.G.; Martin, I.; Zhao, Q.; Amoscato, A.A.; Kagan, V.E. *J.Am.Chem.Soc*. **2004**, 126, 9221-9232.

(92) Fairfull-Smith, K. E.; Bottle, S. E. *Eur. J. Org. Chem*., **1998**, 32, 5391-5400.

(93) Herbelin, S.E.; Blough, N.V. *J.Phys.Chem.B*. **1998**, 102, 8170-8176.

(94) Ingold, K.U.; *In Landolt-Bornstein Numerical Data and Functional Relationships in Science and Technology, Subvolume C, Radical Reaction Rates in Liquids; Fischer, H., Ed.*; Springer-Verlag: New York, **1983**; Vol. 13, pp 166-270.

(95) Li, B.; Gutierrez, P.L.; Blough, N.V. *Anal.Chem*.**1997**, 69, 4295-4302.

(96) Li, B.; Gutierrez, P.L.; Blough, N.V. *Methods.Enzymol*.**1999**, 300, 202-216.

(97) Li, B.; Gutierrez, P.L.; Amstad, P.; Blough, N.V. *Chem.Res.Toxicol*. **1999**, 12, 1042-1049.

(98) Thomas-Smith, T.E.; Blough, N.V. *Environ.Sci.Technol*. **2001**, 35, 2721-2726.

(99) Vaughan, P.P.; Blough, N.V. *Environ.Sci.Technol*. **1998**, 32, 2947-2953.

(100)Johnson, C.G.; Caron, S.; Blough, N.V. *Anal.Chem*. **1996**, 68, 867-872;

(101)Kieber, D.J.; Johnson, C.G.; Blough, N.V. *Free Rad. Res. Comm*. **1992**, 16, 35-39.

(102)Maillard, B.; Ingold, K.U.; Scaiano, J.C. *J.Am.Chem.Soc*. **1983**,105, 5095-5099.

(103) Goldstein, S.; Samuni, A.; Hideg, K.; Merinyi, G. *J.Phys.Chem.A*. **2006**, 110, 3679-3685.

(104)Krishina, M.C.; Grahame, D.A.; Samuni, A.; Mitchell, J.B.; Russo, A. *Proc.Natl.Acad.Sci.USA*. **1992**, 89, 5537-5541.

(105)Darmanyan, A.P.; Tatikilov, A.S. *J.Photochem*. **1986**, 32, 157.

(106) Nortre Dame Radiation Chemistry Data Center: http://www.rcdc.nd.edu/Solnkin2/

(107)Yamamoto, Y.; Niki, E.; Kamiya, Y. *Lipids*, **1982**, 17, 870-877.

(108)Yamamoto, Y.; Niki, E.; Kamiya, Y.; Shimasaki, H. *Biochimica et Biophysica Acta*, **1984**, 332-340.

(109)Takahashi, M.; Tsuchiya, J.; Niki, E. *J.Am.Chem.Soc*. **1989**, 111, 6350-6353.

(110) Lardinois, O.; Maltby, D.; Medzihradszky, K.; Montellano, P.R.; Tomer, K.; Mason, R.; Deterding, L. *Chem. Res. Toxicol*. **2009**, 22(6), 1034-1049.

(111)Tang, Y. Ph.D thesis, the Michigan Techonological University, **2005**.